The spatio-temporal regulation of Polo-like kinase 1 in DNA repair

Kirsten Joanne Legg

A thesis submitted for Doctor of Philosophy in

Chromosome and Developmental Biology



Lincoln College

Sir William Dunn School of Pathology

University of Oxford

Hilary Term 2019

Abstract

The G2/M cell cycle kinase Polo-like kinase 1 (PLK1) was recently discovered to play an active role in DNA repair by phosphorylating the RAD51 recombinase to aid homologous recombination. This occurs at a much shorter timeframe than the well-characterised downregulation of PLK1 activity via the DNA damage checkpoint. In this thesis, I expand upon this by investigating the regulation of PLK1 during this earlier timeframe post-damage. Laser microirradiation experiments observe fluorescently-tagged PLK1 localising to DNA damage sites within 15 minutes, in both S/G2 and, unexpectedly, G1 cells. In S/G2, this recruitment is dependent on PLK1's polo-box domain binding sites primed by the cyclin-dependent kinase CDK2. Activity of the DNA damage response kinase ATM is also required for PLK1's localisation to damage in both phases of the cell cycle. Meanwhile, a proteomics approach identified novel DNA repair-related PLK1 binding partners, including the E3 ubiquitin ligase UBR5 and the protein kinase DYRK2. DYRK2 increases in association with PLK1 within 30 minutes post-damage and can induce PLK1 activation by phosphorylation of its T-loop. These findings shed light onto how PLK1 is regulated to carry out its repair function, open up new avenues of future investigation into this topic, and even suggest the possibility of PLK1 playing further as-yet-uncharacterised roles in DNA repair.

Contents

Abstract iii

List of Figures x

List of Tables xiii

Abbreviations xv

Acknowledgements xxi

1 Background 1

1.1 Double-strand breaks and HR 1

1.1.1 Major mechanisms of double-strand break repair . . . 1

1.1.2 Initial sensing and response to a double-strand break 3

1.1.3 Promotion of homologous recombination over non-homologous end joining 5

1.1.4 Recruitment of RAD51 to resected DNA 7

1.1.5 Double Holliday junction formation and resolution . . . 9

1.2 PLK1 and its role in the cell cycle 11

1.2.1 Structural mechanism of PLK1 activation and localisation 12

1.2.2 PLK1 activity and mitotic entry 15

1.2.3 Roles of PLK1 during mitosis 16
1.3 The DNA damage checkpoint 17
1.3.1 Checkpoint kinases CHK1 and CHK2 induce cell cycle arrest 18
1.3.2 PLK1 as a target of the DNA damage checkpoint . . . 19
1.3.3 PLK1 in checkpoint recovery 20
1.4 Cell cycle drivers promoting DNA repair 21

2 Materials and Methods 29
2.1 Cell lines and antibodies 29
2.1.1 Cell lines 29
2.1.2 Culture of cell lines 30
2.1.3 Antibodies 31
2.2 Generation of stable cell lines 32
2.2.1 Generation of plasmid constructs 32
2.2.2 Transfection of plasmid constructs 34
2.2.3 Antibiotic selection 34
2.2.4 Confirmation of stable clones 35
2.3 Cell synchronisation 36
2.3.1 Double thymidine block 36
2.3.2 Mitotic arrest 36
2.3.3 FACS analysis of cell cycle profile 36
2.4 Ionising radiation treatment 37
2.5 Transfection of siRNAs 37
2.6 Cell lysis and immunoprecipitation 38
2.6.1 Cell lysis 38
2.6.2 Cell fractionation 39
2.6.3 Crosslinking of beads to antibodies 39

2.6.4 Pre-washing of beads 40
2.6.5 Pre-clearing 40
2.6.6 Immunoprecipitation 40
2.6.7 Washing beads 41
2.6.8 Glycine elution 41
2.6.9 Boiling beads 42
2.7 Mass spectrometry and proteomics 42
2.7.1 TCA precipitation method of protein digestion 42
2.7.2 In-solution method of protein digestion 43
2.7.3 FASP method of protein digestion 44
2.7.4 C18 sample preparation 45
2.7.5 Mass spectrometry 45
2.7.6 Database searching and filtering 46
2.7.7 Statistical analysis 47
2.8 Live-cell microscopy and laser microirradiation 48
2.8.1 Preparation of cells for live cell microscopy 48
2.8.2 Microscope setup and image capture 48
2.8.3 Quantification of signal in images 49
2.9 Fixed-cell microscopy 50
2.9.1 Cell fixation and immunostaining 50
2.9.2 Microscope setup and image capture 51
2.10 *In vitro* kinase assay 52
2.11 Bacterial protein purification 52
2.12 Quantitative real-time PCR 53
2.12.1 RNA extraction and reverse transcription 53
2.12.2 Real-time PCR 54
2.13 Tables of materials used 55

3 PLK1 localisation to DNA damage sites 63

3.1 Introduction 63

3.2 Results 64

3.2.1 Cell lines containing fluorescently-tagged PLK1 64

3.2.2 PLK1 does not form cytologically visible foci upon ionising radiation treatment 66

3.2.3 PLK1 localises to damage sites within 15 minutes in G1 and G2 cells 66

3.2.4 PLK1 recruitment to damage in G2 is dependent on the PBD and primed by CDK2 but not CDK1 72

3.2.5 PLK1 localisation to damage is dependent on ATM activity 74

3.2.6 Effect of PLK1 activity on its recruitment to damage is unclear but unrelated to ATM activity 76

3.2.7 BRCA2 localises to DNA damage in late S phase with faster kinetics than PLK1 81

3.2.8 Attempts to generate cells with a cell cycle-dependent reporter 83

3.3 Discussion 86

4 PLK1 interaction partners upon damage 93

4.1 Introduction 93

4.1.1 Outline and optimisation of experimental setup 94

4.2 Results 99

4.2.1 PLK1 interaction partners related to the cell cycle . . . 100

4.2.2 PLK1 interaction partners related to the DNA damage response 104

4.2.3 Change in PLK1 interaction partners upon DNA damage . . . 107
4.3 Discussion . . . 110

5 PLK1 interaction with DYRK2 and UBR5 115
5.1 Introduction . . . 115
5.1.1 A brief overview of DYRK2 . . . 115
5.1.2 A brief overview of UBR5 . . . 118
5.2 Results . . . 119
5.2.1 DYRK2 phosphorylates PLK1 *in vitro* . . . 119
5.2.2 Confirmation of DYRK2 inhibition and knockdown . . . 121
5.2.3 DYRK2 affects PLK1 T210 phosphorylation *in vivo* . . . 123
5.2.4 PP6 has no effect on PLK1 T210 phosphorylation in mitosis . . . 124
5.2.5 Preliminary experiments on UBR5's interaction with PLK1 . . . 126
5.2.6 Laser microirradiation experiments with DYRK2 and UBR5 . . . 130
5.2.7 Setup of a CRISPR interference system for live-cell microscopy . . . 133
5.3 Discussion and further work . . . 137

6 Conclusions and overall discussion 141
6.1 PBD- and CDK2-dependent PLK1 recruitment in S/G2 . . . 141
6.2 ATM-dependent PLK1 recruitment in G1 and S/G2 . . . 147
6.3 DYRK2 association with and activation of PLK1 . . . 150
6.4 Concluding remarks . . . 154

References 157

List of Figures

1.1 Non-homologous end-joining and homologous recombination 2

1.2 Establishment of DNA damage-dependent chromatin 4

1.3 Recruitment of RAD51 to resected DNA 8

1.4 Synthesis-dependent strand annealing and double Holliday junction formation 10

1.5 Mutual autoinhibition between the kinase domain and polo-box domain of PLK1 14

1.6 FRET detection of DNA damage-induced PLK1 activation . . 24

1.7 Potential change in PLK1 activity upon DNA damage 26

3.1 Lack of PLK1 foci formation upon ionising radiation treatment 65

3.2 PLK1 localisation to laser-induced DNA damage in G1 and G2 cells 69

3.3 PLK1 localisation to damage is dependent on its PBD and CDK2 activity 73

3.4 PLK1 localisation to damage sites is dependent on ATM activity 75

3.5 Effect of PLK1 activity on its recruitment to damage 78

3.6 BRCA2 localisation to laser-induced DNA damage 82

3.7 Expression of CDT1-BFP did not vary throughout the cell cycle 85

4.1 Confirmation of cell synchronisation for proteomics 98
4.2 Volcano plots of notable significant PLK1 interaction partners 101
4.3 PLK1 interaction partners of interest 109

5.1 DYRK2 phosphorylation of PLK1 123
5.2 PP6 has no effect on phosphorylation of PLK1 T210 in mitosis 125
5.3 Generation and testing of UBR5 truncation constructs 129
5.4 UBR5 and DYRK2 in laser microirradiation experiments . . . 131
5.5 Attempts to set up a CRISPRi system for live-cell experiments 134

6.1 Models for PLK1's interaction with its CDK2- and PBD-dependent binding scaffold upon damage 144

List of Tables

2.1 Sequences of primers used in this thesis 55
2.2 Sequences of primers and oligos used by collaborators in generating CRISPRi plasmids 57
2.3 siRNA and sgRNA sequences 58
2.4 Suppliers of reagents used 58

4.1 Optimisation attempts for mass spectrometry protocol 97

Abbreviations

53BP1	TP53-binding protein 1
ACN	Acetonitrile
ANR28	Ankyrin repeat domain-containing protein 28
ANR52	Ankyrin repeat domain-containing protein 52
APC/C	Anaphase promoting complex/cyclosome
AS	Asynchronous
ATP	Adenosine triphosphate
ATR	Ataxia telangiectasia and Rad3-related protein
ATRIP	ATR-interacting protein
ATM	Ataxia telangiectasia mutated
BAC	Bacterial artificial chromosome
BFP	Blue fluorescent protein
BLM	Bloom syndrome protein
BRCA1	Breast cancer type 1 susceptibility protein
BRCA2	Breast cancer type 2 susceptibility protein
BSA	Bovine serum albumin
bSAF	bait-normalised SAF
CDC6	Cell division cycle 6
CDH1	CDC20 homolog 1
CDK	Cyclin-dependent kinase
CDK1	Cyclin-dependent kinase 1
CDK2	Cyclin-dependent kinase 2

CENP-A	Centromeric protein A
CENPQ	Centromere protein Q
CENPU	Centromere protein U
CEP78	Centrosomal protein of 78 kDa
CEP97	Centrosomal protein of 97 kDa
CFP	Cyan fluorescent protein
ChIP	Chromatin immunoprecipitation
CHK1	Checkpoint kinase 1
CHK2	Checkpoint kinase 2
CINP	Cdk2-interacting protein
CK2	Casein kinase 2
CMV	Cytomegalovirus
CP110	Centriolar coiled-coil protein of 110 kDa
CRISPR	Clustered regularly interspaced short palindromic repeat
CRISPRi	CRISPR interference
CtIP	CtBP-interacting protein
CycA	Cyclin A
CycB	Cyclin B
dHJ	double Holliday junction
DIM-PIM	Dimethyl pimelimidate dihydrochloride
DMEM	Dulbecco's Modified Eagle Medium
DMSO	Dimethyl sulfoxide
DNA	Deoxyribonucleic acid
DNA-PK	DNA-dependent protein kinase
DTT	Dithiothreitol
DSB	Double-strand break
dsDNA	double-stranded DNA
DYRK1A	Dual-specificity tyrosine-phosphorylation-regulated kinase 1A

DYRK2	Dual-specificity tyrosine-phosphorylation-regulated kinase 2
EDTA	Ethylenediaminetetraacetic acid
EDVP complex	EDD, DDB1 and VPRBP complex
EGFP	Enhanced green fluorescent protein
EXO1	Exonuclease 1
FASP	Filter-assisted sample preparation
FBS	Foetal bovine serum
FRET	Förster resonance energy transfer
FUCCI	Fluorescent ubiquitination-based cell cycle indicator
γH2AX	Histone H2AX phosphorylated at serine 139
GFP	Green fluorescent protein
GST	Glutathione S-transferase
HECT	Homologous to E6-AP carboxylterminus
HPRT	Hypoxanthine-guanine phosphoribosyltransferase
HR	Homologous recombination
HRP	Horseradish peroxidase
IF	Immunofluorescence
IgG	Immunoglobulin G
IP	Immunoprecipitation
IPTG	Isopropyl ß-D-1-thiogalactopyranoside
IR	Ionising radiation
kDa	kiloDaltons
KRAB	Krüppel-associated box
LAP	Localisation and affinity purification
LC-MS/MS	Liquid chromatography tandem mass spectrometry
MDC1	Mediator of DNA damage checkpoint 1
MISP	Mitotic interactor and substrate of Plk1
MLH1	MutL protein homolog 1
MMEJ	Microhomology-mediated end joining

MOPS	3-(n-Morpholino)propanesulfonic acid
MRG15	Mortality factor 4-related gene 15 protein
MRGX	Mortality factor 4-related gene X protein
MRN complex	MRE11, RAD50 and NBS1 complex
NA	Numerical aperture
NBS1	Nijmegen breakage syndrome 1
NCS	Neocarzinostatin
NHEJ	Non-homologous end joining
NLS	Nuclear localisation sequence
Noc	Nocodazole
NSAF	Normalised spectral abundance factor
NUCKS1	Nuclear ubiquitous casein and cyclin-dependent kinase substrate 1
PALB2	Partner and localiser of BRCA2
PAR	Poly(ADP-ribose)
PARP-1	Poly(ADP-ribose) polymerase 1
P/S	Penicillin/Streptomycin
PBD	Polo-box domain
PBS	Phosphate buffered saline
PI	Propidium iodide
PICH	Plk1-interacting checkpoint helicase
PLGEM	Power law global error model
PLK1	Polo-like kinase 1
PLK2	Polo-like kinase 2
PLK3	Polo-like kinase 3
PLK4	Polo-like kinase 4
PMT	Photomultiplier tube
PP1	Protein phosphatase 1
PP2A	Protein phosphatase 2A
PP6	Protein phosphatase 6

PP6C	Protein phosphatase 6 catalytic subunit
PP6R1	Protein phosphatase 6 regulatory subunit 1
PP6R2	Protein phosphatase 6 regulatory subunit 2
PRC1	Protein regulator of cytokinesis 1
PSM	Peptide spectral match
RFP	Red fluorescent protein
RMI1	RecQ-mediated genome instability protein 1
RMI2	RecQ-mediated genome instability protein 2
RNA	Ribonucleic acid
RPA	Replication protein A
SAF	Spectral abundance factor
SAPS	Sit4-associated proteins
SCF	Skp1-cullin-F-box
siRNA	small interfering RNA
SEM	Standard error of the mean
SLX4IP	SLX4-interacting protein
ssDNA	single-stranded DNA
STN	Signal-to-noise ratio
TEAB	Triethylammonium bicarbonate
TCEP	Tris(2-carboxyethyl)phosphine
TFA	Trifluoroacetic acid
TOPBP1	DNA topoisomerase 2-binding protein 1
UBA	Ubiquitin-associated
UBR5	Ubiquitin protein ligase E3 component N-recognin 5
UV	Ultraviolet
WCE	Whole cell extract
WT	Wild-type
XPF	Xeroderma pigmentosum group F-complementing protein
YFP	Yellow fluorescent protein

Acknowledgements

To the Esashi lab, including several members who are no longer here, for being a lovely group that I felt at home amongst almost as soon as I began my rotation project here. To Fumiko, of course, for all of her suggestions and advice, as well as always being approachable and enthusiastic about my work. Marjorie deserves special mention for her immense help regarding mass spectrometry, without which half of this thesis would not exist. In relation to that, I have to thank her, Isabel and Josh for creating the final optimised mass spec prep protocol I used, saving me from slaving away trying to optimise it for even longer than I'd been doing, which was far too long already. To Anthony as well for the help with using qPCR, which I'd had bad experiences with figuring out on my own in my undergrad project but which he managed to make relatively painless here. And those who didn't directly help with a particular part of my project still deserve mention just for being there and being who they were: to Jean-Yves for seemingly always having the answers to any general lab-related questions I had, to Chris for basically being my lab mum, to Isabel and Federico for being there to share this DPhil journey with, and to Lucia and Xanita, whom I can't think of anything poetic and specific to say about but who are also great people I didn't want to go without mentioning.

This work relied a lot on the help of people outside the Esashi lab as

well, especially Svenja for operating the mass spectrometer and also being a huge help with that section of my thesis, and Alan for teaching me how to use the confocal microscope and being there to ask whenever something went wrong with it, along with several other people in charge of various facilities and services who helped in more minor ways. The Dunn School in general was a pleasant department to work in, particularly thanks to the GSA committee for organising all sorts of events for DPhil students, and the members of the Nieduzynski lab for being a group I almost felt like a part of too thanks to our labs' joint meetings.

Putting the science aside... during my time here, I found myself suddenly struggling with anxiety and depression. This was a thing I'd maybe always had rattling around in my brain, but it had never been enough of a problem to be noticeable until I was doing something more challenging to me than anything I'd done before. So the rest of these acknowledgements are for everyone who helped me with that, since it turns out that not being emotionally willing to do the science due to stress and exhaustion is a much bigger problem than just not knowing how to.

Again, I have to thank the members of the Esashi lab for being completely accepting of this, especially Fumiko and Jean-Yves for briefly sharing similar experiences they'd had or were having and making me feel less like the only one, and Chris, whose lab-mum powers were probably the most helpful in this regard. To all the various counsellors and doctors I saw on the rare occasions I felt like I should try some more professional help, none of whom made a particularly huge difference if I'm honest, but who each helped at least a little and I'm grateful that the University of Oxford gave me so many options I could turn to for this kind of thing. To my parents, of course, for taking this in their stride despite having no experience

with matters like this and being totally okay with the fact that I'm much less able to be a functional adult than my brothers. And to my small handful of very close friends, both from "real life" and from online, for being there and being the best. (Also for reminding me that the science I was doing was super cool and exciting, which should be obvious but is easy to forget when you do it every day while surrounded by people doing even cooler science than you.)

Last of all, and I don't care how silly this sounds because it's true: I absolutely have to thank all the works of fiction I've been invested in and the characters within them, for giving me something I was always able to care about even when the science had sometimes lost its spark. I'm not exaggerating when I say this was just as much of a help in me pushing through my mental illness and sticking with my DPhil as the real people in my life. So here's to everyone, even if they were all just fictional, who helped me understand that it's okay to feel weak and scared sometimes, that ignoring how I felt and running away from it would just make it worse, and that despite it all I could keep on fighting anyway, because no matter how impossible something might seem, if you just up and do it, you'll make it possible.

Chapter 1

Background

1.1 Double-strand breaks and homologous recombination

The genetic material of living cells is constantly being assaulted by many different forms of damaging lesions. One of the most deleterious kinds of DNA damage is the double-strand break (DSB), which can cause genome rearrangements and cell death if not repaired, to the point that defective DSB repair mechanisms are a major driving factor in many genetic disorders as well as cancer [1].

1.1.1 Major mechanisms of double-strand break repair

Cells have two main mechanisms of repairing DSBs. The first is non-homologous end joining (NHEJ), where the broken ends are simply religated back together [2]. Since most DSBs are ragged, nucleases and polymerases are needed to trim or fill in the ends before they can be cleanly ligated, often resulting in small sequence errors (Figure 1.1A). More severely, chromosome translocations can occur if NHEJ joins broken ends that were

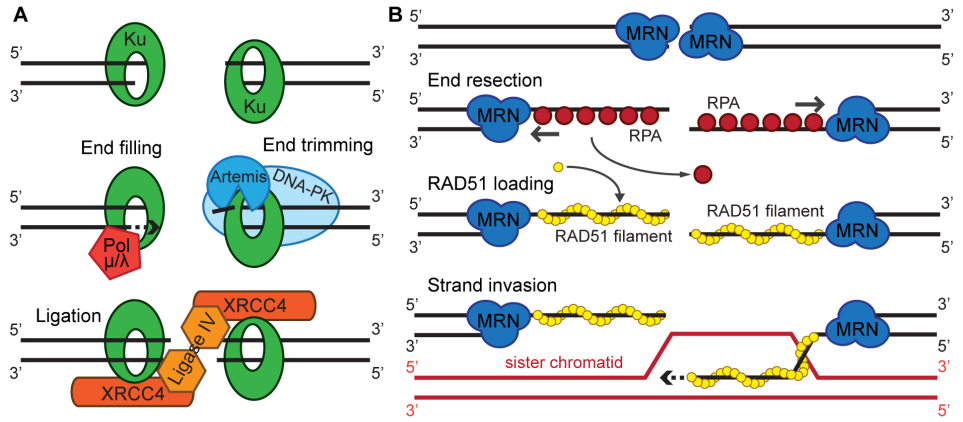


Figure 1.1: **Diagrams depicting the basic mechanisms of non-homologous end-joining and homologous recombination. A:** Non-homologous end-joining. DSBs are bound by the Ku70/80 heterodimer, which recruits several enzymes for end-processing, including polymerases μ and λ for end filling, the nuclease Artemis in complex with DNA-PK for end trimming, and DNA ligase IV in complex with XRCC4 to ligate the broken ends. **B:** Homologous recombination. DSBs are bound by the MRN complex, of which the MRE11 subunit carries out end resection, producing long ssDNA tracts bound by RPA. RAD51 is then recruited to the break and replaces RPA to form a helical filament around the ssDNA, and this RAD51-ssDNA filament can perform strand invasion into a homologous sister chromatid, giving a template for error-free repair.

not originally together. Despite its error-prone nature, NHEJ is advantageous in that it can be carried out at any stage of the cell cycle, whether or not the cell's genome has already been replicated.

The second and largely error-free mechanism of DSB repair is homologous recombination (HR). It is initiated by the resection of broken ends to form long 3' single-stranded overhangs onto which the RAD51 recombinase is loaded. The RAD51-ssDNA filament invades a homologous double-stranded DNA template, allowing it to be used as a template for DNA synthesis (Figure 1.1B). The repaired strands are then rejoined either by re-annealing or by formation of a double Holliday junction which can be resolved in different ways to form either crossover or non-crossover products

[3] (Figure 1.4). Due to the requirement for a homologous template, HR must be restricted to S phase onwards, once an identical sister chromatid has been synthesised during DNA replication. As such, the initiation of HR must be regulated in a cell cycle-dependent manner.

1.1.2 Initial sensing and response to a double-strand break

As soon as a double-strand break occurs, several factors respond by sensing the lesion and signalling repair pathways. One of the first factors to sense a DSB is the Ku70/80 heterodimer [4]. Ku binds to the broken ends to hold them in proximity, and there it also activates the kinase DNA-PK, which promotes the NHEJ pathway [2].

Another early sensor of DSBs is the MRN complex, which consists of MRE11, RAD50 and NBS1 [5]. MRE11 and RAD50 bind the broken ends directly, while RAD50 forms a flexible linker tethering them together [6]. The MRN complex activates ATM, a protein kinase that is a key regulator of the DNA damage response [7] [8]. One of the many targets of ATM is the histone variant H2AX, resulting in an S139-phosphorylated form of it known as γH2AX [9]. γH2AX is bound by the checkpoint mediator protein MDC1 [10], which also binds to MRN via NBS1 [11] [12] and to ATM [13]. This causes a positive feedback loop amplifying ATM activation and H2AX phosphorylation, resulting in a widespread γH2AX signal around the damage site that is required for the recruitment of further factors important for repair [14] (Figure 1.2).

MDC1 is itself phosphorylated by ATM, and these ATM-dependent phosphosites on MDC1 recruit the ubiquitin ligase RNF8, which ubiquitylates histones H2A and H2AX around the damage site [15] [16] [17]. A second ubiquitin ligase, RNF168, binds to these ubiquitylated histones and further

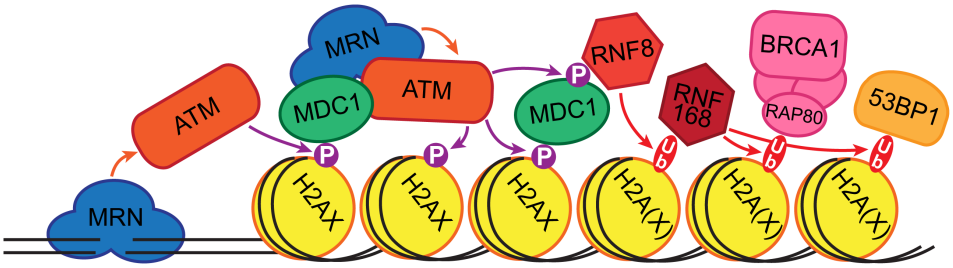


Figure 1.2: **A diagram depicting establishment of DNA damage-depentent chromatin.** From left to right: the MRN complex binds to a DNA double-strand break, stimulating activation of ATM, which phosphorylates H2AX on serine 139, creating γH2AX. The phosphorylated serine on γH2AX is bound by MDC1, which recruits more molecules of MRN and ATM, enabling more activated ATM to phosphorylate more H2AX and resulting in a positive feedback loop that spreads the γH2AX signal. Additionally, ATM phosphorylates MDC1 itself, which is then bound by RNF8, and RNF8 ubiquitylates H2A/H2AX. This ubiquitylation is bound by RNF168, which ubiquitylates more histones, also spreading the ubiquitylation signal in a positive feedback manner. Ubiquitylated histones can be bound by either BRCA1 in a complex with RAP80, or by 53BP1 directly. Orange arrows depict activation, purple arrows depict phosphorylation, and red arrows depict ubiquitylation. Other histones in a nucleosome and the fact that not all nucleosomes contain the variant H2AX have been omitted for simplicity.

ubiquitylates them to form lysine 63-linked ubiquitin chains [18] [19]. These ubiquitin chains are bound directly by 53BP1 [20] and also by RAP80, which recruits BRCA1 via Abraxas [21] [22] [23] [24], resulting in the accumulation of both 53BP1 and BRCA1 in DNA damage-induced foci (Figure 1.2).

A third sensor that binds quickly to DSBs is PARP-1 [25], which catalyses the formation of poly(ADP-ribose) (PAR) chains on itself, H1 and H2B. These PAR chains recruit a number of factors involved in chromatin modification [26] and promoting an alternative NHEJ pathway instead of the classical NHEJ pathway [25]. More relevantly to HR, PARylation also aids in the early recruitment of ATM [27] and MRN [28]. PAR is also bound by BRCA1, allowing BRCA1 to be recruited to DSBs by a means other than

RAP80 [29].

If damage occurs during mitosis, these signalling pathways are partially inhibited. One reason for restricting DNA repair during mitosis is that telomeres are deprotected at this time, meaning that mitotic DNA repair, especially NHEJ, can cause unwanted telomere fusions [30]. Most of the aforementioned damage-sensing factors are still recruited to damage sites, but RNF8, RNF168, 53BP1 and BRCA1 are not [31] [32]. This is due to high cyclin-dependent kinase (CDK) and PLK1 activity in mitosis. CDK1 phosphorylates RNF8 which prevents its recruitment to MDC1 and therefore prevents ubiquitylation of histones [32], and CDK1 and PLK1 phosphorylate 53BP1 to prevent it binding to nucleosomes [30]. PLK1 also phosphorylates the NHEJ factor XRCC4 to inhibit the NHEJ pathway during mitosis [33]. Mitotic cells that are exposed to DNA damage exit mitosis while still damaged before repairing the damage in G1 phase [31].

1.1.3 Promotion of homologous recombination over non-homologous end joining

In order to commit a break to be repaired by HR as opposed to NHEJ, the first step that must occur is end resection, the digestion of a single 5' strand from each end to leave a 3' ssDNA overhang. This is carried out by two key nucleases: first, MRE11, a subunit of the MRN complex, nicks the DNA around 300 bp from the break and then digests in a 3' to 5' direction towards the break. Then, EXO1 digests from the nick in a 5' to 3' direction away from the break [34], leaving a long tract of ssDNA which is promptly stabilised by the ssDNA-binding protein RPA [35].

MRE11 is stimulated to begin end resection by a protein called CtIP [36]. The ability of CtIP to stimulate resection is regulated on two levels by

its phosphorylation, first in a cell cycle-dependent manner by CDKs from S phase onwards [37] [38] [39], and then in a DNA damage-dependent manner by ATM [40] [41]. A further level of cell cycle-dependent regulation also exists, in that CtIP is degraded in G1 phase by APC/C(CDH1) [42]. EXO1 is regulated similarly by phosphorylation from CDKs [43] and ATM [44].

Binding of the NHEJ-promoting factor Ku to DSBs also needs to be alleviated for HR to proceed [45] [46]. Experiments in fission yeast suggest Mre11 resection activity removes Ku from broken ends [47]. Mre11's ability to first nick the DNA some distance away from the end and then digest towards the end [34] supports the idea that both MRN and Ku could bind to the break at slightly different positions and then compete for retention based on whether or not Mre11 initiates resection. However, experiments in human cells suggest that, unlike in yeast, MRE11 resection activity alone cannot remove Ku, and so higher levels of regulation must be in play [48].

BRCA1 is also part of a complex with MRN and CtIP [49], dependent on the phosphorylation of CtIP by CDKs [50]. BRCA1's interaction with the complex is not required to stimulate resection [36] [51] [52], but it increases the speed and length of it [53].

53BP1 inhibits resection in a manner antagonised by BRCA1 [54] [55]. This requires the phosphorylation of 53BP1 by ATM, leading to the recruitment of RIF1 [56] [57] [58] [59] [60]. Recent work suggests RIF1 acts by ultimately recruiting CST-Polα to bind to and fill in ssDNA ends, promoting NHEJ over HR [61]. This is opposed in S and G2 by BRCA1 in a CtIP-dependent manner [59] [58]. A proposed mechanism for this is that BRCA1-CtIP promotes 53BP1 dephosphorylation and therefore dissociation of RIF1 [62].

Surprisingly, the portion of BRCA1 that is associated with damage-induced foci in a ubiquitin- and RAP80-dependent manner (as depicted in Figure 1.2) is inhibitory to HR [63]. However, BRCA1 binds to either CtIP or to Abraxas (and therefore RAP80) via the same BRCT domain, making its interaction with these proteins mutually exclusive [64]. The difference between these HR-repressive and HR-promoting complexes of BRCA1 is likely a spatial one. Bekker-Jensen *et al* identified a distinction between different subcompartments of damage-associated proteins: a directly ssDNA-associated microcompartment defined by the presence of RPA that only exists during S and G2 phases when resection occurs, and a wider area of DSB-associated chromatin defined by γH2AX signal that is cell cycle-independent [65]. BRCA1 was identified in both subcompartments, suggesting that even if the repressive RAP80-BRCA1 complex is present in the wider area, BRCA1-CtIP complexes can still stimulate resection closer to the actual break. This is supported by super-resolution microscopy showing BRCA1 accumulating in the core of pre-existing 53BP1 foci, excluding 53BP1 from the core and allowing RPA foci to form there instead [66] [67].

1.1.4 Recruitment of RAD51 to resected DNA

Once resection occurs, RPA bound to the ssDNA tract needs to be replaced with RAD51 in order for the strand invasion step of HR to occur [68]. This replacement is mediated by BRCA2, which contains BRC repeats that promote RAD51 assembly and RPA replacement on ssDNA, while preventing RAD51 assembly on dsDNA [69] [70] [71] [72].

Recruitment of BRCA2 to damage sites is partly mediated by BRCA1, via PALB2, which bridges the two BRCA proteins [73] [74] [75] (Figure 1.3A). This most likely involves the population of BRCA1 that is associated

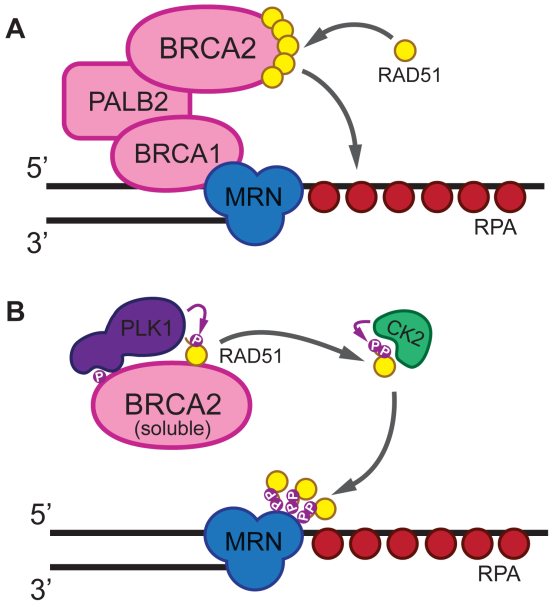


Figure 1.3: **Diagrams depicting mechanisms of RAD51 recruitment to resected DNA. A:** Canonical method of recruitment. RAD51 is recruited directly by BRCA2 as part of the BRCA1-PALB2-BRCA2 complex. **B:** PLK1-dependent method of recruitment. PLK1 phosphorylates RAD51 on S14 in a manner bridged by BRCA2 or another scaffold protein. CK2 binds to pS14 RAD51 and phosphorylates it further on T13. RAD51 phosphorylated on T13 can then associate with the NBS1 subunit of the MRN complex at damage sites.

with ssDNA and CtIP/MRN, rather than the population that is part of the repressive RAP80-based complex associated with chromatin [65]. PALB2 binds via BRCA1's central coiled-coil domain and not the BRCT domain that CtIP binds to, so it is possible for BRCA1 to bind PALB2 and CtIP at the same time [64]. In support of this, PALB2 IPs pull down CtIP along with BRCA1 and BRCA2 [74].

BRCA1 recruitment is upstream of that of PALB2 and BRCA2 [75], but PALB2 and BRCA2 are still partially recruited without BRCA1 [74], so they must have other, BRCA1-independent ways of associating with damaged chromatin. Indeed, PALB2 contains a chromatin-association motif [76] and

interacts with MRG15 [77] [78], which binds to K36-trimethylated histone H3, an epigenetic mark associated with active genes that is also induced at DSB sites [79]. PALB2 has additionally been shown to bind to DNA and stimulate RAD51 strand invasion without BRCA2 [80] [81]. Meanwhile, BRCA2 has its own DNA-binding activity through its oligonucleotide-binding folds, which can bind both ssDNA [82] [71] and PAR chains [83]. This oligonucleotide-binding domain displays redundancy with the PALB2-interacting domain; BRCA2 retains its HR function upon deletion of either one domain or the other, but not both at once [84].

However, BRCA2 is not always required to directly recruit RAD51 to resected DNA. RAD51 foci formation is BRCA2-independent in S-phase [85]. More recently, work by the Esashi lab found that PLK1 phosphorylates RAD51 at S14, causing subsequent phosphorylation by CK2 at T13, and phospho-T13 RAD51 can associate directly with NBS1 at damage sites [86] (Figure 1.3B). PLK1 does not directly interact with RAD51 in order to phosphorylate it; instead, this interaction is bridged by BRCA2, which PLK1 can bind to in a manner dependent on the phosphorylation of BRCA2 by CDKs [87]. RAD51 phosphorylation can also occur in BRCA2-deficient cells [87], suggesting that other proteins, including TOPBP1 [88] but potentially also others, can also act as mediators between PLK1 and RAD51.

1.1.5 Double Holliday junction formation and resolution

Once the RAD51 filament catalyses strand invasion into a homologous template, two possible pathways can occur (Figure 1.4). Synthesis of a new DNA strand using the homologous template will cause the D-loop to either migrate or extend depending on whether branch migration occurs behind the DNA synthesis. D-loop migration will likely eventually result

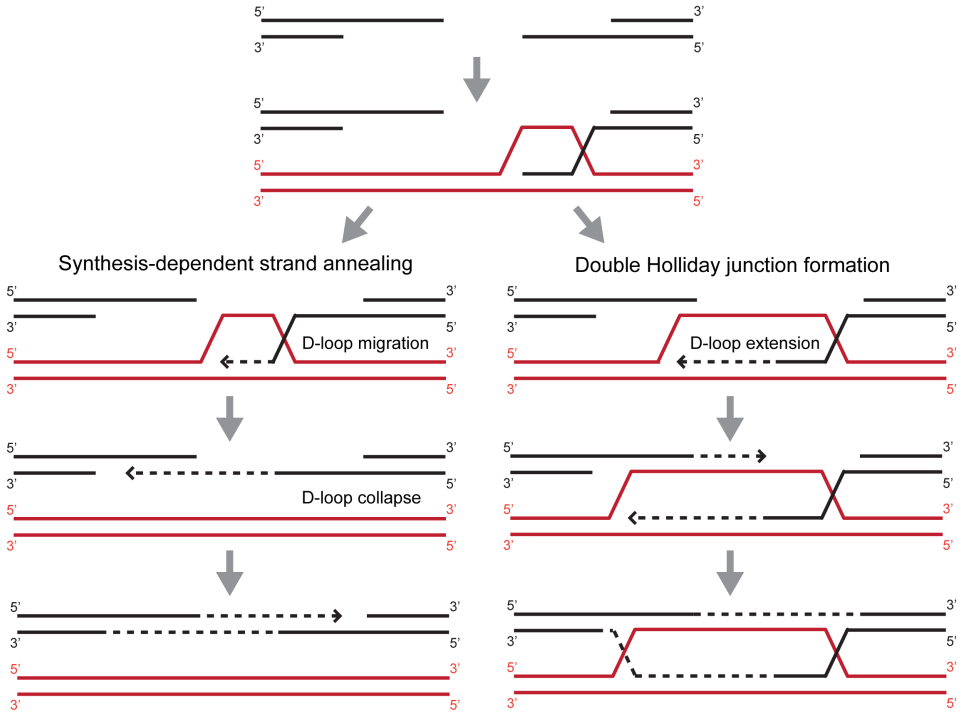


Figure 1.4: **A diagram depicting the mechanisms of synthesis-dependent strand annealing and double Holliday junction formation.** One resected end of a DSB (black) invades a homologous sister chromatid (red). DNA synthesis along the template (dotted line) may result in either D-loop migration (left) or D-loop extension (right). This ultimately determines whether the second resected end anneals to the extended first resected end, resulting in no crossovers (left), or to the other strand of the sister chromatid, resulting in a double Holliday junction which must then be resolved (right).

in the D-loop collapsing and the extended ssDNA potentially being recaptured by annealing to the other resected ssDNA tract, known as synthesis-dependent strand annealing. Alternatively, D-loop extension will expose more of the D-loop's ssDNA until the other resected ssDNA tract can anneal to it, resulting in formation of a double Holliday junction (dHJ) once synthesis is completed and the ends are religated [3].

Before chromosome segregation in mitosis, any dHJs that formed as a result of HR must be removed, otherwise chromosome breakage will occur.

There are two possible mechanisms for this: either dissolution, mediated by the BTR complex (BLM-Topoisomerase IIIα-RMI1-RMI2), in which the junction is untangled through topoisomerase activity; or resolution, in which the junctions are cut by structure-selective endonucleases and then religated [89]. The nucleases involved in resolution can either be GEN1, or the SLX-MUS complex, consisting of SLX4-SLX1 and MUS81-EME1 [90]. To avoid competing with dissolution, which is the preferred pathway as it never results in crossover products, activity of the resolution-mediating nucleases is restrained until late in the cell cycle, shortly before mitosis. GEN1 is restricted to the cytoplasm, rendering it only able to cleave DNA after nuclear envelope breakdown at the onset of mitosis. SLX-MUS, meanwhile, is regulated via phosphorylation by cell cycle kinases. Association between SLX4 and MUS81 to form the SLX-MUS holoenzyme that can cleave dHJs is promoted by phosphorylation of SLX4 by CDKs and also, to a lesser extent, by PLK1. This restricts SLX-MUS association and therefore dHJ cleavage activity to G2/M phase [90], without which SLX-MUS would cause unwanted cleavage during replication in S phase, leading to shearing of chromosomes [91]. As such, dHJ resolution is another aspect of HR which is controlled in a cell cycle-dependent manner to avoid potentially deleterious consequences.

1.2 PLK1 and its role in the cell cycle

PLK1 (Polo-like kinase 1) is a cell cycle kinase which is most highly expressed and active in G2 and M phase [92] [93]. It is important not only for promoting mitotic entry but also for regulating many different processes during mitosis [94].

1.2.1 Structural mechanism of PLK1 activation and localisation

PLK1 is a serine/threonine protein kinase with target motif of D/E-X-**S**/**T**-Φ-X-D/E [95] [96]. Its activation is dependent on the phosphorylation of threonine 210 in its T-loop; phosphomimetic mutants T210D/E are constitutively active [97] [98]. The serine 137 residue was also thought to have a role in PLK1 activation, in part because phosphomimetic S137D mutation causes an S-phase arrest, implying phosphorylation of this residue plays a role in the G1-S transition [98]. However, S137A PLK1 mutants are viable [98] [99] and S137A/T210D mutants of PLK1 still show activity via a FRET-based probe [100]. Lasek *et al* [99] more recently showed a possible role for the phosphorylation of threonine 214 in the T-loop, as T214V mutants were inviable. Meanwhile, phosphorylation of tyrosine 217 appears to have an inhibitory effect on PLK1 activity [101].

While the N-terminus of PLK1 is its kinase domain, the C-terminus is a Polo-box domain (PBD), containing two tandem Polo boxes which bind specifically to substrates with phosphorylated serines or threonines [102] [103]. PBD binding strictly requires a serine residue at position -1 relative to the phosphorylated serine/threonine and is also partially dependent on a proline at position +1 [103]. PLK1 residues H538 and K540 directly contact the phosphate group of the substrate in a pincer-like arrangement, such that a double mutant of these residues abrogates PBD binding to phosphopeptides entirely [103]. Since CDKs are proline-directed kinases and the PLK1 PBD binding motif includes a proline, PLK1 will bind to many substrates primed by CDK phosphorylation, enabling it to further phosphorylate either these proteins or other proteins closely associated with them [104]. PLK1 can also prime its own PBD binding sites [105] [106].

Binding of the PBD to a phosphoprotein stimulates PLK1 activity [103]. When not bound to a substrate, the PBD binds instead to PLK1's kinase domain and inhibits kinase activity [107] [108], as well as causing the inter-domain linker to sequester the T-loop and prevent access for activating kinases [109]. Binding of the PBD to a phosphoprotein relieves this autoinhibition, stimulating kinase activity and opening up the T-loop for phosphorylation to further increase the activity of PLK1 [108] [109]. The effect of PBD inhibition is reduced when T210 is phosphorylated, suggesting that the kinase domain also reciprocally inhibits the PBD when inactive, and T-loop phosphorylation relieves this [107][108] [109] (Figure 1.5). Additionally, S137 phosphorylation directly blocks PBD autoinhibition, clarifying the role for S137 in PLK1 activation [109]. Thus, once PLK1 is activated by T-loop phosphorylation, or when S137 is phosphorylated, its PBD is freed up to localise it to the appropriate subcellular locations for it to carry out its function.

Recent work on the *Drosophila* homologue Polo suggests the PBD also controls PLK1 by controlling its nuclear import [110]. A bipartite NLS in the kinase domain is masked by autoinhibitory PBD binding, but when the autoinhibition is relieved by T-loop phosphorylation, the NLS is exposed and Polo can move to the nucleus [110]. Human PLK1 also contains this bipartite NLS in its kinase domain [111], and the localisation conferred by it is important for mitotic progression [112]. It is currently unclear whether relief of the PBD's autoinhibition by T-loop phosphorylation is required for PLK1 nuclear localisation outside of *Drosophila*, though this would explain the finding that PLK1 is activated by T-loop phosphorylation in the cytoplasm yet first displays kinase activity in the nucleus [112].

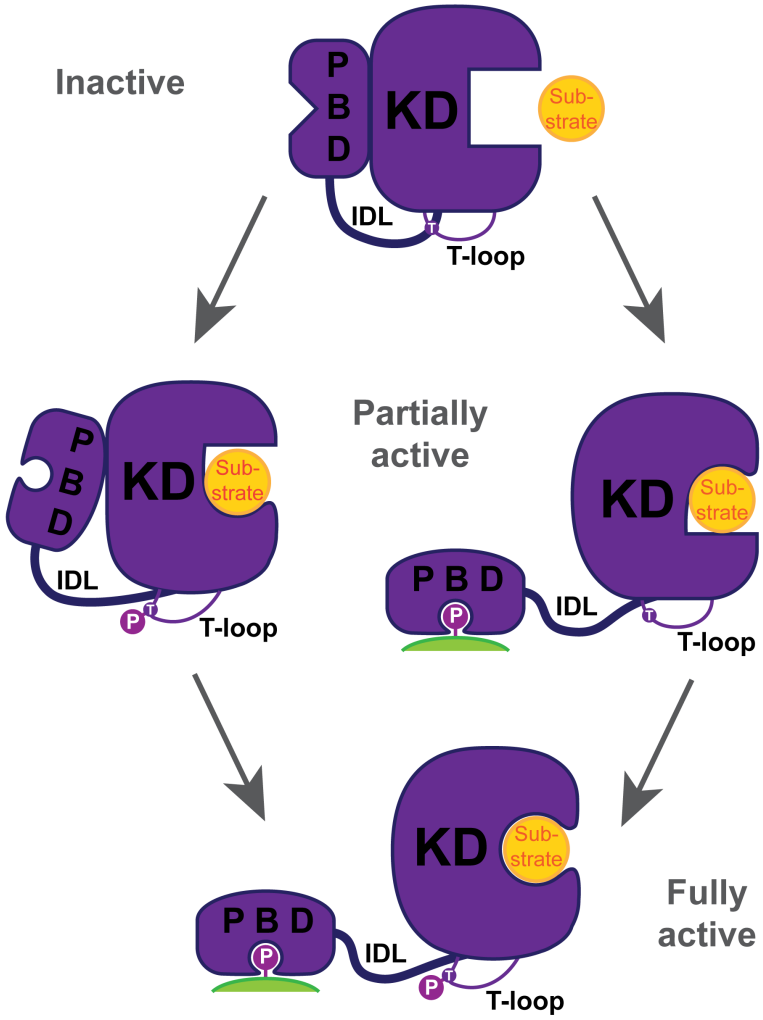


Figure 1.5: **A diagram showing the mechanism of mutual autoinhibition between the kinase domain and polo-box domain of PLK1.** KD: kinase domain. PBD: Polo-box domain. IDL: Inter-domain linker. In the inactive form, the KD and PBD interact in a conformation that inhibits both from binding efficiently to their substrates, while the IDL sequesters the T-loop, preventing access by activating kinases such as Aurora A. Upon binding of the PBD to a phosphoprotein, inhibition of the KD is partially relieved and the IDL no longer sequesters the T-loop. Alternatively, upon phosphorylation of the T-loop, the KD changes to a more active conformation that also shifts the PBD into an open conformation better able to bind phosphopeptides. Both T-loop phosphorylation and PBD binding to a phosphopeptide together render the KD fully active.

1.2.2 PLK1 activity and mitotic entry

PLK1 initially becomes activated in G2 phase [93], which is mediated by phosphorylation of T210 by the kinase Aurora A, with the help of its cofactor Bora [100] [113]. Bora binds the PBD and relieves its autoinhibition to allow Aurora A access to the T-loop to phosphorylate T210 [113]. The timing of this during the cell cycle is determined by the phosphorylation of Bora on multiple residues by CDKs, without which Bora cannot promote PLK1 activation [114] [115]. This appears to be controlled not by Cyclin B but by the earlier-accumulating Cyclin A based on evidence that Cyclin A2 relocalisation to the cytoplasm at the S/G2 transition coincides with PLK1 activation, and that CycA2/CDK2 can also phosphorylate Bora *in vitro* [116] [117]. Vigneron *et al* later confirmed, through immunodepletion of different factors in cell-free *Xenopus* extracts, that it is Cyclin A bound to CDK1, not CDK2, which initially phosphorylates Bora to activate PLK1 *in vivo* [118]. Phosphorylation of Bora by CycB/CDK1 has also been observed [114] [115], but this presumably serves to maintain PLK1 activation later on in G2 phase.

PLK1 promotes mitotic entry by contributing to the activation of Cyclin B/CDK1. CDK1 activity is inhibited in early G2 by phosphorylation by WEE1, and this inhibitory phosphorylation is relieved by CDC25 phosphatase activity. Active CDK1 can phosphorylate WEE1 to inhibit it and CDC25 to activate it, resulting in a positive feedback loop that enhances its activation [119]. Similarly, PLK1 phosphorylates both WEE1, to target it for degradation [120], and CDC25, to activate it [121] [122] and induce its localisation to the nucleus [123] [124]. Since PLK1 is itself kept active by CDK1 phosphorylating Bora, this adds another layer to the WEE1/CDC25 positive feedback loop. It was originally thought that PLK1 was not strictly necessary for mitotic entry in unperturbed cells [125] and that inhibiting

PLK1 merely causes a delay in prophase before arresting cells in prometaphase [126]. However, more recent research indicates that whether or not PLK1 activity is required for mitotic entry varies depending on cell type and is even non-genetically heterogeneous in individual cells within the same population [127].

1.2.3 Roles of PLK1 during mitosis

PLK1 localises dynamically at centrosomes from interphase through to prometaphase [128] [129] [130]. Centrosome maturation requires PLK1 activity, without which centrosomes cannot properly nucleate microtubules to form a mitotic spindle [131] [132] [133] [126]. PLK1 is also required for disjunction of the two centrosomes in G2 to allow the mitotic spindle to become bipolar [131] [132] [126] [134]; the *Drosophila* homologue Polo gets its name from the fact that mutants often display a monopolar spindle with chromosomes arranged around it in a circle [131]. Other PLK family members are also involved with centrosomes: PLK4 is required for duplication of centrioles [135], and PLK2 helps initiate centriole duplication upon the G1-S transition by increasing levels of cyclin E [136].

PLK1 also localises at the kinetochores of chromosomes [129] beginning in G2, as it becomes activated [93]. Here, during prometaphase, PLK1's T-loop is kept phosphorylated by Aurora B rather than Aurora A [137], and it is important in helping spindle microtubules form bipolar attachments to kinetochores, thereby allowing proper segregation of chromosomes during metaphase. This is based on evidence that a PLK1 depletion- or inhibition-based prometaphase arrest is alleviated by inactivation of the spindle assembly checkpoint [133] [138] [126]. This is independent of PLK1's role at centrosomes in promoting the formation of proper bipolar

spindles in the first place: cells with mislocalised PLK1, which does not affect centrosome maturation or disjunction, still arrest in metaphase due to impaired chromosome alignment [139]. Additionally, phosphorylation of BUBR1 by PLK1 at kinetochores is required for BUBR1's function in promoting stable kinetochore-microtubule attachments [140].

PLK1 relocalises to the central spindle during anaphase [128]. While degradation of Cyclin B deactivates CDK1 upon anaphase entry, meaning that most of PLK1's usual PBD binding sites are no longer phosphorylated, PLK1 primes its own docking to a central spindle-associated protein PRC1. Prior to anaphase, this association was blocked by a CDK1 phosphorylation that blocked PLK1 binding [105]. Inhibition of PLK1 after the onset of anaphase, to avoid impairing its role in earlier stages of mitosis, shows that PLK1 is required for spindle elongation in anaphase B and for the initiation of cytokinesis. The latter is due to a requirement for PLK1 in localising RhoA, a key mediator for assembly and ingression of the contractile ring, and its activator ECT2, to the central spindle [141] [142] [143] [144]. PLK1 is not required for mitotic exit itself, as these cells did not divide but nonetheless entered G1 as binucleate tetraploids.

1.3 The DNA damage checkpoint - the DNA damage response and cell cycle drivers in opposition

When DNA damage occurs, DNA repair must be allowed time to occur before the cell cycle progresses. As such, cells have evolved pathways to allow the DNA damage response to downregulate cell cycle drivers such as CDKs and halt the cell cycle [145].

1.3.1 Checkpoint kinases CHK1 and CHK2 induce cell cycle arrest

Upon its activation by MRN at sites of damage, ATM phosphorylates the checkpoint kinase CHK2 to activate it [146], and activated CHK2 disperses throughout the nucleus to phosphorylate many different substrates [147]. If resection occurred at the DSB (which is dependent on ATM and CDK activity, as discussed in section 1.1.3), RPA bound to the resected DNA recruits and activates the ATM-related kinase ATR [148], with the help of ATRIP and TOPBP1 [149] [150]. ATR phosphorylates another checkpoint kinase, CHK1 [151], with the help of Claspin [152] [153]. Like CHK2, CHK1 also disperses throughout the nucleus to carry out its functions [154].

The main pathway through which CHK1 and CHK2 halt the cell cycle is through downregulation of CDC25, preventing it from activating CDK1 and thus leading to G2/M arrest [155]. CHK1 and CHK2 can both phosphorylate CDC25C on its S216 residue, causing it to be bound by the 14-3-3 protein, which sequesters it in the cytoplasm away from CDK1 [156] [157] [146]. CHK1 and CHK2 also phosphorylate CDC25A to target it for degradation [158], although a later paper argued that only CHK1 is required for this [159].

Another PLK family member, PLK3, is partially involved in promoting the checkpoint response. PLK3 expression is fairly constant throughout the cell cycle, but its activity rapidly increases upon DNA damage induction in an ATM- and CHK2-dependent manner [160] [161]. PLK3 phosphorylates CHK2 to prime it for activatory phosphorylation by ATM, such that in PLK3-deficient cells, CHK2 is much less active upon DNA damage [162]. This suggests that PLK3 and CHK2 work in a positive feedback loop to maximally activate each other upon damage. Similarly to CHK1 and CHK2,

PLK3 phosphorylates CDC25C on S216 to sequester it with 14-3-3 [163], and CDC25A to target it for degradation [164], thus promoting cell cycle arrest.

1.3.2 PLK1 as a target of the DNA damage checkpoint

PLK1 is another major target of the DNA damage checkpoint. PLK1 activity is lower in damaged cells compared to undamaged cells due to to less phosphorylation of T210 [165] [166] [167]. ATM and ATR are important for this [165] [166], as are CHK1 and CHK2 [167].

On one level, this occurs through preventing the usual increase in activity of PLK1 during G2. Aurora A activity is inhibited upon damage [168]. Bora is also phosphorylated by ATM/ATR and targeted for degradation, although this only happens upon UV- but not IR-induced damage, implying this is for a pathway other than DSB repair [169]. Aurora A inhibition was found to not be the only factor preventing PLK1 activation; work expressing a constitutively-active Aurora A showed that Aurora A recruitment to PLK1 by Bora was also lost upon DSB induction. [170]. Bruinsma *et al* [170] used a FRET sensor for PLK1 activity and saw that activity not only stopped increasing but in fact decreased, albeit at a slower rate that it was originally increasing, suggesting that some already-active PLK1 is dephosphorylated at T210. They ruled out PP1 as the phosphatase that could have been doing this.

Other papers that looked at M-phase DNA damage gave a clearer picture of PLK1 dephosphorylation, since PLK1 is already maximally activated in M phase. PLK1 dephosphorylation was seen upon damage in M phase [165] [171] and is carried out by the PP2A phosphatase [172] in a manner dependent on the unusual combination of ATM and CHK1 [173]. However, it

is strange that these groups were able to induce a DNA damage-dependent arrest and downregulation of PLK1 in mitosis by using the topoisomerase inhibitor adriamycin, because separate work has indicated that inducing DNA damage in mitosis, including with adriamycin, does not cause a mitotic delay [174]. Additionally, as discussed in Section 1.1.2, the general picture of how cells respond to mitotic damage is that they should continue with mitotic exit and repair the damage only in G1 in order to avoid potentially-deleterious consequences of repair during mitosis [31] [30]. Regardless, experiments in Xenopus extracts suggest that PP2A can also dephosphorylate PLK1 upon damage in interphase [175], so it is likely that PP2A could be the phosphatase responsible for the damage-induced decrease in PLK1 activity in G2 seen by Bruinsma *et al* [170].

There is also evidence to suggest that that PLK1 abundance is regulated upon damage: ATR/CHK1 activates APC/C(CDH1), which degrades PLK1 [176]. Meanwhile, p53, a transcription factor and target of ATM, represses PLK1 gene expression [177].

1.3.3 PLK1 in checkpoint recovery

Once damage is repaired and checkpoint signalling has been silenced, cells need to resume the cell cycle. While PLK1 is not always required for mitotic entry in unperturbed cells, it has been shown to be necessary for mitotic entry during checkpoint recovery, along with CDC25B and inactivation of WEE1, both of which are downstream of PLK1 [125]. As in unperturbed cells, this also requires Aurora A-mediated activation of PLK1 [100].

PLK1 activity in turn deactivates checkpoint signalling, both via phosphorylation of Claspin leading to its degradation and thereby preventing

it from aiding ATR-induced activation of CHK1 [178] [179] [180], and via phosphorylation of CHK2 to directly inhibit its activity [181]. This could explain why Lee *et al* [173] found the unusual combination of ATM/CHK1 to be required for PLK1 dephosphorylation in mitosis: when PLK1 activity is high, CHK2 is completely inactive and CHK1 cannot be activated by ATR, so the only way to activate a CHK kinase is for ATM to activate CHK1.

Liang *et al* [182] investigated PLK1 activity during checkpoint recovery in individual cells using a FRET reporter and found that mitotic entry after DNA damage occurs when PLK1 activity rises above a threshold, regardless of varying levels of checkpoint signalling between cells. Contrary to what Bruinsma *et al* [170] observed using the same FRET reporter, Liang *et al* observed that PLK1 activity continues to increase after damage, albeit more slowly than it was increasing prior to damage. The higher the initial PLK1 activity, the less that DNA damage induction was able to slow the rate of increase in PLK1 activity, and the shorter the duration of arrest, since PLK1 activity would reach the required threshold for mitotic entry sooner. Thus, cells with high initial PLK1 activity upon damage induction enter mitosis with some damage still unrepaired, supporting the idea that PLK1 not only promotes recovery after damage has been fixed but also opposes checkpoint signalling while it is still ongoing, such as through the aforementioned downregulation of CHK1 and CHK2 activity.

1.4 Cell cycle drivers promoting DNA repair

At first glance, it seems paradoxical that cell cycle kinases such as CDKs and PLK1 can both oppose the DNA damage checkpoint response and yet also positively regulate DNA repair by promoting HR in G2. Perhaps

because the study of HR regulation and the study of the checkpoint response are different enough that no one research group focuses fully on both, there is relatively little literature that properly acknowledges this conundrum and discusses how this might be resolved. One exception is a review by Wohlbold and Fisher [183], which talks about this question in regards to CDKs.

In the case of CDKs, the solution appears to be one of different proteins playing specific roles. While CDK1 is the kinase that promotes mitosis and is downregulated by the checkpoint, CtIP phosphorylation and therefore initiation of resection is carried out by the S-phase kinase CDK2 [39]. Further evidence suggests other roles for CDK2 in DNA repair. Selective inhibition of an analogue-sensitive CDK2 showed an increase in cell death after DNA damage [184]. CDK2 has also been shown to help initiate DNA damage checkpoint signalling through its phosphorylation of ATRIP [185], and to promote NHEJ through its interaction with Cyclin A1, the expression of which is upregulated upon damage [186]. Wohlbold and Fisher [183] suggest a reason why these two CDKs could have such separate roles upon DNA damage: CDK2 is not as strongly regulated by inhibitory phosphorylation as CDK1 is [187], and would therefore potentially be able to remain active even while the DNA damage checkpoint is inhibiting CDK1 activity through phosphorylation.

Wohlbold and Fisher [183] also discuss how this could work in yeasts, which only have one Cdk. In budding yeast, the DNA damage checkpoint does not inhibit Cdk and instead acts on the PLK1 homologue Cdc5 to arrest cells at prometaphase [188]. As such, the cell cycle kinase involved in promoting resection (Cdk) and the cell cycle kinase inhibited by the checkpoint (Cdc5) are still two separate proteins. In fission yeast, Cdk is inhibited

by the DNA damage checkpoint, but interestingly, unlike in most organisms, there are two different cyclin-activating kinases. One of these is essential for normal cell cycle progression, while the other is dispensable for cell cycle progression but is required for homologous recombination [189]. Thus, again, the DNA damage response appears to be acting differently upon two different cell cycle-related proteins. Meanwhile, in plants, which have yet another different system of CDKs to those of yeast and of animal cells, a specific CDK in *Arabidopsis* that is not normally crucial for mitotic entry was recently found to be upregulated upon damage and to phosphorylate RAD51, without which RAD51 cannot be recruited to sites of damage [190]. While this is still very new research, this mechanism is intriguingly similar to the one in which human PLK1 phosphorylates RAD51 to enable it to be recruited to damage sites via NBS1 [86].

Since PLK1 is only one protein, its own opposing roles upon DNA damage in humans instead appear to be a matter of timeframes. Very few papers draw attention to this, but work on PLK1 downregulation by the DNA damage checkpoint consistently shows that this occurs at around 3-4 hours after damage. On the other hand, RAD51 phosphorylation by PLK1 increases noticeably by around 20 minutes post-damage induction [86]. Separate work found that inhibition of PLK1 shortly before damage induction decreases the amount of RAD51 foci formation [191], supporting the idea that PLK1 activity is important early on to promote DNA repair. This same paper also found that PLK1 phosphorylates BRCA1 upon damage, which occurs no later than 1 hour after damage induction (although unfortunately they did not test any earlier timepoints than this), and that this phosphorylation aids BRCA1 recruitment to damage foci.

Unpublished data generated and shared with us by Dr. Arne Lindqvist

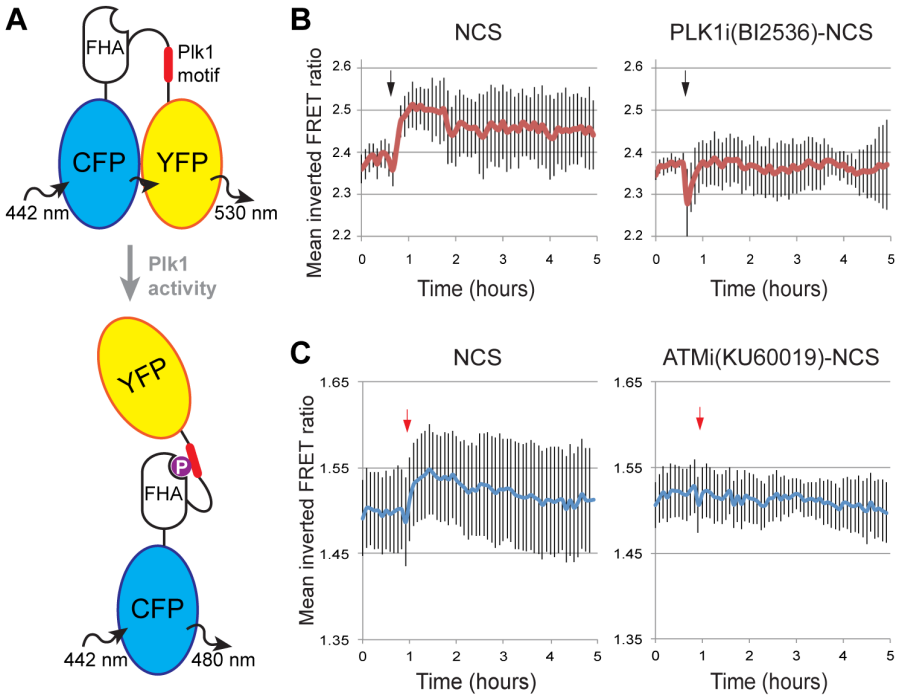


Figure 1.6: **FRET detection of DNA damage-induced PLK1 activation.** All data from this figure was generated and kindly shared with us by Dr. Arne Lindqvist. **A:** Diagram of the the FRET PLK1 activity reporter [100]. The phospho-binding domain FHA binds to the PLK1-phosphorylated substrate, resulting in a conformational change that reduces FRET between the FRET donor (CFP) and the FRET acceptor (YFP). **B:** U2OS cells stably expressing the FRET PLK1 activity reporter and grown asynchronously were followed live at 37℃ in L15 media using a Deltavision spectris imaging system or an Image Xpress imaging system with 20x NA 0.4 or NA 0.75 objectives. The inverted FRET ratio was calculated by, after background subtraction, dividing YFP excitation-YFP emission with CFP excitation-YFP emission, using ImageJ [192]. The graphs depict the mean value from cells that had a low base-line inverted FRET ratio, thus excluding cells with already active PLK1. Arrows indicate the time of DNA damage induction by addition of 10 nM NCS. Error bars = standard deviation. BI-2536 was added where indicated at 100 nM shortly prior to imaging. **C:** FRET graphs as in **B**. KU-60019 was added where indicated at 10 µM shortly prior to imaging.

of the Karolinska Institutet suggests that PLK1 activity as sensed by a FRET reporter increases rapidly at around 15 minutes after DNA damage induction with the DSB-inducing agent NCS in asynchronous cells (Figure 1.6B). Both Bruinsma *et al* [170] and Liang *et al* [182] have used the same FRET reporter to examine PLK1 activity after damage induction in G2-synchronised cells and found contradicting results of PLK1 activity either decreasing [170] or continuing to increase albeit more slowly than before [182]. The discrepancy between these published accounts and the unpublished data could be explained by the fact that Dr. Lindqvist's data was collected from asynchronous cells, and cells with a high base-line of PLK1 activity (and therefore likely in G2) were specifically excluded from the analysis in order to examine the effect of DNA damage on currently-inactive PLK1. It is possible that a rapid increase in PLK1 activity is necessary in cells with initially low PLK1 activity in order to reach a threshold required for the phosphorylation of RAD51, while PLK1 activity in late G2 is already above this threshold and so a further increase upon damage is not needed in these cells (Figure 1.7). This does, however, then raise the question of if this rapid damage-induced increase in PLK1 activity seen by Dr. Lindqvist's data is even occuring in G1 cells, which should not be carrying out RAD51 phosphorylation for HR in the first place.

A potential caveat of Dr. Lindqvist's data is that the rapid increase in FRET signal seen could instead be caused by the increase in PLK3 activity known to occur upon DNA damage [160], since the PLK1 target motif in the FRET sensor may potentially also be a target for PLK3, and BI-2536, the PLK1 inhibitor used as a negative control, can also inhibit PLK3 at only a 10-fold lower selectivity [126]. Even if this is the case, data from Yata *et al* (2012) still supports the idea that PLK1 activity can increase somewhat

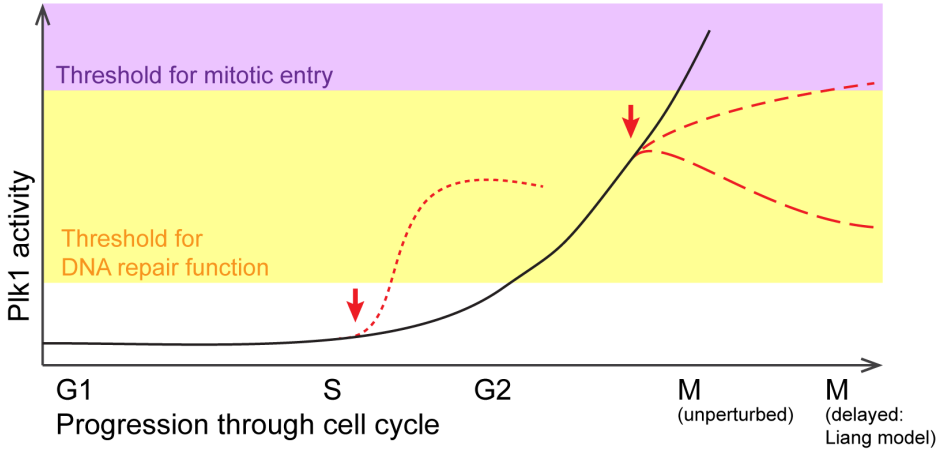


Figure 1.7: **Potential change in PLK1 activity upon DNA damage.** A model showing how PLK1 activity may change upon DNA damage at various points in the cell cycle. The black curve depicts PLK1 activity in unperturbed conditions: it begins to rise in G2 until it reaches the threshold for mitotic entry and triggers mitosis. If DNA damage (denoted by a red arrow) occurs in G2, PLK1 activity is affected in one of two possible ways. Large-dashed red curve: the Bruinsma model, in which PLK1 activity decreases, preventing mitotic entry [170]. Medium-dashed red curve: the Liang model, in which PLK1 activity continues to increase albeit a slower rate, and mitotic entry may still be achieved after a delay if initial PLK1 activity was high enough [182]. In both cases, PLK1 activity remains above the threshold for its functions in DNA repair, such as RAD51 phosphorylation. However, if damage occurs earlier in the cell cycle, when PLK1 activity is still below the threshold for repair function, its activity may need to increase in order to carry out these functions, denoted by the small-dashed red curve. This could be what is being seen in the FRET data from Dr. Lindqvist in asynchronous cells.

upon DNA damage if it is not already high, because while RAD51 phosphorylation is high in G2/M phase in unperturbed cells, there is still an increase in RAD51 phosphorylation detected around 20-40 minutes after damage induction in asynchronous cells [86].

Relatively little work has been done to examine the regulation of PLK1 after DNA damage in an earlier timeframe before PLK1 becomes downregulated by the DNA damage checkpoint. The work carried out here in this

thesis aims to shed more light on this matter by examining PLK1 localisation and interaction partners at these earlier timeframes post-damage. Live-cell microscopy approaches observe PLK1 localising to sites of laser-induced DNA damage as early as 15 minutes post-damage, in a manner dependent on ATM, CDK2 and PLK1's PBD. Meanwhile, proteomics approaches identify novel PLK1 interaction partners involved in the DNA damage response, including DYRK2, a kinase which only begins to associate with PLK1 at around 15-30 minutes post-damage. These results suggest possible answers to the question of how PLK1 is regulated at an earlier timeframe upon DNA damage in order to actively promote DNA repair.

Chapter 2

Materials and Methods

2.1 Cell lines and antibodies

2.1.1 Cell lines

HeLa cells stably expressing EGFP were a kind gift from Chih-Chao Liang of the Cohn lab. HeLa Kyoto cells stably expressing PLK1-LAP on a BAC vector [193] were a kind gift from Anthony Hyman, and a clonal cell line with PLK1-LAP expression levels similar to that of endogenous PLK1 was generated in our lab by Vito Katis. HeLa Kyoto cells with one PLK1 allele fused to YFP using CRISPR/Cas9 gene editing were a kind gift from Iain Cheeseman [194]. HeLa Kyoto WT and HeLa Kyoto NFLAP-BRCA2 cells were a kind gift from Mark Petronczki [195]. HEK293T WT cells were from the American Type Culture Collection.

All other cell lines used were generated in this study. PLK1-YFP m-Cherry BP1 cells, PLK1-LAP mCherry BP1 cells, NFLAP-BRCA2 mCherry BP1 cells and HeLa Kyoto mCherry-BP1 cells were generated by stably transfecting the relevant parental cell lines with pLPC-Puro mCherry BP1-2 plasmid. The HeLa Kyoto mCherry-BP1 cell line was then further stably

transfected with pDEST53 GFP-PLK1, with the PLK1 sequence being either wild-type or containing one of several mutations: K82R, T210D, or H538A/L540M (PBD dead). Several of these cell lines were also further stably transfected with pCEP4 CDT1-BFP, of which only GFP-PLK1 WT mCherry-BP1 CDT1-BFP and NFLAP-BRCA2 mCherry-BP1 CDT1-BFP have data shown in this thesis.

CRISPRi cell lines were generated by first transfecting PLK1-YFP mCherry BP1 cells with both pAAVS1-NDi-CRISPRi (Gen2) plasmid which had been modified to contain a hygromycin resistance gene, along with pSpCas9(BB)-2A-puro (PX459) expressing AAVS1 gRNA, which would theoretically cleave the AAVS1 locus to allow integration of the pAAVS1-NDi-CRISPRi (Gen2) plasmid into that locus. Only the pAAVS1-NDi-CRISPRi (Gen2), which expresses inducible dCas9-KRAB, was selected for using hygromycin. A clonal cell line from this which had been confirmed to express dCas9-KRAB upon doxycycline induction was then further stably transfected with pX330 EGFP-P2A-Blast-ΔCas9 expressing either DYRK2-9 or UBR5-8 sgRNA.

2.1.2 Culture of cell lines

All cells were cultured in DMEM supplemented with with 10% FBS and 1% P/S, plus additional antibiotics depending on the stably expressed constructs they contained: for mCherry-BP1, 0.5 µg/ml puromycin; for PLK1-LAP, GFP-PLK1 (wild-type and all mutants) or NFLAP-BRCA2, 400 µg/ml G418; for CDT1-BFP or dCas9-KRAB, 200 µg/ml hygromycin; for sgRNAs targeting UBR5 or DYRK2, 5 µg/ml blasticidin.

2.1.3 Antibodies

The following commercial primary antibodies were used for Western blotting and IF: ANR28 (A300-974A-T, Bethyl), ATM (sc-23921, Santa Cruz Biotechnology), ATM phospho-S1981 (ab81292, Abcam), Cas9 (7A9, Sigma Aldrich), DYRK2 (MAB5408, Novus Biologicals; ab37912, Abcam; ab116674, Abcam), FLAG (F1804, Sigma Aldrich), GFP (G1544, Sigma Aldrich, for Western blotting; ABX325, Source Bioscience, for IF), H3 phospho-S10 (06-570, EMD Millipore), γH2AX (05-636, EMD Millipore), mCherry (GTX128508, GeneTex), p53 (ab90363, Abcam), p53 phospho-S46 (ab76242, Abcam), PLK1 (P5998, Sigma Aldrich), PLK1 phospho-T210 (558400, BD Pharmingen), PP6C (A300-844A-T, Bethyl), PP6R2 (A-300-969A-T, Bethyl), RFP (AB233, Evrogen), UBR5 (sc-515494, Santa Cruz Biotechnology; except when specifically stated to be A300-573A-T, Bethyl). Monoclonal antibody for Cyclin A was a kind gift from Tim Hunt. RAD51 and RAD51 phospho-S14 antibodies were made by Biogenes as previously described [87] [86].

The following commercial secondary antibodies were used: Goat anti-Rabbit IgG HRP (PO448, Dako) and Goat anti-Mouse IgG HRP (PO447, Dako) for ECL detection with Western blotting; and Goat anti-Rabbit IgG Alexa Fluor 488 (A11070, Invitrogen), Goat anti-Mouse IgG Alexa Fluor 555 (A21425, Invitrogen) and Goat anti-Mouse IgG Alexa Fluor 647 (A21237, Invitrogen) for IF.

2.2 Generation of stable cell lines

2.2.1 Generation of plasmid constructs

pLPC-Puro mCherry-BP1-2 plasmids were originally generated by the de Lange group [196] and obtained from Addgene. pDEST53 plasmid containing GFP-PLK1 WT, K82R and T210D were generated by Keiko Yata. GFP-PLK1 PBD dead pDEST53 was generated in this study using site-directed mutagenesis on pDONR221 PLK1 WT with primers in Table 2.1 and then gateway cloning from this donor plasmid into the GFP-containing pDEST53 vector.

pCEP4 CDT1-BFP plasmids were generated as follows. A codon-optimised fragment of residues 31-120 of human *CDT1* from Integrated DNA Technologies was amplified using PCR primers that added an XhoI restriction site as well as a Met and a Pro codon to the beginning, and a PstI restriction site to the end (Table 2.1). This PCR product was cloned into the multiple cloning site of a pTagBFP-N plasmid (Evrogen). The full *CDT1-BFP* fragment was then cloned into an empty pCEP4 plasmid (Thermo Fisher Scientific) using NheI and NotI.

pDONR223 DYRK2 plasmid from Addgene (generated by the Hahn group [197]) was gateway cloned into pDEST53 to generate GFP-DYRK2 plasmids, and also gateway cloned from pDEST53 back into pDONR221. pDONR221 DYRK2 was then mutagenised into K251R, F301A or F301G using site-directed mutagenesis with primers in Table 2.1. These mutant *DYRK2* sequences were gateway cloned back into pDEST53 to create mutant GFP-DYRK2.

UBR5 fragments were amplified from pcDNA 6.2 N-EmGFP-DEST-V5 with a *UBR5* insert (generated by the Saunders group [198] and obtained

from Addgene) as shown in Figure 5.3B. Primers listed in Table 2.1 were used to add flanking attB gateway cloning sites to the fragments, and optionally also an NLS to the C-terminal end of fragments 3, 4 and 5. These fragments were then gateway cloned into either pDEST53 or pcDNA5/FRT-GWa/N3xFLAG.

pcDNA5/FRT-GWa/N3xFLAG plasmids were generated by Jean-Yves Bleuyard. A HindIII-N3xFLAG-EcoRV-XhoI cassette was first cloned into the HindIII/XhoI sites of pcDNA5/FRT (Thermo Fisher Scientific). The Gateway reading frame A cassette (Thermo Fisher Scientific) was then cloned into the EcoRV site. This plasmid with a *PP6C* insert was also generated previously by Jean-Yves Bleuyard.

pAAVS1-NDi-CRISPRi (Gen2) plasmids were generated by the Conklin lab [199] and obtained from Addgene. The selection marker was changed from NeoR to hygromycin by PCR amplifying the hygromycin resistance gene from pCEP4 using primers that added KpnI and PmeI restriction sites (Table 2.1), then cloning into those sites of the pAAVS1-NDi-CRISPRi plasmid in place of NeoR.

pSpCas9(BB)-2A-puro (PX459) plasmids were generated by the Zhang lab [200] and obtained from Addgene. *AAVS1* guide RNA sequence (Table 2.3) was cloned in by Joey Riepsaame using the method described in Ran *et al* [200].

pX330 EGFP-P2A-Blast-ΔCas9 plasmids were generated as follows by Joey Riepsaame and Christine Ralf. The PGK promoter and an EGFP-T2A-Neo cassette were cloned into the PsiI site of pX330-U6-Chimeric BB-CBh-hSpCas9 (generated by the Zhang lab [201] and obtained from Addgene) using Gibson assembly for 1 hour at 50℃. T2A was then converted into P2A by annealing and Klenow filling oligos listed in Table 2.2 and cloning

the resulting dsDNA fragment into the HindIII/NheI sites of pX330 EGFP-T2A-Neo to generate pX330 EGFP-P2A-Neo. Next, the Cas9 sequence was removed by cutting with KpnI and SbfI and replaced with a short linker sequence to generate pX330 EGFP-P2A-Neo-ΔCas9. The blasticidin resistance gene was PCR amplified from pcDNA 6/TR with primers that added NheI and XhoI sites, then cloned into those sites in place of NeoR to generate pX330 EGFP-P2A-Blast ΔCas9. Finally, a gBlock containing the modified sgRNA scaffold "Qi" with an extended stem-loop 1 and T-A flip [202] (Table 2.2) was subcloned into the AflIII and KpnI sites of pX330 EGFP-P2A-Blast ΔCas9. From this, specific sequences targeting *UBR5* or *DYRK2* (listed in Table 2.3 and designed by Joey Riepsaame) were cloned into the sgRNA scaffold using the method described in Ran *et al* [200].

2.2.2 Transfection of plasmid constructs

Cells growing at 50% confluency in all 6 wells of a 6-well plate were transfected with the relevant plasmid using JetPRIME transfection kit according to the kit's instructions. 2 µg of plasmid DNA, 4 µl of JetPRIME reagent and 200 µl of JetPRIME buffer was added to 2 ml of antibiotic-free medium (DMEM with 10% FBS) in each well. For transfection of the epichromosomal plasmid pCEP4 CDT1-BFP, only 2 wells of a 6-well plate were transfected in the same way.

2.2.3 Antibiotic selection

One day after transfection, the transfected cells from all 6 wells, now at approximately 100% confluency, were trypsinised and transferred onto multiple 15 cm plates with the same media normally used for the parental cell line. After another day, this media was then changed to the same media

plus either 1 µg/ml puromycin for the pLPC-Puro plasmid, 400 µg/ml G418 for the pDEST53 plasmid, 200 µg/ml hygromycin for the pCEP4 or pAAVS1-NDi-CRISPRi plasmids, or 5 µg/ml blasticidin for the pX330 plasmid. These were then left to grow, with regular media replacement, for approximately one week if puromycin or two weeks if G418, hygromycin or blasticidin, until antibiotic-resistant colonies had formed, of which several were picked to grow up as separate clonal cell lines. If the transfected plasmids contained fluorescent constructs, plates containing colonies were first viewed with a Zeiss Axiovert 25 inverted fluorescence microscope to identify colonies displaying the appropriate colour fluorescence, and colonies were picked from among these.

2.2.4 Confirmation of stable clones

Approximately one-third of clonal cell line cells trypsinised from a 100% confluent 75 cm^2 flask were washed twice with PBS and then lysed as in Section 2.6.1. For cells potentially expressing dCas9-KRAB under an inducible promoter, cells were first induced with 2 µM doxycycline for 24 hours prior to lysis. 20 µg of total protein from these lysates was run on an agarose gel, transferred to a membrane and then probed with mCherry antibody, GFP antibody, RFP antibody (for CDT1-BFP), or Cas9 antibody as appropriate. Attempts to confirm stable clones expressing sgRNAs for *UBR5* or *DYRK2* are described in Section 5.2.7 but were not completed.

2.3 Cell synchronisation

2.3.1 Double thymidine block

Approximately 2.5×10^6 cells were seeded onto a 15 cm diameter plate (roughly one-eighth initial confluency). After growth in normal medium for approximately 24 hours, cells were subjected to a thymidine block by changing to medium containing 2 mM thymidine for 18 hours. Cells were then released into normal medium for 9 hours before being blocked with thymidine again for 17 hours. The release after this second thymidine block lasted as long as specified for each experiment. Each time cells were released, removal of thymidine was ensured by washing three times with PBS before adding more media.

2.3.2 Mitotic arrest

Cell cultures at close to maximum confluency were switched to media containing 200 nM nocodazole and left overnight for approximately 17 hours. Only the unattached mitotic cells were harvested by shake-off, while any attached and therefore non-mitotic cells were left behind. For release from nocodazole block, cells were washed twice with PBS before being released in normal medium, taking care to retain any unattached cells during each wash by centrifugation.

2.3.3 FACS analysis of cell cycle profile

Cells were harvested by trypsinisation, centrifuged for at 500 g for 5 minutes at 4℃, washed in PBS, centrifuged again the same way and then resuspended in 70% ethanol for fixation and stored at -20℃ for at least 16 hours. To stain DNA, cells in ethanol were centrifuged at 500 g for 10

minutes at room temperature, the ethanol removed and the cells resuspended in staining solution made up of PBS with 0.1% BSA, 0.1 mg/ml RNase A and 2 µg/ml propidium iodide, then incubated for 30 minutes at room temperature in the dark. Then, after centrifuging the same way and removing the supernatant, cells were resuspended in PBS with 0.1% BSA, transferred to 5ml test tubes and analysed on a Cytek DxP8 flow cytometer.

2.4 Ionising radiation treatment

When indicated, cells were irradiated at the stated dose by a GRAVITRON RX 30/55 (Gravatom).

2.5 Transfection of siRNAs

Cells growing at approximately 25% confluency in 10 cm plates were transfected as follows per plate. 25 µl of DharmaFECT Reagent (Dharmacon) was added to 1225 µl of serum-free DMEM and incubated at room temperature for 5 minutes. Meanwhile, from a 20 µM stock solution of siRNA, either 10 µl for a 20 nM final concentration or 50 µl for a 100 nM final concentration was added to RNAse-free water in a separate tube to a total volume of 625 µl (or simply 625 µl of RNase-free water was used for mock transfection). Another 625 µl of serum-free DMEM was added to this, and then the contents of the two tubes were mixed and incubated at room temperature for 20 minutes. Finally, 7.5 ml of DMEM with 10% FBS was added to the transfection mixture (totaling 10 ml of transfection medium), and the medium on the plates was replaced with this transfection medium. If cells were instead being grown in a well of a 6-well plate, or on a 35 mm dish for live cell microscopy, all volumes listed above were divided by 5.

2.6 Cell lysis and immunoprecipitation

2.6.1 Cell lysis

Cultured cells were first washed with PBS, then harvested with a cell scraper (or simply by pipetting for HEK293T cells, which were more loosely attached) while in PBS + 1x Protease Inhibitor Cocktail + 50 mM NaF and pelleted at 500 g for 5 minutes at 4℃. An exception to this is if the cells had already been removed from the plate without scraping while in their growth medium, such as for the mitotic shake-off described in Section 2.3.2, in which case the cells were pelleted at 500 g for 5 minutes at 4℃, their media removed, and then washed twice with PBS + 1x Protease Inhibitor Cocktail + 50 mM NaF, pelleting between each wash to allow removal of the PBS.

Harvested cell pellets were resuspended in lysis buffer at a ratio of 100µl buffer per 10mg of cells. Lysis buffer was made up of 50 mM Tris-HCl pH 8.0, 150 mM NaCl, 2 mM EDTA, 5 mM $MgCl_2$, 1 mM DTT, 1x Protease Inhibitor Cocktail, 125 U/ml Benzonase and 0.5% NP-40. Additionally, if protein phosphorylation was relevant to the experiment, lysis buffer also contained 50 mM NaF, 1 mM $NaVO_4$ and 20 mM Na-β-glycerophosphate to inhibit phosphatases. Cells in lysis buffer were vortexed briefly and incubated on ice for 1 hour, then the cell debris pelleted at 16,100 g for 30 minutes at 4℃ and the supernatant kept.

For mass spectrometry samples, however, cell lysis protocol was altered due to the fact that the usual detergent, NP-40, would contaminate the mass spectrometer readout. The lysis buffer used for this purpose was the same as described above except that it contained *n*-dodecyl-β-D-maltoside instead of NP-40. For preliminary mass spectrometry preparation attempts,

detergent concentration was still 0.5% and the lysis protocol was otherwise the same. For the final, successful protocol, lysis buffer instead contained only 0.05% *n*-dodecyl-β-D-maltoside, cell pellets were always lysed in exactly 1 ml of this buffer regardless of the mass of the pellet, which for these experiments averaged approximately 250 mg, and the lysis incubation at 4℃ lasted only 30 minutes, with vortexing for 5 seconds every 10 minutes.

2.6.2 Cell fractionation

For cell fractionation, harvested cell pellets were instead resuspended in 100 µl of sucrose buffer per 10 mg of cells. Sucrose buffer was freshly made out of 250 mM sucrose, 10 mM Tris-HCl pH 7.5, 20 mM KCl, 2.5 mM $MgCl_2$, 1x Protease Inhibitor Cocktail (Sigma Aldrich), 1 mM DTT, 0.3% Triton X-100, and if applicable the appropriate phosphatase inhibitors as described in Section 2.6.1. Cells were vortexed three times for 10 seconds, then the nuclei pelleted at 500 g for 5 minutes at 4℃ and the supernatant kept as the cytoplasmic fraction. Nuclei pellets were then washed twice in Triton-free sucrose buffer, then resuspended in the previously-described lysis buffer at 0.4x the volume of sucrose buffer used originally. From here on, extraction proceeded the same way as normal cell lysis to extract the nuclear fraction of protein.

2.6.3 Crosslinking of beads to antibodies

Certain experiments in this work directly immunoprecipitated endogenous untagged PLK1 and therefore used beads crosslinked to PLK1 antibody. AffiPrep Protein A beads were first washed twice in PBS, then incubated with 2.5 µg antibody per 10 µl of beads (diluted in a 10x volume of PBS) and rotated for 3 hours at room temperature. For this and every other method

requiring the separation of beads from their solution between washes or incubations, beads were spun down at 500 g for 5 minutes at 4℃. Beads were then washed three more times in PBS, then twice in coupling buffer consisting of 22 mM boric acid and 22 mM sodium tetraborate. Next, beads were washed once in 10 mg/ml DIM-PIM in 0.1 M boric acid, then resuspended in 1 ml of the same DIM-PIM/boric acid buffer and rotated overnight at 4℃. The next day, beads were washed once in 1 M Tris pH 9.0, resuspended in the same Tris buffer and rotated for 10 minutes at room temperature, then washed three times in storage buffer consisting of 55 mM boric acid and 6 mM sodium tetraborate and stored in said buffer at 4℃ until use.

2.6.4 Pre-washing of beads

All beads used were first pre-washed, including the antibody-conjugated beads prepared beforehand, three times in 1 ml buffer base consisting of 50 mM Tris-HCl pH 8.0, 150 mM NaCl, 2 mM EDTA and 5 mM $MgCl_2$.

2.6.5 Pre-clearing

For mass spectrometry applications, lysates were first pre-cleared to reduce the background of sticky proteins. Lysates were incubated with mouse IgG agarose beads of a volume indicated in Table 4.1 and rotated for 1 hour at 4℃. Afterwards, the beads were discarded and the cleared lysate was kept.

2.6.6 Immunoprecipitation

Prior to immunoprecipitation, a small aliquot of approximately 50 µl of lysate was taken aside for agarose gel analysis as an “input” sample. The remain-

der was incubated with either the volume specified in Table 4.1, or otherwise 15 µl per 1 ml of lysate, of GFP-Trap A beads and rotated for 1 hour at 4℃. For direct PLK1 immunoprecipitation, lysates were incubated with 10 µl antibody-conjugated beads per 1 ml of lysate and rotated for 2 hours at room temperature. Afterwards, the beads were separated from the lysate, the supernatant put aside for agarose gel analysis as a "flow-through" sample, and the beads kept for further washing and elution steps.

2.6.7 Washing beads

Beads bound to proteins were washed to reduce nonspecific binding by incubating with 1 ml wash buffer and rotating for 5 minutes at 4℃. Wash buffer makeup for non mass-spectrometry applications was the same as the lysis buffer described in Section 2.6.1, except without benzonase and with 0.2% NP-40 instead of 0.5%. This wash was repeated two more times with fresh buffer each time.

For mass spectrometry preparation attempts prior to the final, successful one, the wash buffer contained 0.2% *n*-dodecyl-β-D-maltoside and the wash was carried out five times. For the final mass spectrometry sample preparation protocol, the wash buffer contained 0.05% *n*-dodecyl-β-D-maltoside instead of NP-40, and the wash was carried out three times. Everything else in the washing step was identical.

2.6.8 Glycine elution

After discarding the buffer from the final wash, beads were centrifuged again in order to facilitate removing the last remnants of the buffer. Beads were then resuspended in a volume of glycine buffer indicated in Table 4.1, or otherwise equal to twice the volume of beads. Glycine buffer contained

0.2 M glycine pH 2.2, 1x Protease Inhibitor Cocktail (Sigma Aldrich), 1 mM DTT, and, if applicable, the phosphatase inhibitors described in Section 2.6.1. Beads in glycine buffer were incubated at 4℃ with 650 rpm shaking for 7 minutes, then centrifuged and the supernatant transferred to a new tube. Beads were then resuspended again in the same volume of glycine buffer and incubated in the same way, centrifuged again and the supernatant also transferred to the same tube. If indicated in Table 4.1, elution was performed a third time. The pooled elutions were neutralised by adding one-tenth the elution volume of 1 M Tris-HCl pH 8.8.

2.6.9 Boiling beads

If immunoprecipitated proteins only needed to be analysed on an agarose gel and not kept intact for further applications, a quicker, “dirty” method of removing them from the beads was used instead of glycine elution. Beads were resuspended in 20 µl of 1x NuPAGE LDS Sample Buffer + 12.5 mM DTT and boiled for 10 minutes at 85℃. After separating it from the beads by quick centrifugation, the supernatant was then loaded directly onto an agarose gel.

2.7 Mass spectrometry and proteomics

2.7.1 TCA precipitation method of protein digestion

This method was only used for the very first mass spectrometry sample preparation attempt (Table 4.1). Neutralised glycine elutions were diluted 1 in 10 with 0.1 M TEAB, then TCA was added to 20% and samples incubated at 4℃ overnight. Precipitated proteins were pelleted by centrifugation at 16,100 g for 30 minutes at 4℃, then washed twice with 500 µl acetone, air

dried, and resuspended in 20 µl of 8 M urea in 0.1 mM TEAB. From this point on, the digest proceeded in the same manner as described for the in-solution method, albeit in a lower volume of solution.

2.7.2 In-solution method of protein digestion

One-eleventh of the neutralised glycine elution was taken aside for agarose gel analysis before treating the remainder as follows. To denature proteins, urea was added to a final concentration of either 1 M for the "low salt" method or 4 M for the "high salt" method (see Table 4.1), by adding the appropriate volume of of 8 M urea dissolved in 50 mM TEAB, and samples were incubated for 10 minutes at 30℃ shaking at 650 rpm. Next, a final concentration of 10 mM TCEP was added to reduce the proteins for an incubation for 30 minutes at room temperature, then a final concentration of 50 mM chloroacetamide was added to alkylate proteins for an incubation of 30 minutes at room temperature in the dark. 0.1 µg of LysC was then added to pre-digest the proteins for 2 hours at 37℃ with 650 rpm shaking. Then, for the high salt method, the urea concentration diluted to 2 M by adding an equal volume of 50 mM TEAB, or the sample kept as-is for the low salt method, and either 0.1 µg of trypsin, or 0.4 µg for the final version of the protocol, was added along with 1 mM $CaCl_2$ to digest further for 16 hours at 37℃ shaking at 650 rpm. Finally, the digest was stopped by adding TFA to a final ratio of 1%, then the sample was centrifuged at 16,100 g for 30 minutes at 4℃ and the supernatant transferred to Eppendorf LoBind tubes (Sigma Aldrich) and stored at -20℃ until samples were ready to run on the mass spectrometer.

2.7.3 FASP method of protein digestion

"Input" samples for mass spectrometry were taken directly from detergent-containing cell lysates and thus had to be digested using Filter-Assisted Sample Preparation (FASP) to remove the detergent. From lysate aliquots put aside after pre-clearing but before GFP immunoprecipitation, a volume equal to 50 µg of total protein was used. This FASP method, with slight alterations, was also used in certain preliminary attempts at mass spectrometry sample preparation, using the eluates from GFP IPs (see Table 4.1).

Vivacon 500 VN01H02 10 kDa filters (Sartorius) were first pre-washed with 200 µl of 50% ACN + 0.1% TFA, and centrifuged at 16,100 g for 15 minutes at room temperature. All further centrifugation steps for FASP were carried out at 16,100 g for 30 minutes at room temperature. Samples were diluted into to 200 µl of 8 M urea in 100 mM TEAB, then transferred to a pre-washed FASP filter and centrifuged to bind the proteins to the filter. Filters were then washed twice with 200 µl of 8 M urea in 100 mM TEAB, although these wash steps were omitted for IP samples due to the lower amount of detergent. Next, for protein reduction, 200 µl of 20 mM TCEP in 8 M urea + 100 mM TEAB was added to the filters, incubated for 30 minutes at room temperature, then removed by centrifugation. Then, for protein alkylation, 200 µl of 50 mM chloroacetamide in 8 M urea + 100 mM TEAB was added, incubated for 30 minutes at room temperature in the dark then removed by centrifugation. The filters were washed again twice with 200 µl of 1 M urea in 50 mM TEAB. During the washes, before centrifugation, the tubes with the filters were shaken by hand to check if all detergent has been removed. If bubbles formed in the liquid, detergent still remained and the filters would need to be washed further; however, in the case of this experiment, two

washes was enough to remove all detergent. For IP samples, these wash steps were again omitted.

At this point, filters were transferred to new tubes and from here on all flow-throughs were kept. Proteins on the filter were digested by adding 0.05 µg LysC in 200 µl 1 M urea + 50 mM TEAB and incubating at 37℃ with 650 rpm shaking, for 16 hours for input samples, or for 4 hours for IP samples. Then 1 µg trypsin for input samples or 0.1 µg trypsin for IP samples in 100 µl 1 M urea + 50 mM TEAB + 1 mM $CaCl_2$ was added to the 200 µl already in the filter and incubated for a further 16 hours at 37℃ with 650 rpm shaking to continue the digest. Digested peptides were removed from the filter by centrifugation, then washed through further by addition of first 200 µl of 0.1% TFA, then 200 µl 50% ACN + 0.1% TFA, centrifuging each wash. The combined flow-throughs were stored at -20℃ until all samples were ready to run on the mass spectrometer.

2.7.4 C18 sample preparation

C18 tips were made by inserting a 1 mm diameter circle of ENVI-18 DSK SPE Disk membrane into a 100 µl pipette tip. These were pre-washed with 100% ACN, then the sample applied to the membrane and centrifuged to bind the peptides to the resin. Membranes were washed twice with 0.1% TFA, then eluted with 20 µl 50% ACN + 0.1% TFA. This method was only used when indicated in Table 4.1.

2.7.5 Mass spectrometry

Peptides were concentrated on a SpeedVac, resuspended in 5% formic acid and 5% DMSO and then trapped on a C18 PepMap100 pre-column (300µm i.d. x 5mm, 100 Å, Thermo Fisher Scientific) using solvent A (0.1%

Formic Acid in water) at a pressure of 50 bar and analysed on an Ultimate 3000 UHPLC system (Thermo Fisher Scientific) coupled to a QExactive mass spectrometer (Thermo Fisher Scientific). The peptides were separated on an in-house packed analytical column (360µm x 75µm i.d. packed with ReproSil-Pur 120 C18-AQ, 1.9µm,120 Å, Dr. Maisch GmbH) and then electrosprayed directly into an QExactive mass spectrometer (Thermo Fisher) through an EASY-Spray nano-electrospray ion source (Thermo Fisher Scientific) using a linear gradient (length: 60 minutes, 15% to 35% solvent B (0.1% formic acid in acetonitrile), flow rate: 200 nL/min). The raw data was acquired on the mass spectrometer in a data-dependent mode (DDA). Full scan MS spectra were acquired in the Orbitrap (scan range 350-2000 m/z, resolution 70000, AGC target 3e6, maximum injection time 50 ms). After the MS scans, the 10 most intense peaks were selected for HCD fragmentation at 30% of normalised collision energy. HCD spectra were also acquired in the Orbitrap (resolution 17500, AGC target 5e4, maximum injection time 120 ms) with first fixed mass set at 180 m/z.

2.7.6 Database searching and filtering

The mass spectrometry data was searched using the SEQUEST algorithm within Proteome Discoverer (Thermo Fisher Scientific, version 1.4.0.288) against the UniProt 2015-09-25 *Homo sapiens* database containing 20,160 nonredundant protein sequence entries. Contaminants LysC (UniProt accession no. Q7M135, lysyl endopeptidase, *Lysobacter enzymogenes*) and trypsin (UniProt accession no. P00761, trypsin, *Sus scrofa*) were added to this database, and the native PLK1 sequence (UniProt accession no. P53350) was replaced with the PLK1 sequence fused to YFP (designated P00000). The mass tolerance was set to 50 ppm for precursor ions and

0.02 Da for fragment ions, with a maximum of 2 missed cleavages permitted. The search assumed static carbamidomethylation on cysteines (+57 Da) and the possibility of dynamic oxidation of methionines (+16 Da) and phosphorylation of serines, threonines and tyrosines (+80 Da). The list of identified proteins was filtered with a false discovery rate of less than or equal to 5%.

2.7.7 Statistical analysis

In order to quantify relative abundance of a single protein within an entire sample, PSMs were converted into NSAF [203]. SAF was calculated by dividing PSM by the length of the protein, then SAF was converted into NSAF by dividing by the summed SAFs of all proteins in the sample after removing contaminants such as keratins, immunoglobulins, LysC and trypsin. NSAF values were then multiplied by 100 to enable better visualisation of the data. These NSAF datasets were fitted to a power law global error model (PLGEM) [204]. Zero values were replaced by a minimum value from the dataset before log transformation of the data. The signal-to-noise ratio (STN) calculated from the modelled error was used as a measure of protein enrichment in PLK1-LAP versus GFP pulldown, and the p-values for each STN value were calculated using a random resampling procedure as described in Pavelka *et al* 2004 [205]. PLGEM fitting and STN and p-value calculation was carried out by Marjorie Fournier, using code written by Norman Pavelka.

2.8 Live-cell microscopy and laser microirradiation

2.8.1 Preparation of cells for live cell microscopy

Approximately 48 hours prior to microirradiation, cells were seeded in a 35 mm glass-bottomed dish (Grener Bio-One) in DMEM supplemented with 10% FBS, 1% P/S, and 10 µM BrdU to sensitise cells to DNA damage. The number of cells seeded was such that they would be at approximately 80% confluency at the time of microirradiation. 1-2 hours prior to microirradiation, media was changed to Leibovitz's L-15 medium with 10% FBS and 1% P/S. If applicable, DMSO or an inhibitor was added along with this medium, at the following concentrations: 1:1000 DMSO, 9 µM RO-3306, 10 µM NU-6102, 100 nM BI-2536, 10 µM KU-55933, 3 µM KU-60019, 10 µM harmine.

2.8.2 Microscope setup and image capture

Imaging was carried out on an Olympus FV1200 laser scanning confocal microscope fitted with a simultaneous (SIM) scanner and driven by AF 2.0 software. The lens used was an Olympus 60x oil immersion PlanApo N lens with NA of 1.40. Cells were kept at 37℃ throughout imaging.

For fluorophore excitation, a multiline argon laser (488 nm) was used for GFP or YFP and a 559 nm solid-state laser was used for mCherry. Emitted light was passed through a FV12-MHBY emission filter which consisted of a 560 nm dichroic mirror, a 505-540 nm band pass filter for GFP/YFP and a 575-675 nm band pass filter for mCherry, into GaAsP PMT high-sensitivity detectors. The software was set to image GFP/YFP and mCherry channels sequentially per line with a pixel size of 0.159 µm by 0.159 µm and a pixel dwell time of 2.0 µs. Images were saved as 12-bit data.

For bleaching, a 405 nm solid state laser was used, with excitation at 100% laser power for 3 seconds with a pixel dwell time of 0.7 ms per pixel of the laser line.

2.8.3 Quantification of signal in images

PLK1-YFP stripe intensity was quantified using ImageJ. Due to the position of the cells and therefore the irradiated stripes shifting over the time course of the experiment and the fact that the PLK1-YFP stripes were punctate and difficult to see by eye, quantification from the PLK1-YFP images alone was not viable. Instead, the mCherry-BP1 images were used to define the damage stripe and undamaged background regions for each cell at each timepoint by converting the images into binary masks. For stripes, ImageJ's Make Binary command was used with the method "Default", followed by light manual editing to remove unwanted non-stripe foci and use of the Close command to make the shape of the stripe more continuous. For the nuclear background, nuclear masks were first generated using the Make Binary command with the method "MinError", followed by manual editing to fill in gaps and delineate any touching nuclei, then using the Erode command set to erode 6 pixels. The stripe masks were then subtracted from the nuclear masks, and the result eroded by one more pixel. These binary masks were then made into selections for the stripe region and nuclear background region of each cell for each timepoint. Since the pre-bleach images did not have a stripe of mCherry-BP1, the selections generated from the 15 minute images were used to define the stripe and background regions for the pre-bleach timepoint as well, with minor adjustment of their positioning.

The selections created from the mCherry-BP1 images were then opened

over the corresponding PLK1-YFP images, and Mean Gray Value (equivalent to mean pixel intensity) was measured for each. “Absolute PLK1-YFP stripe intensity” was calculated by subtracting the nuclear background values from the stripe values for each cell and timepoint, and then normalised such that the absolute stripe intensity at pre-bleach, as averaged between all cells, was 0. “Relative PLK1-YFP stripe intensity” was calculated by dividing the stripe values by the nuclear background values for each cell and timepoint, and then normalised such that the relative stripe intensity at pre-bleach, as averaged between all cells, was 1.

Statistical analysis was carried out in Prism software (GraphPad). One-phase association curves were fitted to the datasets using the least squares fitting method and constraining Y0 to 1, and an extra sum-of-squares F test was used to determine the probability that one curve adequately fitted both datasets in question.

2.9 Fixed-cell microscopy

2.9.1 Cell fixation and immunostaining

Cells were grown on glass coverslips in 12-well plates. For fixation, coverslips were washed three times in PBS beforehand, fixed by a 10 minute incubation with 4% paraformaldehyde in PBS, then washed again three times in PBS. Cells were then permeabilised by 5 minute incubation with 0.5% Triton X-100 in PBS, then washed again three times in PBS.

Before immunostaining, coverslips were first blocked by incubation for 30 minutes in antibody dilution buffer which consisted of 0.5% BSA, 0.2% Cold Fish Skin Gelatin and 0.05% Triton X-100 in PBS. Coverslips were then incubated with primary antibodies diluted 1:500 in antibody dilution

buffer for 1 hour, then washed three times for five minutes each wash with PBS + 0.05% Triton X-100. Next, secondary antibodies conjugated to fluorophores were also diluted 1:500 in antibody dilution buffer when incubated with coverslips for 30 minutes in the dark. Coverslips were washed three more times for five minutes each with PBS + 0.05% Triton X-100 then mounted on slides in ProLong Gold Antifade Mountant with DAPI, incubated in the dark for 24 hours and sealed with nail varnish.

2.9.2 Microscope setup and image capture

Imaging was carried out on an Olympus FV1000 laser scanning confocal microscope fitted with a simultaneous (SIM) scanner and driven by AF 2.0 software. The lens used was an Olympus 60x oil immersion UPLS APO lens with NA of 1.35. For fluorophore excitation, a 405 nm solid-state laser was used for DAPI, a multiline argon laser (488 nm) for YFP/Alexa Fluor 488, a 559 nm solid-state laser for Alexa Fluor 555, and a 633 nm solid-state laser for Alexa Fluor 647. Emitted light was passed through an emission filter which consisted of a 490 nm dichroic mirror for DAPI, a 640 nm dichroic mirror for YFP/Alexa Fluor 488 in Figure 3.1 or a 560 nm dichroic mirror for YFP in Figure 5.3C, and a mirror for Alexa Fluor 555 or 647, into standard PMT detectors. The software was set to image all relevant channels sequentially per line with a pixel size of 0.207 µm by 0.207 µm and a pixel dwell time of 4.0 µs. Images were saved as 12-bit data.

2.10 *In vitro* kinase assay

A 10 µl volume of glutathione-sepharose beads bound to either GST-PLK1 WT or GST-PLK1 K82R (purified by Keiko Yata) was first equilibriated twice in kinase buffer consisting of 25 mM MOPS pH 7.2, 25 mM Na-β-glycerophosphate, 15 mM $MgCl_2$ and 1% DMSO. Then to the 10 µl of beads was added 10 µl kinase buffer supplemented with 500 µM ATP, 2 mM DTT and 1 µl of commercial active DYRK2 or 1 µl water for negative control. The reaction was incubated with 600 rpm shaking for 30 minutes at 30℃. 6.66 µl of 1x NuPAGE LDS Sample Buffer + 12.5 mM DTT was then added, the beads boiled at 85℃ for 10 minutes and the supernatant loaded onto an agarose gel for electrophoresis. The resulting membrane was probed with a pIMAGO HRP Detection kit according to manufacturer protocols to detect phosphoprotein. The membrane was then treated with Re-Blot Plus Mild Solution before being re-probed with DYRK2 and PLK1 pT210 antibodies.

2.11 Bacterial protein purification

Arctic Express RIL Competent *E. coli* cells expressing GST-PLK1 K82R in pDEST15 were generated by Keiko Yata. An overnight pre-culture grown in 10 ml LB medium containing ampicillin and gentamycin at 37℃ was used to inoculate 400 ml fresh antibiotic-free medium. When cell density had reached OD_{595} = 0.56, 0.1 µM IPTG was added and the culture was incubated at 18℃ for 16 hours. All subsequent steps were carried out at 4℃. The culture was spun down with a JLA 10.500 rotor at 6000 rpm for 20 minutes and the pellet frozen at -20℃ until extraction.

The pellet was resuspended in 20 ml extraction buffer consisting of 40 mM MOPS pH 7.4, 150 mM KCl, 10% glycerol, 1 mM EDTA, 2 mM DTT

and 1x Protease Inhibitor Cocktail, supplemented with 2 mg/ml lysozyme and 0.2% Triton X-100. The cell suspension was lysed by sonication with four 20 second pulses separated by 20 second intervals, incubated on ice for 30 minutes, then spun down with a Ti70 rotor in an ultracentrifuge at 19,000 rpm for 20 minutes and the supernatant kept. 100 µl of glutathione-sepharose beads pre-washed three times in extraction buffer were incubated with the lysate for 2 hours with rotation, then beads were washed three times with 300 µl extraction buffer, three times with 300 µl ATP-Mg buffer consisting of 40 mM MOPS pH 7.4, 0.5 M KCl, 20 mM $MgCl_2$, 10% glycerol, 5 mM ATP and 2 mM DTT, then three times with equilibriation buffer consisting of 40 mM MOPS pH 7.4, 150 mM KCl, 10% glycerol and 2 mM DTT. After the last wash, beads were split into 10 µl aliquots, flash-frozen in liquid nitrogen and stored at -80℃.

2.12 Quantitative real-time PCR

2.12.1 RNA extraction and reverse transcription

Cells were homogenised on the culture dish or flask by removing medium, pipetting 200 µl of TRI Reagent per 10 cm^2 culture area and incubating for 5 minutes at room temperature. Cell debris were pelleted at 12,000 g for 10 minutes at 4℃ and the supernatant kept. One-tenth the TRI reagent's volume of 1-bromo-3-chloropropane was added to the supernatant and incubated for 10 minutes at room temperature, then centrifuged again the same way as before to extract the RNA in the aqueous phase, which was transferred to a fresh tube. Half the TRI Reagent's volume of isopropanol was added, vortexed for 10 seconds and incubated at room temperature for 5 minutes to precipitate the RNA. This was pelleted at 12,000 g for 8

minutes at 4℃, then the pellet was washed with 75% ethanol and air-dried.

RNA pellets were resuspended in RNase-free water and diluted to an RNA concentration of 1 µg/µl. 1 µl of this RNA solution was used in a reverse transcription reaction containing 1x RT Buffer, 1x dNTP Mix, 1x Random Primers, 1 µl Multiscreen RTase, 1 µl RNase Inhibitors (all from a High Capacity cDNA Reverse Transcription kit), with a total volume of 20 µl made up with RNase-free water. This mix was incubated in a PCR machine at 25℃ for 10 minutes, 37℃ for 120 minutes, 85℃ for 5 minutes then stored at 4℃.

2.12.2 Real-time PCR

First, standard curves were generated to verify the two DYRK2 primer pairs (Table 2.1). cDNA libraries were diluted to 1/5, 1/25, 1/125, 1/625 and 1/3125 of their original concentrations, then reaction mixes were made, consisting of 3 µl of each cDNA dilution, 1x SensiFast SYBR No-Rox mix and 0.6 µl each of a 10 µM stock of each forward and reverse primer, in a total volume of 15 µl made up with MilliQ water. These reactions were run on a Rotor-Gene Q (Qiagen) using a two-step protocol consisting of 95℃ for 3 minutes, then 45 cycles of 95℃ for 5 seconds followed by 62℃ for 30 seconds. All reactions were done in duplicate. From the standard curves generated, 1/125 was selected as an appropriate dilution to use, and DYRK2 qPCR primer set 1 was selected due to having a higher quality melt curve.

For quantification of *DYRK2* transcript level, cDNA libraries from samples were used in qPCR reactions in the same way, using a 1/125 dilution, with either DYRK2 qPCR primer set 1 or primers for the housekeeping gene *HPRT* as a control (Table 2.1), with each reaction performed in duplicate.

2.13 Tables of materials used

Table 2.1: **Sequences of primers used in this thesis**

PLK1 PBD dead mutagenesis	
PBD dead Fw	GATCAACTTCTTCCAGGATGCCACCATGCTCATCTTGTGCCCAC
PBD dead Rv	GTGGGCACAAGATGAGCATGGTGGCATCCTGGAAGAAGTTGATC
DYRK2 mutagenesis	
K251R Fw	CATTCCGCACCATCCTTAGGGCCACGTGCTG
K251R Rv	CAGCACGTGGCCCTAAGGATGGTGCGGAATG
F301A Fw	GTTCATGCTCAGCAGCTCAGCCGTCATGCAGATGTGGTTG
F301A Rv	CAACCACATCTGCATGACGGCTGAGCTGCTGAGCATGAAC
F301G Fw	GTTCATGCTCAGCAGCTCACCCGTCATGCAGATGTGGTTG
F301G Rv	CAACCACATCTGCATGACGGGTGAGCTGCTGAGCATGAAC
DYRK2 sequencing	
DYRK2 Seq Fw	ACTCACAGCCTTCGAACACCATG
CDT1-BFP cloning	
XhoI-CDT1 Fw	AGAGAGCTCGAGATGCCATCTCCTGCTAGGCCAGCTC
PstI-CDT1 Rv	AGAGAGCTGCAGCCCGATGGTGTCCTGGTC
HygR cloning	
KpnI-HygR Fw	AGAGAGGGTACCGCCACCATGAAAAAGCCTGAACTCACCGCGAC
PmeI-HygR Rv	AGAGAGGTTTAAACTCAGTTAGCCTCCCCCATCTCC

Table 2.1: **Sequences of primers used in this thesis (continued)**

UBR5 truncations	
attB1 Fw	GGGGACAAGTTTGTACAAAAAAGCAGGCTTC
attB2-UBR5-1 Rv	GGGGACCACTTTGTACAAGAAAGCTGGGTCCGCGGCTATGGTGGAGGACCCATTTCTGTTTTCAC
attB1-UBR5-2 Fw	GGGGACAAGTTTGTACAAAAAAGCAGGCTTCCGGACCATGGAAGCTAAGCCTGAAAGTAAGCAGG
attB2-UBR5-2 Rv	GGGGACCACTTTGTACAAGAAAGCTGGGTCCGCGGCTATACAGATGGCTCTGTGGAAGGACC
attB2-UBR5-3 Fw	GGGGACAAGTTTGTACAAAAAAGCAGGCTTCCGGACCATGGGTCAAGGACCAAGCACCTCC
NLS-UBR5-3 Rv	CGGCTATACCTTTCTCTTCTTCTTCGGATGCTCATCATGTTGTCCCTCTGC
attB2-UBR5-3 Rv	GGGGACCACTTTGTACAAGAAAGCTGGGTCCGCGGCTAATGCTCATCATGTTGTCCCTCTGC
attB1-UBR5-4 Fw	GGGGACAAGTTTGTACAAAAAAGCAGGCTTCCGGACCATGGATGAACAGGAAGAACACGGG
NLS-UBR5-4 Rv	CGGCTATACCTTTCTCTTCTTCTTCGGTGAACTCTCAGTTTCTTCTGGCAGC
attB2-UBR5-4 Rv	GGGGCCACTTTGTACAAGAAAGCTGGGTCCGCGGCTATGAACTCTCAGTTTCTTCTGGCAGC
attB1-UBR5-5 Fw	GGGGACAAGTTTGTACAAAAAAGCAGGCTTCCGGACCATGAAAAAAGAAGGGGAAGAACAGCCC
NLS-UBR5-5 Rv	CGGCTATACCTTTCTCTTCTTCTTCGGCACAAAACCAAAATTCTTGGTCTTAATGGC
attB2 Rv	GGGGACCACTTTGTACAAGAAAGCTGG
NLS-attB2 Rv	GGGGACCACTTTGTACAAGAAAGCTGGGTCCGCGGCTATACCTTTCTCTTCTTCTTCGG
DYRK2 qPCR	
DYRK1 q1 Fw	TCCAAGTTACCTCCACCTTCTA
DYRK2 q1 Rv	CAACACTGTCCTCTGCTGAATA
DYRK2 q2 Fw	ATGGCTCTGTGGTCCTAAAC
DYRK2 q2 Rv	CTGCAGGATCCCACTCTAAAC
HPRT qPCR	
HPRT q1 Fw	GCTATAAATTCTTTGCTGACCTGCTG
HPRT q1 Rv	AATTACTTTTATGTCCCCTGTTGACTGG

Table 2.2: **Sequences of primers and oligos used by collaborators in generating CRISPRi plasmids**

Primers for PCR amplification of PGK promoter	
Fw	cgggctattcttttgatttataaGGGTAGGGGAGGCGCTTT
Rv	tgctcaccatATTGGCTGCAGGTCGAAAG
Primers for PCR amplification of EGFP-T2A-Neo	
Fw	tgcagccaatATGGTGAGCAAGGGCGAG
Rv	gaaatcggcaaaatcccttaGTTTATTGCAGCTTATAATGGTTACAAATAAAG
P2A oligos	
Fw	GACGAGCTGTACAAGCTTGGAAGCGGAGCTACTAACTTCAGCCTGCTGAAGCAGGCTGGA
Rv	GGCCGATCCCATGCTAGCAGGTCCAGGGTTCTCCTCCACGTCTCCAGCCTGCTTCAGCAG
Linker to replace Cas9 sequence	
cAGATCTGATATCGTCGACcctgca	
Primers for PCR amplification of Blasticidin resistance gene	
Fw	agagaagctagcATGGCCAAGCCTTTGTCT
Rv	ttctctctcgagTTAGCCCTCCCACACATA
gBlock containing modified sgRNA scaffold	
ctttgctggccttttgctcacatgtgagggcctatttcccatgattccttcatatttgcatatacgatacaaggctgttagagagataattggaattaatttgactgtaaacacaaagatattagtac aaaatacgtgacgtagaaagtaataatttcttgggtagtttgcagttttaaaattatgttttaaaatggactatcatatgcttaccgtaacttgaaagtatttcgatttcttggctttatatatcttGTG GAAAGGACGAAACACCggGTCTTCgaGAAGACctGTTTAagagctaTGCTGgaaaCAGCAtagcaagttTaaataaggctagtccgttatcaacttgaaaa agtggcaccgagtcggtgcTTTTTTgttttagagctagaaatagcaagttaaaataaggctagtccgtTTTTagcgcgtgcgccaattctgcagacaaatggctctagaggtacccg ttacataacttacggtaaatggc	

Table 2.3: **siRNA and sgRNA sequences**

siRNAs	
siDYRK2 #1	GGACUAAUUUGGCGCAGAU
siDYRK2 #2	GGUGCUAUCACAUCUAUAU
siDYRK2 #3	AUACCUGUAAGCCACGUGAUCGUGG
sgRNAs	
AAVS1-1	CCCCACAGTGGGGCCACTACGG
DYRK2-1	GCGAGGCATGTGCACGGGCCGG
DYRK2-9	CGCCCCTATGTGAGGGAGACGG
UBR5-3	CTACGGGGACGGTCTGGTCCCGG
UBR5-4	AGCTTCTCGCTAGTGACGCGCGG
UBR5-8	GGCGGACGGGGTCCGGACTAGGG

Table 2.4: **Suppliers of reagents used**

Reagent	**Supplier**
Dulbecco's Modified Eagle Medium	Gibco
Heat-Inactivated FBS (EU approved)	Gibco
Penicillin-Streptomycin	Gibco
Trypsin (Tryple Express Enzyme)	Gibco
G418 disulfate salt	Sigma Aldrich
Puromycin	Invivogen
Hygromyin B Gold	Invivogen
Blasticidin	Invivogen
Doxycycline	Sigma Aldrich
JetPRIME transfection reagent and buffer	Polyplus-transfection
Plasmid PlusMidi kit	Qiagen
GeneJET Plasmid Miniprep kit	Thermo Fisher Scientific

Table 2.4: **Suppliers of reagents used (continued)**

Reagent	**Supplier**
QIAquick PCR purification kit	Qiagen
QIAquick gel extraction kit	Qiagen
Gateway LR/BP Clonase II Enzyme kits	Invitrogen
Restriction enzymes and buffers	New England Biolabs
Calf Intestinal Alkaline Phosphatase	New England Biolabs
DNA Ligation kit, Mighty Mix	Takara
PCRBio HIFI Polymerase and buffer	PCR Biosystems
LB broth	EMD Millipore
LB agar	EMD Millipore
SOB broth	Fisher BioReagents
Ampicillin sodium salt	Melford
Kanamycin sulfate	Sigma Aldrich
Spectinomycin dihydrochloride pentahydrate	Sigma Aldrich
Gentamycin Sulphate salt, VETRANAL	Fluka
Lysozyme	Sigma Aldrich
IPTG	Melford
Ultra Pure Agarose	Invitrogen
Ethidium bromide	Sigma Aldrich
DNA ladders (100 bp; 1 kB)	New England Biolabs)
DNA Loading dye Purple (6x)	New England Biolabs)
NuPAGE 4-12% Bis-Tris protein gels	Thermo Fisher Scientific
BlueEasy Pre-stained protein ladder	Geneflow
NuPAGE LDS Sample Buffer	Invitrogen
Dried skimmed milk	Marvel

Table 2.4: **Suppliers of reagents used (continued)**

Reagent	**Supplier**
Tween 20	Sigma Aldrich
0.45 µm Nitrocellulose membrane	GE Healthcare
Ponceau	Sigma Aldrich
ECL Western Blotting detection reagents	GE Healthcare
Bradford protein assay	Bio-Rad
pIMAGO HRP Detection kit	Tymora Analytical
Re-Blot Plus Mild solution	EMD Millipore
Thymidine	Sigma Aldrich
Nocodazole	Calbioochem
Bovine Serum Albumin	Sigma Aldrich
RNase A	Sigma Aldrich
Propidium iodide	Sigma Aldrich
Protease Inhibitor Cocktail	Sigma Aldrich
Benzonase Nuclease	EMD Millipore
10% NP-40 solution	Thermo Fisher Scientific
n-dodecyl-β-maltoside	EMD Millipore
AffiPrep Protein A beads	Bio-Rad
Mouse IgG Agarose beads	Sigma Aldrich
GFP-Trap A beads	Chromotek
Endoproteinase LysC	Roche
Sequencing grade modified trypsin (lyophilised)	Promega
ENVI-18 DSK SPE Disk	Supelco
BrdU	Sigma Aldrich
Leibovitz's L-15 medium	Gibco

Table 2.4: **Suppliers of reagents used (continued)**

Reagent	**Supplier**
DMSO	Sigma Aldrich
RO-3306	Axon Medchem
NU-6102	EMD Millipore
BI-2536	Axon Medchem
ATM inhibitor (KU-55933)	Calbiochem
KU-60019	TOCRIS
Harmine	BioVision
Leucettine L41	BioVision
Camptothecin	Sigma Aldrich
Triton X-100	Sigma Aldrich
Cold Fish Skin Gelatin	Sigma Aldrich
ProLong Gold Antifade Mountant	Life Technologies
DharmaFECT 1 Reagent	Dharmacon
SmartPool siRNAs	Dharmacon
Nuclease-free water	Fisher BioReagents
Lipofectamine 2000	Thermo Fisher Scientific
MISSION siRNA Universal Negative Control #1	Sigma Aldrich
Glutathione-sepharose 4 FastFlow beads	GE Healthcare
Active DYRK2	EMD Millipore
TRI Reagent	Applied Biosystems
High Capacity cDNA Reverse Transcription kit	Applied Biosystems
SensiFAST SYBR No-Rox mix	Bioline

Chapter 3

PLK1 localisation to DNA damage sites

3.1 Introduction

Recently, there has been growing evidence of PLK1 playing an active role in HR by phosphorylating substrates including RAD51 [86] and BRCA1 [191], prior to its downregulation by the DNA damage checkpoint, as discussed in Section 1.4. Despite this, it remains unclear how PLK1 acts upon these substrates: whether it does so by phosphorylating them while they are mobile in the nucleus before they translocate to damage sites, or whether PLK1 itself becomes more closely associated with damage sites to carry out these functions. On the one hand, one might expect PLK1 to have easier access to its repair-related substrates by localising to damage, especially given the fact that PLK1 requires bridging proteins such as BRCA2 and TOPBP1 to be able to phosphorylate RAD51 [87] [88]. On the other hand, the only currently known function of RAD51 phosphorylation by PLK1 is to facilitate RAD51 association with resected DNA via NBS1, so PLK1

phosphorylating RAD51 while already located near the damage seems unnecessary.

In this chapter, I set out to investigate PLK1 localisation to damage sites by using laser microirradiation and found that PLK1 is indeed recruited to laser-induced damage as early as 15 minutes after induction, in both G2 and, surprisingly, G1 cells. Investigation of factors that regulate this localisation revealed that PLK1's PBD likely binds to CDK2-phosphorylated substrates at damage sites in G2, and that its recruitment in both G2 and G1 is also dependent on ATM activity. Experiments to determine whether PLK1's own activity was a factor in its recruitment to damage returned conflicting results. Nonetheless, these findings not only demonstrate PLK1 localisation to DNA damage but also uncover parts of the mechanism behind its recruitment.

3.2 Results

3.2.1 Cell lines containing fluorescently-tagged PLK1

For this chapter, I initially used two different cell lines of fluorescently-tagged PLK1. One was PLK1-LAP, a Hela Kyoto cell line with PLK1 fused to a GFP-containing LAP tag expressed within *PLK1*'s native locus on a BAC vector, thus in theory retaining the natural expression pattern of PLK1 [193]. The other cell line was PLK1-YFP, a HeLa Kyoto cell line in which in which one PLK1 allele had been tagged with YFP at the C-terminus using CRISPR/Cas9 technology [194], and should therefore be more likely to display a native expression pattern for the tagged PLK1.

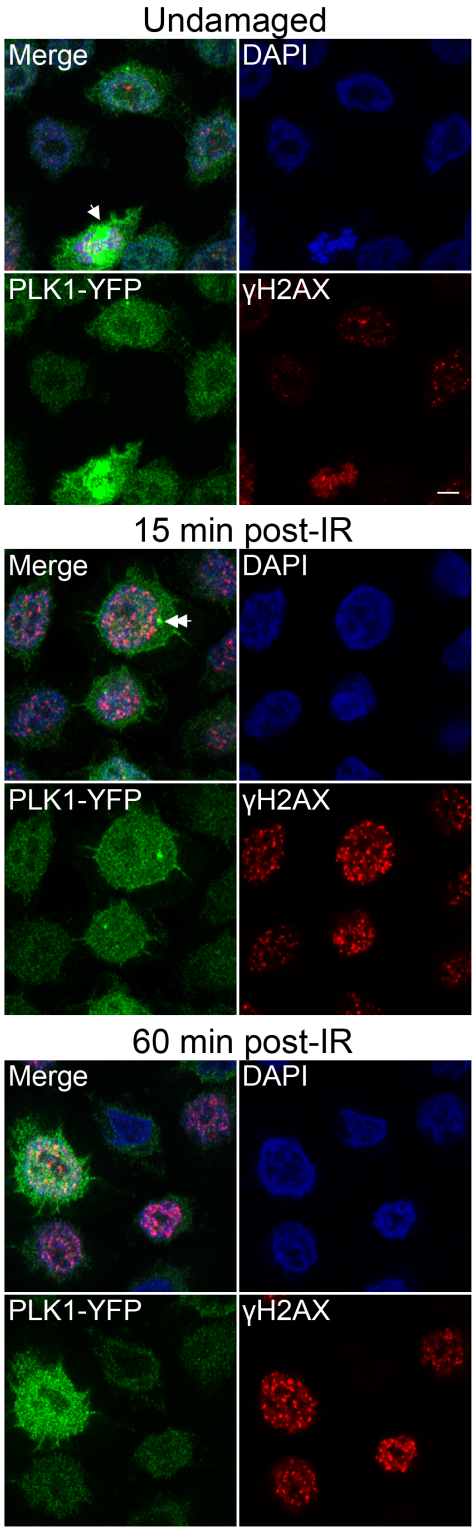


Figure 3.1: **Lack of PLK1 foci formation upon ionising radiation treatment.** PLK1-YFP cells were either left untreated or irradiated with 4 Gy of ionising radiation and incubated for the indicated amount of time before fixation. Fixed cells were then stained with DAPI and immunofluorescence, targeting GFP with a green fluorophore to amplify the PLK1-YFP signal and targeting γH2AX with a far-red fluorophore. Images are blue, green and far-red channels of representative cells. Single arrowhead denotes a cell in prometaphase: note chromosomes beginning to align and high PLK1-YFP signal on spindles. Double arrowhead denotes a centrosome. Scale bar = 10 µm.

3.2.2 PLK1 does not form cytologically visible foci upon ionising radiation treatment

As a preliminary line of investigation, I examined whether PLK1 forms foci upon ionising radiation-induced DNA damage. I fixed PLK1-YFP cells either before irradiation or 15 or 60 minutes afterwards, then immunostained for γH2AX. A preliminary attempt found the PLK1-YFP signal to be very dim, so this signal was also amplified by immunostaining using a GFP antibody with a green fluorophore. I could be confident that the green signal was indeed showing PLK1-YFP due to observing high signal at certain features PLK1 is known to localise to. In Figure 3.1, in the non-irradiated sample, a cell in prometaphase displays high PLK1-YFP signal at the spindle poles, while in other cells, bright green dots just outside of the nucleus are likely a sign of PLK1-YFP accumulation at centrosomes. (A similar experiment carried out in PLK1-LAP cells did not show these distinctive features of PLK1 localisation (data not shown).) Nonetheless, PLK1-YFP did not form visible nuclear foci upon DNA damage, despite the presence of γH2AX foci indicating that damage induction was successful.

3.2.3 PLK1 localises to damage sites within 15 minutes in G1 and G2 cells

Since immunofluorescence did not produce visible PLK1 localisation to damage sites, I moved to using live-cell laser microirradiation instead. As a positive control to confirm that the microirradiation setup induced DNA damage, I stably transfected both PLK1-LAP and PLK1-YFP cell lines with mCherry-BP1. This construct consists of mCherry fused to the minimal focus-forming region of 53BP1, residues 1220-1711 [196], which contains

an oligomerisation domain (OD) [206], a Tudor domain which binds dimethylated lysine 79 on histone H3 [207], and a ubiquitination-dependent recruitment (UDR) motif, which binds ubiquitin [20] (Figure 3.2A). This region confers binding to DNA damage-associated chromatin but no repair function and therefore acts as a neutral marker for DNA damage. Upon introducing a stripe of DNA damage into these cells using laser microirradiation, I observed faint but noticeable PLK1-LAP or PLK1-YFP recruitment to the laser stripe (Figure 3.2B shows representative PLK1-YFP cells; PLK1-LAP cells looked similar).

I was able to estimate the cell cycle phase of each irradiated cell by using the level of PLK1-LAP or PLK1-YFP expression, since PLK1 is more highly-expressed in S and G2 [92]. Cells with lower PLK1 expression also showed predominantly cytoplasmic localisation of PLK1, while cells with higher expression had roughly equal PLK1 levels in both the cytoplasm and the nucleus. Since PLK1 begins to localise to the nucleus in S phase [111], this further supported that the latter were S/G2 phase cells. The PLK1-YFP cell line also had further features helpful for cell cycle identification: certain cells displayed high levels of PLK1-YFP signal which decreased more substantially than usual over the course of the experiment, indicating these were in fact early G1 cells prior to full PLK1 degradation [208]. Such cells were always found in neighbouring pairs with a midbody high in PLK1-YFP signal between them [129], signifying that they had recently divided, and often showed visible PLK1-YFP association with centromeres, observed to be a G1-specific phenomenon by the creators of this cell line [194] (Figure 3.2C).

The mCherry-BP1 signal also helped identify cell cycle phase. S/G2 cells had larger nuclei, which was more easily determined by looking at the

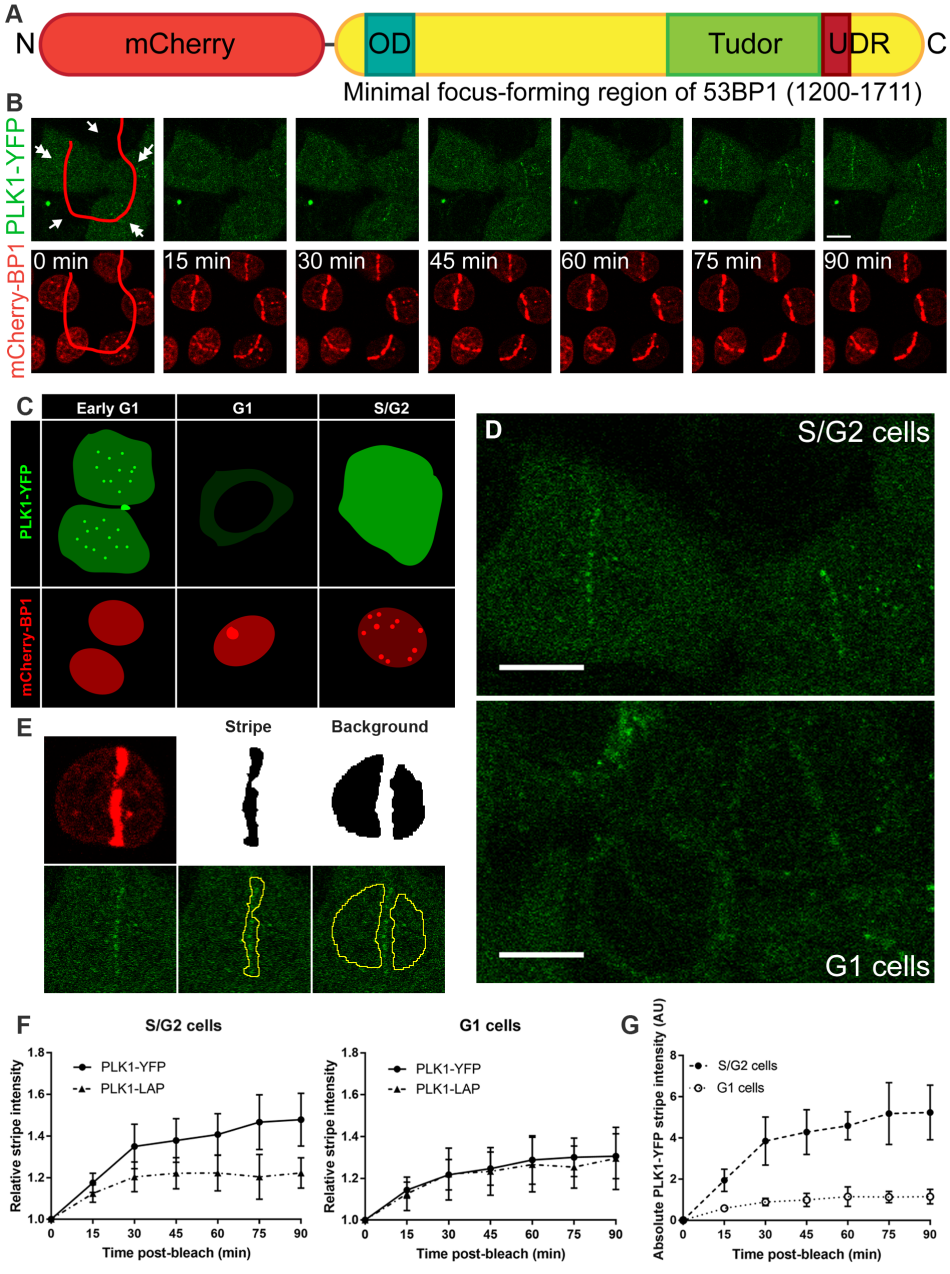

A
N
mCherry
OD
Tudor
UDR
C
Minimal focus-forming region of 53BP1 (1200-1711)
B
PLK1-YFP
mCherry-BP1
0 min
15 min
30 min
45 min
60 min
75 min
90 min
C
Early G1
G1
S/G2
PLK1-YFP
mCherry-BP1
D
S/G2 cells
G1 cells
E
Stripe
Background
F
S/G2 cells
G1 cells
PLK1-YFP
PLK1-LAP
Relative stripe intensity
Time post-bleach (min)
G
S/G2 cells
G1 cells
Absolute PLK1-YFP stripe intensity (AU)
Time post-bleach (min)

Figure 3.2: **PLK1 localisation to laser-induced DNA damage in G1 and G2 cells. A:** Diagram of the mCherry-BP1 construct. OD: oligomerisation domain. UDR: Ubiquitination-dependent recruitment motif. The Tudor domain binds H3K79Me2 chromatin marks. **B:** Images of green and red channels for representative PLK1-YFP mCherry-BP1 cells at indicated times post-bleaching. Red line: laser path. Single arrowheads: G1 cells. Double arrowheads: S/G2 cells. Scale bar: 10 µm. **C:** Cartoon depiction of microscope images of cells showing representative features used to determine cell cycle phase. G1 cells have smaller nuclei (as delineated by mCherry-BP1), and foci of mCherry-BP1 are typically larger and few in number. PLK1-YFP signal in G1 cells is low in intensity, and even lower in the nucleus than the cytoplasm. S/G2 cells have larger nuclei, typically with multiple smaller mCherry-BP1 foci, and higher PLK1-YFP intensity with no obvious nuclear/cytoplasmic boundary. Early G1 cells also have high PLK1-YFP intensity but can be identified by the presence of a PLK1-YFP-rich midbody between two such cells and bright PLK1-YFP spots in the nuclei from centromeres. **D:** Images of the green channel of irradiated cells at 90 minutes post-bleach. Top: PLK1-YFP mCherry-BP1 cells, zoomed-in image from **B**, focusing on two S/G2 cells. Bottom: GFP-PLK1 mCherry-BP1 cells (used in Figure 3.3B; this cell line is shown because the G1 stripe is more easily visible), focusing on two G1 cells. Scale bar: 10 µm. **E:** Method of quantifying stripe and background intensity. Binary masks are generated for“stripe” and “background” using the mCherry-BP1 signal, then selections taken from these masks are applied to the PLK1-YFP images and average pixel intensity is calculated for each selection. **F:** Quantification of relative PLK1-YFP or PLK1-LAP stripe intensity against time in G1 and G2 cells. **G:** Quantification of absolute PLK1-YFP stripe intensity against time in G1 and G2 cells. **F-G:** n values (G1—G2) as follows. PLK1-YFP: 41—26. PLK1-LAP: 40—21. Error bars: SEM for three biological replicates.

nuclear-only mCherry-BP1. These larger nuclei frequently showed multiple small mCherry-BP1 foci, likely marking endogenous DNA damage caused by replication stress from S phase, while the smaller G1 nuclei only occasionally displayed low numbers of larger mCherry-BP1 foci, consistent with G1-specific 53BP1 nuclear bodies found to be a result of natural levels of replication stress occasionally remaining throughout mitosis [209] (Figure 3.2C).

Due to how relatively faint the fluorescently-tagged PLK1 stripe was against the nuclear background, the intensity of the stripes was difficult to quantify directly. Fortunately, the mCherry-BP1 signal proved useful as marker to enable fluorescent PLK1 quantification (Figure 3.2E; more details in Section 2.8.3). Quantification determined that PLK1-LAP and PLK1-YFP are recruited to DNA damage sites in S/G2 cells as early as 15 minutes post-damage (Figure 3.2F). Surprisingly, despite it being difficult to spot by eye, the quantification also determined that PLK1-LAP and PLK1-YFP are recruited to damage sites in G1 cells, again as early as 15 minutes post-damage (Figure 3.2F). In both cell cycle phases, PLK1 association with the damage stripe continued to increase after 15 minutes but reached an approximate plateau by around 60 minutes. This suggests that at this point either recruitment had stopped and PLK1 association remained stable, or that the association and dissociation rates of PLK1 with the damage sites had reached equilibrium - more likely the latter, since PLK1 turnover at most subcellular structures is relatively fast [130]. Since PLK1-YFP cells showed a greater intensity of fluorescent PLK1 at the stripe than PLK1-LAP cells in S/G2, possibly due to the more natural expression of the fluorescently-tagged PLK1, PLK1-YFP was chosen as the cell line to continue using for these experiments.

Figure 3.2F shows the relative stripe intensity of fluorescent PLK1 calculated by dividing stripe intensity by background. Both are similar between G1 and S/G2 cells once a plateau is reached, suggesting that approximately the same proportion of nuclear PLK1 is recruited to damage sites regardless of cell cycle phase. However, it is important to note that the absolute stripe intensity, calculated by subtracting background from stripe intensity, is much higher in S/G2 than G1 (Figure 3.2G). This is to be expected considering that PLK1 expression and nuclear localisation in S/G2 is higher overall, and as such, a higher overall amount of PLK1 molecules are recruited to damage sites in S/G2 than in G1.

The pattern of PLK1-YFP at laser stripes in S/G2 cells was relatively faint and punctate compared to the thicker, bolder stripe of mCherry-BP1 signal (Figure 3.2B/D). This suggests that, rather than binding to the wider area of DNA damage-associated chromatin that 53BP1 is found in, PLK1 binds more directly to ssDNA-containing microcompartments, as classified by Bekker-Jensen *et al* [65], where resection has occurred. In G1 cells, as expected given the lack of resection activity, the appearance of the PLK1 stripe was broader and more even in intensity across the whole stripe, indicating PLK1 association with the wider chromatin at the damage sites (Figure 3.2D).

I initially expected any observed localisation of PLK1 to damage sites to be confined to S/G2 cells, when HR can occur. As such, the observation of PLK1 associating with DNA damage during G1 is very surprising. This suggests that PLK1 may have an as-yet unidentified role in DNA repair pathways other than HR. It is also surprising since the majority of PLK1 molecules still present in G1 should be inactive and unable to carry out any function that would require its localisation at damage. However, there

is some precedent for PLK1 functioning in G1. McKinley and Cheeseman found that PLK1 licenses the deposition of CENP-A at centromeres during G1 [194], although this only indicates a function for the small fraction of G1 PLK1 that is associated with centromeres.

3.2.4 PLK1 recruitment to damage in G2 is dependent on the PBD and primed by CDK2 but not CDK1

Encouraged by this initial finding that PLK1 localises to damage sites, I set out to identify possible factors that regulated this. Since PLK1's PBD is required for much of its subcellular localisation and mediates its binding to many substrates, a logical first step was to ask if the PBD was important for PLK1's recruitment to DNA damage. To this end, I generated cell lines stably expressing mCherry-BP1 along with N-terminal GFP-tagged PLK1 that was either wild-type or containing a H538A/K540M mutation that renders the PBD unable to bind to phosphopeptides [103] (henceforth referred to as "PBD dead") (Figure 3.3A). While the GFP-PLK1 construct was expressed from a constitutive CMV promoter, I was fortunately still able to obtain clones which showed a cell-cycle dependent difference in GFP-PLK1 expression, likely due to its degradation from the end of anaphase to early G1 [208]. Perhaps due to somewhat higher GFP-PLK1 expression in G1 compared to that of PLK1-YFP, it was easier to see the recruitment of GFP-PLK1 WT to laser stripes in G1 by eye (Figure 3.2D).

The PBD dead cell line, using the WT cell line as a control, showed that PBD dead PLK1 recruitment to damage sites was significantly reduced compared to WT in S/G2 cells, but not in G1 cells (Figure 3.3B). This indicates a requirement for the PBD for PLK1 binding to damage sites in S/G2 only, which strongly suggests that an S/G2-specific CDK may be the

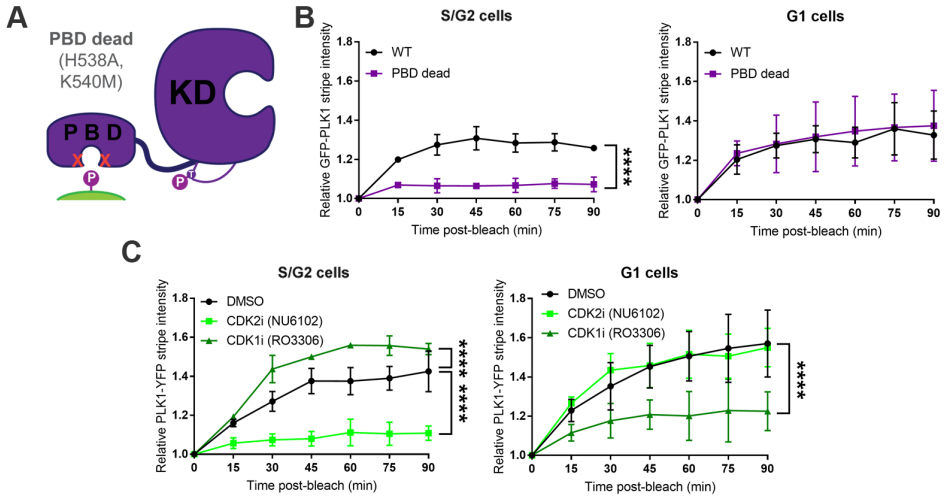


Figure 3.3: **PLK1 localisation to damage is dependent on the PBD and CDK2 activity. A:** Diagram of the PBD dead mutant. Two mutated residues in the PBD abrogate binding to phosphopeptides. **B:** Quantification of relative GFP-PLK1 stripe intensity against time in G1 and G2 cells, for either wild-type or PBD dead GFP-PLK1. **C:** Quantification of relative PLK1-YFP stripe intensity against time in G1 and G2 cells, treated with either 1:1000 DMSO, 9 µM RO-3306 or 10 µM NU-6102 1-2 hours prior to bleaching as indicated. **B-C:** n values (G1—G2) as follows. **B:** WT: 34—37; PBD dead: 43—20; **C:** DMSO: 62—31; RO-3306: 46—28; NU-6102: 30—44. Error bars: SEM for three biological replicates. **** = p-value <0.0001.

priming kinase for the phosphoprotein that the PBD binds to.

To determine whether this was the case, I used small-molecule CDK inhibitors to examine this using the PLK1-YFP cell line. Inhibition of CDK1 using RO-3306 [210] showed a small increase, rather than a decrease, of PLK1-YFP recruitment to damage in S/G2, and a decrease of PLK1-YFP recruitment to damage in G1 (Figure 3.3C). Meanwhile, inhibition of CDK2 using the small-molecule inhibitor NU-6102 [211] showed a decrease of PLK1-YFP recruitment to damage in S/G2 similar to that seen in PBD dead compared to wild-type, while having no effect on recruitment in G1 (Figure 3.3C). NU-6102 does inhibit CDK1 as well, but at a 50-fold lower selectivity than for CDK2 [212], while RO-3306 also inhibits CDK2 but with a 10-fold

lower selectivity than for CDK1 [210]. However, when taken together, the data for both inhibitors' effect on S/G2 PLK1 recruitment strongly supports that CDK2 and not CDK1 is the crucial kinase for PLK1 recruitment to damage. Thus, this and the PBD dead data together suggest a model in which PLK1 PBD binding at sites of DNA damage is primed in S and G2 phase by CDK2.

CDK1 inhibition was instead seen to cause an increase in the amount of PLK1 associating to damage sites in S/G2. A potential explanation for this is inhibition of CDK1 activity relieves CDK1 priming of PBD binding sites on proteins elsewhere in the nucleus, thus freeing up a larger portion of nuclear PLK1 to relocalise to damage sites. In G1 cells, however, CDK1 appears to be partially required for PLK1 localisation to damage, which is especially surprising given that CDK1 should not be active in G1 either. The paper characterising RO-3306 did note that use of the inhibitor caused a 4 hour delay of S-phase entry in HeLa cells at the concentrations used here, suggesting either a role for CDK1 in G1 progression in HeLa cells or an off-target effect of the inhibitor in G1 [210]. Given that the cells used for these experiments are also HeLa cells, this could potentially be related to the observed effect of CDK1 inhibition on PLK1 localisation to damage in G1. Repeating the experiments in a different cellular background would shed more light upon whether or not this observation is merely a cell line-specific effect.

3.2.5 PLK1 localisation to damage is dependent on ATM activity

Another relevant question to ask was whether PLK1 recruitment to damage was affected by DNA damage signalling, such as that of ATM. At first, I

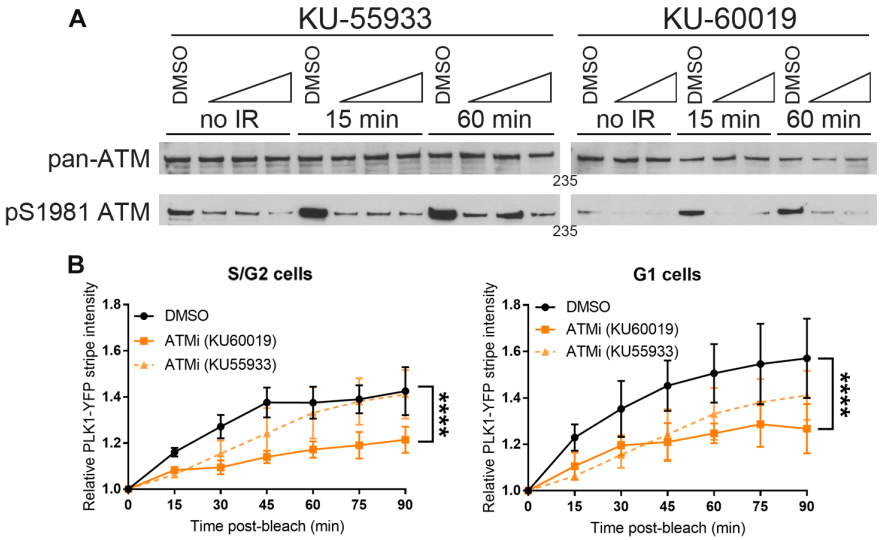


Figure 3.4: **PLK1 localisation to damage sites is dependent on ATM activity. A:** Verification of ATM inhibitors. PLK1-YFP cells were treated with either 1:1000 DMSO; KU55933 at 10 µM, 20 µM or 50 µM; or KU-60019 at 3 µM or 10 µM, as indicated, 1 hour prior to irradiation. Then cells were either harvested without irradiation or irradiated with 4 Gy and harvested the indicated times after irradiation. Lysates were probed with the indicated antibodies. **B:** Quantification of relative PLK1-YFP stripe intensity against time in G1 and G2 cells, treated with either 1:1000 DMSO, 10 µM KU-55933 or 3 µM KU-60019 1-2 hours prior to bleaching as indicated. n values as follows. DMSO: 62—31; KU-55933: 39—29; KU-60019: 46—25. Error bars: SEM for three biological replicates. **** = p-value $<$0.0001.

tried using the small molecule inhibitor KU-55933 [213], which gave some level of decrease in PLK1-YFP recruitment to damage in G1 and S/G2 (Figure 3.4B). However, this was somewhat unconvincing, particularly in S/G2 cells. Verification of the inhibitor's potency by examining autophosphorylation of ATM on S1981 [214] showed that KU-55933 did not completely inhibit ATM activity (Figure 3.4A). I therefore tried using an improved version of KU-55933, KU-60019 [215]. Verification of KU-60019 showed that it inhibited ATM activity to a greater extent than KU-55933 (Figure 3.4A). Using this inhibitor in the microirradiation experiment resulted in a more dramatic

decrease of PLK1-YFP recruitment to damage sites in both G1 and S/G2 cells (Figure 3.4B). This decrease was still not as complete as was seen for PBD mutation and CDK2 inhibition in Figure 3.3, suggesting that either KU-60019 still does not fully inhibit ATM, or that another mechanism can partially compensate for the loss of ATM activity.

Given this requirement of ATM for PLK1 recruitment to damage not only in S/G2 but also in G1 when the PBD and CDK2 are not required, ATM is most likely upstream of the PBD binding and acting via a different mechanism not directly involving the PBD. However, since ATM is important for so many parts of DNA damage signalling, the exact mechanism by which it is affecting PLK1 localisation to damage is still unclear and would require further experiments inhibiting various factors downstream of ATM to clarify this.

3.2.6 Effect of PLK1 activity on its recruitment to damage is unclear but unrelated to ATM activity

Another question I was interested in answering was whether PLK1 needs to be active before it can be recruited to damage sites. For this purpose, I generated cell lines stably expressing mCherry-BP1 along with GFP-PLK1 containing either the catalytically inactive K82R mutation, or the constitutively active T210D mutation (Figure 3.5A). These mutants of GFP-PLK1 showed lower expression that did not noticeably vary throughout the cell cycle, likely because their effect on PLK1 activity meant that overexpression caused dominant-negative cell viability defects. As such, I could not determine cell cycle stage in these cells. As an appropriate control, I used a different clonal cell line of GFP-PLK1 WT with a similarly low and non-varying GFP-PLK1 expression level. Laser microirradiation using these cell

lines showed the T210D mutant having a small but significant increase and the K82R having a small but significant decrease in recruitment to damage compared to wild-type (Figure 3.5B), both of which support a hypothesis that PLK1 being active aids in its recruitment to damage sites.

Our collaborator Dr. Lindqvist had also used the FRET sensor for PLK1 activity to show that the possible increase he observed in PLK1 activity upon DNA damage in asynchronous cells is dependent on ATM activity (Figure 1.6C). Therefore, I examined the possibility that the decrease I observed in PLK1 recruitment to damage sites upon ATM inhibition was the result of the ATM inhibition causing a decrease PLK1 activation. To test this, I looked at the effect of ATM on PLK1 T210D recruitment to damage. If the requirement of ATM for PLK1 recruitment is due to ATM causing activation of PLK1 upon damage, I would expect to see the constitutively-active PLK1 T210D recruited to damage even upon ATM inhibition. However, ATM inhibition resulted in the same decrease in recruitment for PLK1 T210D as for PLK1 WT (Figure 3.5C). Thus, whatever mechanism is behind the requirement of ATM in PLK1 recruitment to damage, it is not related to its possible role in PLK1 activation.

As a parallel approach to the activity mutants, I examined the effect of directly inhibiting global PLK1 activity using the small-molecule inhibitor BI-2536 [126] in the PLK1-YFP cell line. This resulted in a small increase in PLK1-YFP recruitment to damage in S/G2 cells, and no change in PLK1-YFP recruitment to damage in most G1 cells (Figure 3.5D). This increase in S/G2 cells is similar to that observed for CDK1 inhibition (Figure 3.3C) and could be explained in the same way: PLK1 can prime its own PBD binding sites, so PLK1 inhibition may reduce the number of PBD binding sites elsewhere in the nucleus and free up more PLK1 to bind to damage.

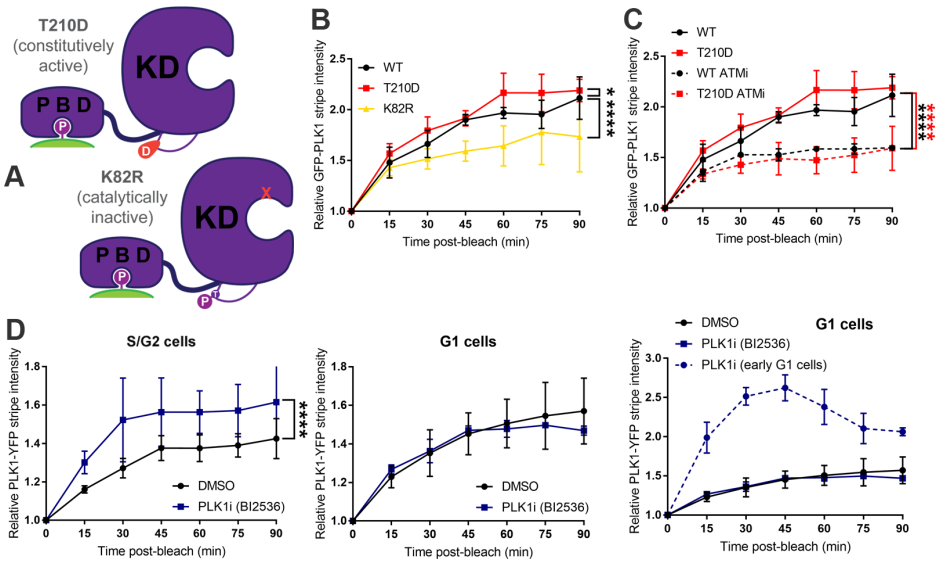


Figure 3.5: **Effect of PLK1 activity on its recruitment to damage. A:** Diagram of T210D and K82R mutations. T210D is a phosphomimetic mutation on the T-loop, causing the T-loop to behave as if it is constitutively phosphorylated and therefore rendering PLK1 constantly active. K82R is a mutation of the active site, rendering the kinase domain unable to catalyse phosphorylation, without affecting its interaction with the PBD. **B:** Quantification of relative GFP-PLK1 stripe intensity against time, for either wild-type, T210D or K82R GFP-PLK1. Due to the low GFP-PLK1 expression of these mutants, cell cycle phase could not be estimated. GFP-PLK1 WT cell line was a different clone to the one used in Figure 3.3B to match this expression level. **C:** As **B**, but also including cells treated with 3 µM KU-60019 1-2 hours prior to bleaching. **D:** Quantification of relative PLK1-YFP stripe intensity in G1 and G2 cells against time, treated with either 1:1000 DMSO or 100 nM BI-2536 1-2 hours prior to bleaching as indicated. Early G1 cells were identified by features depicted in Figure 3.2C. **B-D:** n values as follows. **B:** WT: 65; K82R: 61; T210D: 65; **C:** WT ATMi: 40; T210D ATMi: 63. **D:** (G1—G2) DMSO: 62—31; BI-2536: 33—23—(early G1: 12). Error bars: SEM for three biological replicates. * = p-value <0.05, **** = p-value <0.0001.

Contrary to the data from the activity mutants, the PLK1 inhibition data does not support the hypothesis that PLK1 activity is required for its recruitment to damage. There are possible explanations for these conflicting results. The T210D mutation increasing PLK1's recruitment to damage sites could potentially be related to the PBD instead of being directly related to activity. As discussed in Section 1.2.1, PLK1's kinase domain and polo-box domain are mutually autoinhibitory: not only does the PBD inhibit the kinase domain's activity, but the kinase domain inhibits the PBD's binding activity (Figure 1.5). Upon phosphorylation of the T-loop – or a phosphomimetic mutation such as T210D – this inhibition of the PBD is relieved. Therefore, it is possible that PLK1 T210D mutants localise more to damage because their PBD is freed up to bind to the appropriate CDK2-phosphorylated substrate at damage sites. Were this true, the T210D mutant would only have this effect in G2 cells; unfortunately, since it was not possible to determine cell cycle phase in this cell line, this cannot be confirmed from this data alone.

However, this PBD-related explanation does not apply to the K82R mutant. K82R is a minor mutation of a key catalytic residue in the active site, which is not the region of the kinase domain that binds the PBD during autoinhibition [109], and as such the mutation should not affect PBD binding activity. Nonetheless, an important difference between the K82R mutant and the PLK1 inhibitor treatment is that the inhibitor causes a global inhibition of PLK1, whereas in the K82R mutant cell line, endogenous untagged PLK1 is still functioning normally. Therefore, it is possible that the decrease in damage recruitment seen by GFP-PLK1 K82R is due to it being partially outcompeted at damage sites by the non-fluorescent, active PLK1, whereas this would not occur during global inhibition of PLK1 by BI-2536.

Another possibility is that inhibiting PLK1 with BI-2536 does in fact cause a small defect in its ability to bind to damage, but this effect is masked by the reduction of PLK1-primed PBD binding sites elsewhere in the nucleus and as such the association with damage still ends up being higher than for control.

In a small subset of G1 cells, PLK1-YFP recruitment appeared to be drastically increased upon PLK1 inhibition, with a peak at around 30 to 45 minutes (Figure 3.2J). These cells were determined to be very early in G1 based on the initially high PLK1-YFP levels that rapidly decreased, the presence of a PLK1-YFP-rich midbody nearby from recent division, and the presence of bright nuclear spots of PLK1-YFP indicating centromeres [194] (Figure 3.2C). Before reading too much into this, however, it is important to consider that relative stripe intensity is calculated relative to the background PLK1-YFP intensity in the rest of the nucleus. Thus, this apparent drastic increase is likely due to a combination of the rapid degradation of background PLK1-YFP in these cells and a partial protection from degradation of damage-associated PLK1-YFP, rather than necessarily a meaningful increase in the amount of PLK1-YFP associating with damage in the first place. Regardless, it is still of note that this pattern was only seen upon PLK1 inhibition and not in DMSO-treated early G1 cells, suggesting that PLK1 inhibition exacerbates this effect, presumably by either increasing the rate of PLK1 degradation in G1 or by increasing the extent to which damage-associated PLK1 is protected. This finding is intriguing, but since this project was mostly interested in examining the damage-induced regulation of PLK1 during HR in G2, in which PLK1 degradation is not relevant until a much later timeframe post-damage, I did not follow this observation up with further experiments.

3.2.7 BRCA2 localises to DNA damage in late S phase with faster kinetics than PLK1

I initially looked at the localisation of BRCA2 to damage for the sake of an unrelated line of investigation that I did not end up pursuing very far. However, given the fact that PLK1 is known to bind to BRCA2 in a PBD and CDK-dependent manner [87], and my earlier finding that PLK1 localisation to damage in G2 is dependent on the PBD and CDK2, it is possible that BRCA2 could be playing a role in delivering PLK1 to damage sites. Therefore, I considered this data relevant to include in order to provide evidence addressing this possibility.

For this, I used NFLAP-BRCA2 cells expressing BRCA2 fused to a FLAP tag, which contains GFP [193], and then stably transfected them with mCherry-BP1. At first, I attempted laser microirradiation in asynchronous cells, but this resulted in only some cells displaying noticeable NFLAP-BRCA2 localisation to laser stripes. I assumed this to be cell cycle-dependent, since BRCA2 is involved only in HR, which is S/G2-specfic. As such, I repeated the experiment while synchronising the cells in late S phase with a double thymidine block and 6 hour release (Figure 3.6A). As expected, this resulted in NFLAP-BRCA2 localising to damage sites in all microirradiated cells.

Much like PLK1-YFP in G2 cells, the NFLAP-BRCA2 localisation pattern included punctate spots of very high intensity (Figure 3.6B). As BRCA2 is well-characterised as associating with ssDNA-containing microcompartments [65], I can confidently assume that this is what is being reflected by this pattern here. Since the PLK1-YFP punctate pattern looks similar (Figure 3.2B), this lends support to the idea that PLK1-YFP is also localising to resected ssDNA. Aside from the extremely bright ssDNA spots, the rest

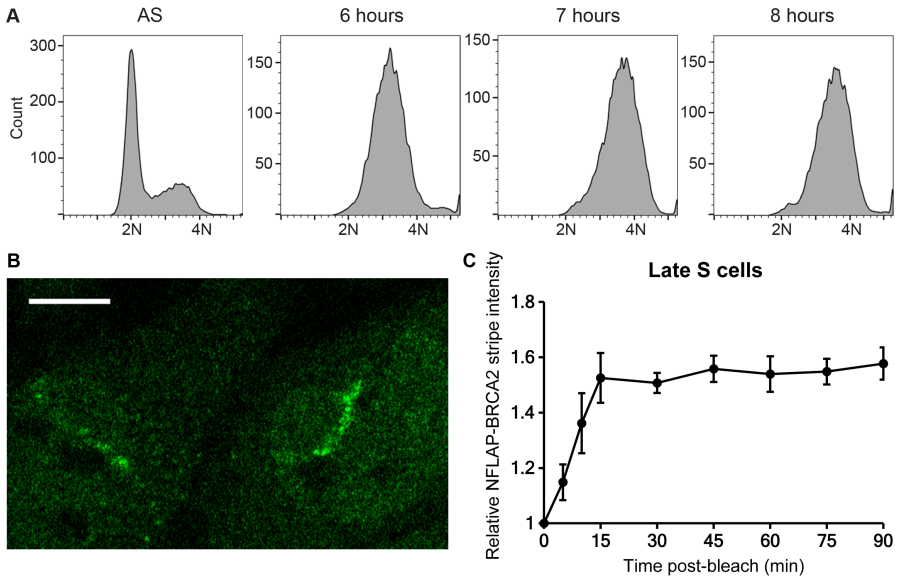


Figure 3.6: **BRCA2 localisation to laser-induced DNA damage. A:** FACS profiles of NFLAP-BRCA2 mCherry-BP1 cells either grown asynchronously or released for the indicated times following a double thymidine block. **B-C:** NFLAP-BRCA2 mCherry-BP1 cells were synchronised in late S with a 6-hour release from double thymidine block and then subjected to laser microirradiation. **B:** Part of the green channel at 90 minutes post-bleach, showing two representative cells. Scale bar: 10 µm. **C:** Quantification of NFLAP-BRCA2 stripe intensity against time. n value: 60 cells. Error bars = SEM for three biological replicates.

of the laser stripe for NFLAP-BRCA2 still showed a somewhat higher intensity of signal than the nuclear background, indicating that BRCA2 also associates to some extent with the wider damage-associated chromatin, which is again consistent with Bekker-Jensen et al [65].

Quantification of the NFLAP-BRCA2 signal at stripes found that BRCA2 has already reached a plateau of association by 15 minutes and begins to associate as early as 5 minutes after damage (Figure 3.6C). BRCA2 localisation to laser-induced damage has in fact already been investigated by Zhang *et al* [83]; in this study, BRCA2 displayed a two-wave retention at damage sites, with the earlier wave peaking at around 30 seconds

and being dependent on PAR binding, and the second wave being PAR-independent and beginning to increase at around 5 to 10 minutes before reaching a plateau, similar to what I see here. I did not observe the earlier rapid wave of BRCA2 recruitment at all, despite having taken images within 1 minute of damage (which were not included in the quantification due to showing no visible BRCA2 recruitment). This discrepancy may be due to the different experimental systems used: Zhang *et al* transiently overexpressed GFP-BRCA2 in mouse embryonic fibroblasts, whereas my system stably expresses a more physiological level of NFLAP-BRCA2 in HeLa cells.

Regardless, the rate of BRCA2 recruitment that I did observe is notably faster than the rate of PLK1-YFP association with laser stripes, which does not begin to reach a plateau until at least 30 minutes if not longer (Figure 3.2). As such, it seems unlikely that PLK1 association with damage in S/G2 is a result of it binding to BRCA2 and being recruited along with it, since one would expect the association kinetics to appear the same if this were the case. Even so, it might be worthwhile to test this possibility further by examining PLK1 recruitment to damage in the absence of BRCA2.

3.2.8 Attempts to generate cells with a cell cycle-dependent reporter

Instead of having to estimate cell cycle phase based on the pattern of PLK1-YFP expression, synchronise cells prior to imaging, or not know the cell cycle phase of imaged cells at all (as was the case for the GFP-PLK1 activity mutants), it would be ideal to create a system in which cells also expressed a fluorescent reporter that labels cells depending on their position in the cell cycle. This is a similar concept to that of the FUCCI cell line

created by Sakaue-Sawano *et al*, in which G1-phase nuclei are labelled red and S/G2/M-phase nuclei are labelled green [216]. However, this exact system would not be compatible with my existing cell lines containing green-labelled PLK1 and a red-labelled DNA damage marker. As such, I attempted to use the same principle to create a single blue fluorescent marker, such that cell cycle phase could be determined by the presence or absence of blue fluorescence, which I could then express in my existing cell lines.

I generated a construct fusing blue fluorescent protein (BFP) to the minimum region of CDT1 (residues 30-120) that confers cell cycle-dependent degradation upon S phase entry but does not alter cell cycle progression [216]. The plasmid I created this construct in was pCEP4, for two reasons: the first was that it has a different antibiotic resistance marker than the tagged PLK1 and mCherry-BP1 constructs already present in my cell lines, and the second was that, as an epichromosomal plasmid, it should be retained upon cell division even with its low copy number, in theory making it easier to obtain stable transformants without the plasmid needing to integrate into the genome. Despite this, upon transfecting this plasmid into several of my existing microirradiation cell lines and selecting with antibiotic, not all colonies exhibited blue fluorescence. As such, it was still necessary to test individual clones.

In theory, these cell lines should exhibit CDT1-BFP expression in G1 phase but not in S, G2 or M phase. Unfortunately, attempts to verify this showed instead that CDT1-BFP expression remained constant throughout the cell cycle. I synchronised cells in mitosis using nocodazole and then released them into G1, expecting to see CDT1-BFP expression be minimal or nonexistent in mitosis, to increase upon G1 entry and then to decrease

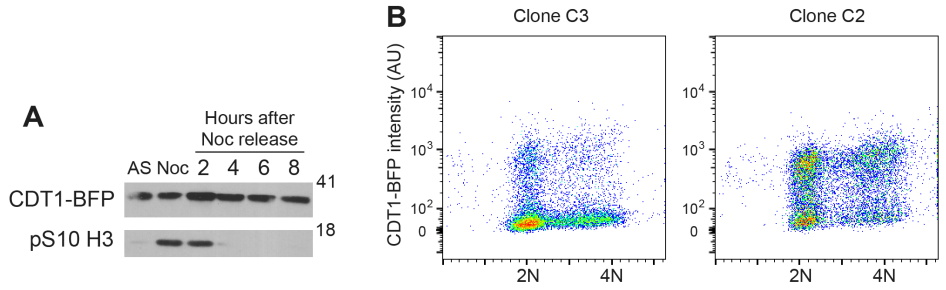


Figure 3.7: **Expression of CDT1-BFP did not vary throughout the cell cycle. A:** GFP-PLK1 mCherryBP1 CDT1-BFP cells were synchronised in mitosis with nocodazole and then released for the indicated amount of hours and the lysates probed via Western blot. CDT1-BFP was detected using anti-RFP. This was attempted with multiple cell lines; this cell line displayed the most successful mitotic release based on loss of the mitotic marker pS10 H3. **B:** FACS analysis of NFLAP-BRCA2 mCherry-BP1 CDT1-BFP cells grown asynchronously and stained with PI to mark DNA content, plotting BFP signal against PI signal. Two different stable CDT1-BFP clones (C2 and C3) are shown; other clones were also tested and most looked similar to clone C3.

as cells entered S phase if it was reached over the time course of the experiment. However, CDT1-BFP expression remained constant throughout (Figure 3.7A). As another, perhaps more robust way of testing this, I stained cells' DNA content with PI and used FACS analysis to compare DNA content with BFP fluorescence, hoping to see high BFP signal in 2N cells and low BFP signal in cells with a DNA content of greater than 2N. However, while some cells within a population did display a higher BFP content than others, this was completely independent of DNA content and therefore of cell cycle phase.

In hindsight, seeing this result for a CDT1-BFP construct should have been expected, as the original FUCCI paper mentions that the 30-120 fragment of CDT1 did not undergo cell cycle-dependent degradation when fused with certain fluorophores, including RFP [216], and BFP is an altered

version of RFP. In future, if I were to try again to create a construct to label cell cycle phase using blue fluorescence, it might be more promising to use Geminin, the protein used to mark S/G2/M phase in FUCCI cells, since this did not display any problems with cell cycle-dependent degradation when fused to a variety of different fluorophores. Such a cell line would instead exhibit blue fluorescence in S/G2/M phase and no fluorescence in G1 phase, but this would still allow identification of cell cycle phase in my existing cell lines using a single reporter.

3.3 Discussion

The work done in this chapter shows that PLK1 localises to sites of DNA damage in both S/G2 and, surprisingly, G1 cells. While I could not visualise PLK1 colocalisation with γH2AX foci in irradiated fixed cells, this is less surprising upon seeing the appearance of PLK1 at laser-induced damage stripes. Since PLK1 accumulation at damage is still relatively faint even when damage is so concentrated in a small area this way, it follows that PLK1 localising to more scattered damage foci might be so faint that it is difficult to see at all.

Laser microirradiation showed PLK1 localising to damage sites within 15 minutes of damage induction. This is a similar timeframe to that seen for RAD51 phosphorylation by PLK1 after damage [86], and for possible PLK1 activation upon damage in asynchronous cells as seen in our unpublished data from Dr. Lindqvist (Figure 1.6). This finding further backs up the idea that PLK1 is playing an active role in DNA repair during this earlier timeframe prior to being downregulated by the DNA damage checkpoint after 3-4 hours. In particular, this rate of PLK1 recruitment to damage sites

is similar to that seen for RAD51 and several other HR factors, while factors involved in other repair pathways or earlier steps in HR are recruited faster [217], which supports the idea that PLK1 is playing a role specifically in HR. Interestingly, a very recently published paper also briefly used laser microirradiation to investigate GFP-PLK1 localisation to damage sites and found recruitment within less than 60 seconds [218] (Figure S8 in the referenced paper). These much faster recruitment kinetics may be due to the fact that they overexpressed GFP-PLK1 rather than having it stably expressed at a more physiological level or tagging one of the endogenous alleles. Regardless, another group independently finding that PLK1 localises to laser-induced damage is encouraging.

The punctate appearance of the PLK1-YFP stripe in S/G2 cells suggests that PLK1 binds directly to ssDNA-associated microcompartments. This is supported by the fact that this matches the pattern I observed from NFLAP-BRCA2 under the same experimental conditions, and BRCA2 is already known to bind to these sites [65]. Use of RPA as a marker in future PLK1-YFP microirradiation experiments could help to confirm this further. Association of PLK1 directly with the resected DNA and not merely the wider DSB-flanking chromatin is perhaps unexpected given that PLK1's main currently-known function in repair is to phosphorylate RAD51 to facilitate its association with ssDNA via binding to MRN. PLK1 carrying out this function directly at sites of damage is potentially unnecessary, since any RAD51 it can access would therefore already be where it needs to be. This suggests that PLK1 might be performing a different, as-yet-unknown role at these sites instead. It is also relevant to note that only a small portion of nuclear PLK1 localises to damage sites, raising the question of whether only the damage-associated portion is playing a role in DNA repair, or whether

the non-damage-associated portion also contributes by targeting diffusible substrates (such as RAD51) that then relocalise to damage sites.

Perhaps unsurprisingly given PLK1's usual mechanism of localising to various subcellular compartments, PLK1 localisation to damage in G2 cells was found to be dependent on the PBD, and based on the evidence, these PBD binding sites are most likely primed by CDK2, but not CDK1. The question still remains of which CDK2-phosphorylated protein or proteins the PBD is binding to. Based on the PLK1-YFP localisation pattern, it may be another protein which is also associated with ssDNA-containing micro-compartments. However, this protein is unlikely to be BRCA2, as I found that BRCA2 localises to damage sites much faster than PLK1 does. Since the aim of Chapter 4 of this thesis is to identify interaction partners that PLK1 increases association with upon DNA damage, this question shall be discussed more later.

The effect of inhibiting CDK1 and PLK1 in G2 cells conversely suggests that relieving PBD binding sites elsewhere in the nucleus frees up more PLK1 molecules to localise to damage. This could be confirmed in future by inhibiting CDK1 and PLK1 in the PBD dead cell line; if the increase in damage association seen upon CDK1/PLK1 inhibition were PBD-dependent, it would not be seen there. Assuming this is the case, it suggests that the level of PLK1 association to damage sites seen in normal conditions is limited by the amount of free PLK1 molecules in the nucleus, rather than by PLK1 molecules at the damage sites having reached saturation. This would also potentially explain the discrepancy between my data and that from Li *et al* [218] which found much faster GFP-PLK1 recruitment kinetics when it was overexpressed. Overexpression would vastly increase the amount of unbound, freely-available PLK1 molecules in the nucleus, which, if this

limiation model is true, would naturally lead to more GFP-PLK1 being recruited, and perhaps faster as well. I never attempted laser microirradiation with transient overexpressed GFP-PLK1, but this could also be worth trying to corroborate this and determine if this, rather than other differences in experimental conditions, is the reason for the discrepancy between my data and Li *et al*'s.

PLK1 localisation to damage sites was also found to be dependent on ATM activity. This raises the question of which of the many functions of ATM is important for this localisation. PLK1's localisation to resected DNA in S/G2 might suggest that the requirement of ATM involves ATM's role in activating resection. It is also possible that ATM's effect on PLK1 localisation in S/G2 is due to it conferring damage recruitment of a PBD- and CDK2-dependent binding partner of PLK1. However, this cannot be the full story, as ATM is also required for PLK1 localisation to damage in G1 cells, in which resection does not occur and PLK1's localisation pattern indicates binding to the wider damage-associated chromatin, and in which PLK1's PBD and CDK2 activity are not required for its recruitment.

The fact that PLK1 was seen localising to damage in G1 cells is in and of itself remarkable, since PLK1's main characterised roles in active repair relate to HR, which does not take place in G1. This could support the possibility that PLK1 plays a role in repair pathways other than HR, although it is still questionable whether its localisation to G1 damage sites necessarily means it is carrying out a function there, since PLK1 should be largely inactive in G1. The apparent requirement of CDK1 activity for PLK1 damage association in G1 does little to shed light on this, since CDK1 should also be largely inactive in G1, and as such this may simply be a HeLa cell line-specific effect which would need to be confirmed by repeating these

experiments in a different cellular background. However, the observed requirement for ATM activity in order for PLK1 to associate with damage in G1 could be a useful clue. Given that ATM is required in both G1 and S/G2, its important function in terms of PLK1 damage association is most likely one of the cell cycle-independent roles of ATM and not only its S/G2-specific role in activating resection.

This important role of ATM might potentially be its involvement in generation of γH2AX-containing chromatin around damage sites and the many proteins that associate with it. Despite the pattern of PLK1-YFP damage association in S/G2 suggesting direct binding close to resected DNA, it is possible that some PLK1-YFP is also associating with the wider γH2AX-containing chromatin to an extent that is not notably visible over the nuclear background signal in S/G2 cells. This initial association could potentially serve to concentrate PLK1 near damage to aid its PBD in binding directly to the sites of resected DNA. It would be difficult to determine whether or not PLK1 truly is binding to damage-associated chromatin in S/G2 despite the nuclear background signal, however. Perhaps using fixed-cell microscopy methods with a pre-clearing step to wash out the majority of PLK1 not strongly associated to chromatin would help with this, or ChIP-based approaches to determine PLK1's proximity to γH2AX in the genome upon damage. If it were true that PLK1 partly associates with the wider damage-induced chromatin in S/G2, PLK1 also associating with damage-induced chromatin in G1 cells may merely be a result of the fact that it does so in a cell cycle-independent manner and not necessarily a reflection of PLK1 having any repair-related function at damage sites during G1.

I ruled out the possibility that ATM's requirement for PLK1 localisation to damage is related to PLK1 activity by showing that even constitutively-

active T210D PLK1 is still just as affected by ATM inhibition. As such, even if ATM is helping to activate PLK1 upon damage, as our data from Dr. Lindqvist may be indicating, and PLK1 activity aids its recruitment to damage, ATM must also play another upstream role in PLK1 recruitment.

However, my data does not clearly answer the question of whether PLK1 activity is important for its localisation to damage in the first place. The effect of the activity mutants of GFP-PLK1 on localisation indicates that activity is at least partially important, although the increase seen in the T210D mutant could be PBD-related, since T-loop phosphorylation and PBD binding activity in PLK1 are closely linked. On the other hand, the effect of inhibiting PLK1 using a small-molecule inhibitor suggests that PLK1 activity is not so important. However, the global nature of this inhibition could be causing wider effects unrelated to the damage-associated portion of PLK1 that mask the effect on PLK1 specifically at the damage sites.

Given the association of PLK1 to damage sites in G1 as well as S/G2, it perhaps makes sense that PLK1 activity may not be especially important for its recruitment, since only a minimal portion of PLK1 in G1 should be active. Approximately the same fraction of nuclear PLK1 is recruited to damage in G1 and S/G2, which, combined with the fact that a much larger fraction of PLK1 should be active in S/G2, suggests that activity of an individual molecule is not a strong requirement for localisation to damage. However, the model discussed in Figure 1.7, which is potentially supported by our FRET data from Dr. Lindqvist (Figure 1.6), suggests the possibility that basal PLK1 activity could increase upon damage, in order to facilitate its roles in DNA repair. This could mean that PLK1 association to damage in G1 is still mostly the portion of PLK1 which is active, if it is true that a higher portion of G1 PLK1 becomes activated after damage induction. The

inability to determine cell cycle phase in my PLK1 activity-mutant cell lines makes this difficult to confirm or deny from the data presented here alone. My attempts to generate a PLK1-independent fluorescent reporter for cell cycle phase were unsuccessful, but successfully doing so in future would enable investigation into how the cell cycle regulates the effect of these activity mutants of PLK1 on its localisation to damage.

Chapter 4

PLK1 interaction partners upon damage

4.1 Introduction

Most work so far examining PLK1 in early timeframes upon DNA damage has been focused on the downstream effects of PLK1: its role in phosphorylating substrates such as RAD51 and the function this serves for repair. Currently, very little is known about the upstream factors. What, if anything, regulates PLK1 in a damage-dependent manner to allow it to carry out these specific repair-related functions during this early timeframe? It is true that the phosphorylation of RAD51 by PLK1 is not only restricted to damage conditions but also occurs in unperturbed cells, suggesting it is in part a passive process. Still, the peak of pS14 RAD51 seen at 20-40 minutes post damage implies a specific regulation of PLK1 during this timeframe upon damage [86]. This regulation could be on one or multiple levels: increasing the activation level of PLK1; increasing the binding of PLK1 to specific proteins, such as to BRCA2 or TOPBP1 to bridge the interaction with its

substrate RAD51; or increasing the amount of PLK1 localised directly at the site of damage, as I discovered was the case in Chapter 3.

While my work in the previous chapter identified certain upstream regulators of PLK1's localisation to damage, namely ATM and CDK2, and ruled out others like CDK1, I was limited to a top-down approach, investigating known factors that I could already expect to potentially play a role. In this chapter, I employ a bottom-up approach, using quantitative shotgun proteomics to find novel PLK1 binding partners. Specifically, I do so across a DNA damage time course in the hope of identifying proteins whose association with PLK1 changes during early timepoints after damage induction. This should reflect a damage-specific functional interaction of such proteins with PLK1, opening up new avenues of investigation into how PLK1's role in DNA repair is regulated.

4.1.1 Outline and optimisation of experimental setup

The design of the proteomics experiment was to pull down tagged PLK1 in cells across a DNA damage time course and then analyse the immunoprecipitated proteins via liquid chromatography tandem mass spectrometry (LC-MS/MS) to examine PLK1 interaction partners at different timepoints post-damage. Like for the microscopy experiments in Chapter 3, I initially tested out two different cell lines for this: HeLa Kyoto PLK1-LAP cells or HeLa Kyoto PLK1-YFP cells, so that I could use anti-GFP beads for the pulldown. In both cases, HeLa cells stably expressing GFP alone were used as a negative control.

The protocol I used to lyse cells, pull down tagged PLK1 and prepare the eluted proteins for LC-MS/MS analysis underwent many attempted optimisations, detailed in Table 4.1. My aim was to create a protocol which con-

sistently obtained an adequate number of peptide spectral matches (PSMs) of both total proteins and PLK1. The protocol performed on 16/06/2015 as shown in Table 4.1 managed to produce a more than satisfactory amount of PSMs: over 10,000 total PSMs and over 1,000 PLK1-LAP PSMs. However, this was only carried out with an undamaged sample of cells, and attempts to perform this with multiple samples of cells harvested at different timepoints post-damage did not produce results consistent with this. As such, I continued to attempt to optimise my protocol to find one that was more consistent. I switched between PLK1-LAP and PLK1-YFP cell lines with the hope that the native expression of the CRISPR-tagged PLK1-YFP might work better than the pseudo-native expression of PLK1-LAP in PLK1's surrounding locus on a BAC vector. I tried fractionating cells and using only the nuclear fraction, with the logic that any PLK1 interaction partners restricted to the cytoplasm would not be playing a role in DNA repair and would therefore not be relevant to my investigation. I adjusted the number of plates of cells used, the amount of beads used for the pre-clearing and pulldown steps, and the methods used for digesting and de-salting the eluted proteins to prepare them for mass spectrometry, all of which is listed in Table 4.1 and described in more detail in Sections 2.6 and 2.7. Unfortunately, for a long time, nothing worked to bring my output of PSM numbers close to what they had once been.

The breakthrough came with the help of other members of the lab, who had been working on similar mass spectrometry-based analyses of different proteins. They had optimised a protocol for cell lysis and immunoprecipitation which was somewhat different from the one I had been using, and which fortunately turned out to work well for PLK1 as well. This new protocol used a much lower amount of detergent for both the cell lysis and bead

Date	cell line	# 15 cm plates per sample	extract type	mg of protein extracted	IgG beads per ml lysate	GFP beads per ml lysate	elution volume	digest method	C18?	# total PSMs	# PLK1 PSMs
01/05/2015	PLK1-LAP	3	whole cell	8.64	None	10 µl	1x bead volume, thrice; 1/3 used	TCA precipitation, then high salt	yes	3499	13
02/06/2015	PLK1-LAP	3	whole cell	12.18	12.5 µl	5 µl	1x bead volume, twice	FASP	yes	28273	120
16/06/2015	PLK1-LAP	3	whole cell	22.48	12.5 µl	5 µl	1x bead volume, twice; 1/2 used	FASP	yes	15049	1385
15/08/2015	PLK1-YFP	4	nuclear	7.2	20 µl	10 µl	1x bead volume, twice	low salt in-solution	no	14000	400
16/10/2015	PLK1-YFP	4	nuclear	9.6	20 µl	10 µl	2x bead volume, twice	high salt in-solution	yes	1800	180
04/12/2015	PLK1-YFP	1	whole cell	2.5	40 µl	10 µl	2x bead volume, twice	high salt in-solution	yes	3000	210
27/01/2016	PLK1-YFP	1	whole cell	9.83	40 µl	10 µl	2x bead volume, twice	high salt in-solution	yes	9452	36
10/03/2016	PLK1-YFP	2	whole cell	12.57	40 µl; overnight	6.6 µl	2x bead volume, twice	high salt in-solution	yes	4374	195
24/03/2016	PLK1-YFP	1	whole cell	not recorded	40 µl	6.6 µl	2x bead volume, twice	high salt in-solution	yes	800	80
12/04/2016	PLK1-LAP	1	whole cell	not recorded	40 µl	6.6 µl	2x bead volume, twice	high salt in-solution	yes	2000	550
21/04/2016	PLK1-LAP	1	whole cell	6.15	40 µl	6.6 µl	2x bead volume, twice	low salt in-solution	no	3004	182
	PLK1-LAP	1	whole cell	6.15	20 µl	10 µl	2x bead volume, twice	low salt in-solution	no	3407	21
29/09/2016 & onwards (final)	PLK1-LAP	2	whole cell; synchronised	4.5 (average)	50 µl	15 µl	2x bead volume, twice	high salt in-solution	no	6500 (average)	850 (average)

Table 4.1: **Optimisation attempts for mass spectrometry protocol.** Each row represents a different attempt at preparing samples for mass spectrometry and lists the different conditions and methods used. Further details of these protocols can be found in Chapter 2. The bottom row represents the final, successful protocol: all biological repeats used to generate the data presented henceforth in this chapter were prepared using these conditions.

washing steps (described in more detail in Section 2.6), which still extracted a similar amount of protein but perhaps resulted in less interference with the mass spectrometer, even though the detergent we used was already mass spectrometry-compatible.

The other major factor that I changed for this final attempt was the decision to prepare cells by synchronising them in G2 phase. This would both maximise PLK1 expression and therefore amount of PLK1 pulled down, and also enrich for cells in which HR was occurring, reducing the proportion of interaction partners that would be less relevant to the main purpose of my experiment. PLK1-LAP cells (chosen for this simply because they displayed a slightly higher expression of tagged PLK1 than PLK1-YFP cells) were synchronised through a double thymidine block followed by a release of 8 hours, which I determined gave the highest proportion of cells in G2 (Figure 4.1A). Preliminary LC-MS/MS analysis on a PLK1-LAP pulldown in a G2-synchronised sample versus an asynchronous sample confirmed the effectiveness of the synchronisation: the G2 sample contained many more PSMs for PLK1 than the asynchronous sample and identified known PLK1 interaction partners, such as Bora, which were not identified in the asynchronous sample (data not shown). Most importantly, with this synchronisation and this new protocol, I was able to obtain a satisfactory number of PSMs for total protein as well as PLK1 (Table 4.1; 29/09/2016). This was

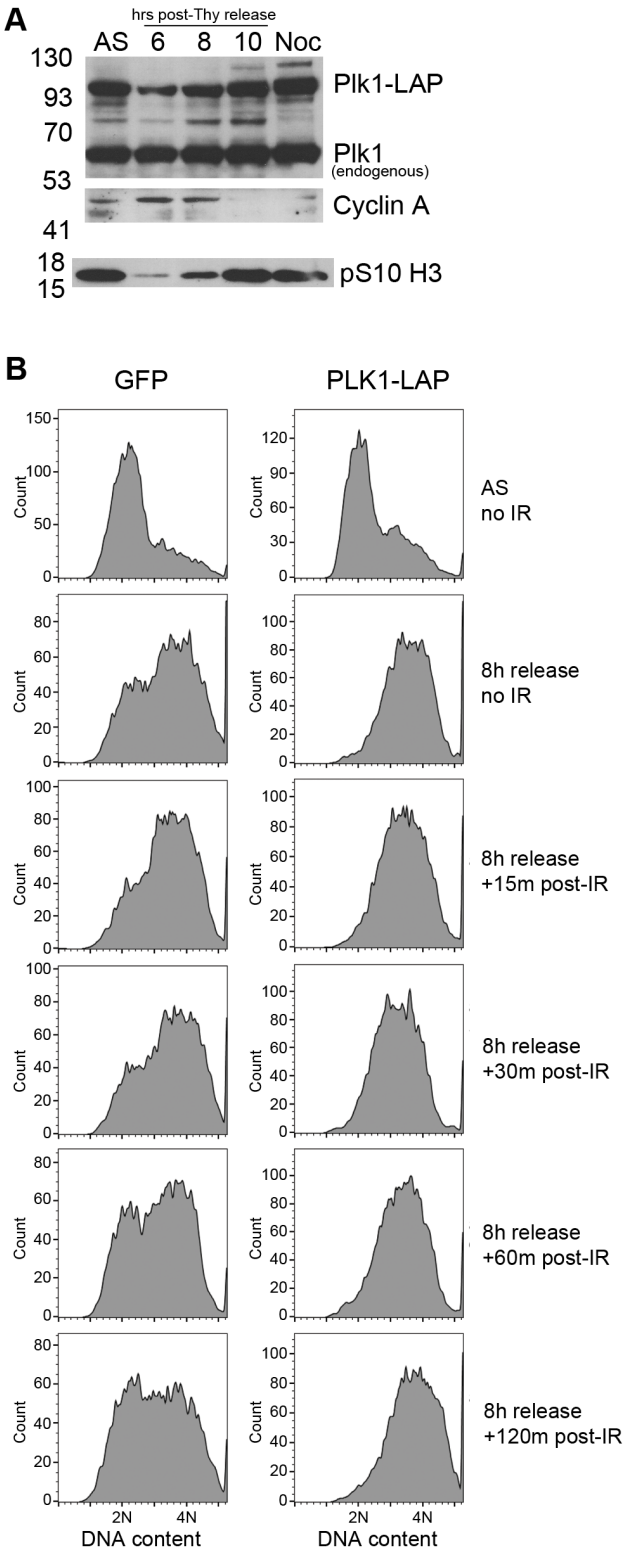


Figure 4.1: **Confirmation of cell synchronisation for proteomics. A:** PLK1-LAP cells either grown asynchronously, synchronised with a double thymidine block and released for the indicated time or synchronised with nocodazole for 16 hours were lysed and the lysates blotted with antibodies for PLK1, Cyclin A (S-phase marker) and phospho-S10 H3 (M-phase marker). The 8-hour release was chosen due to having the best middle-ground between these two markers and therefore presumably the most cells in G2. **B:** GFP or PLK1-LAP cells were either grown asynchronously or released for 8 hours from a double thymidine block. Cells were then irradiated if indicated with 4 Gy of radiation and allowed to recover for the indicated times, then fixed, stained with propidium iodide and analysed with flow cytometry. Each histogram contains approximately 10,000 cells.

still not as good an output as the sample from 16/06/2015 had produced, but it would be adequate for statistical analysis.

To carry out a DNA damage time course, cells were first synchronised in G2 as above, then either harvested while still undamaged (hereafter referred to as the ”0 minute” sample), or irradiated with 4 Gy and then harvested at 15, 30, 60 or 120 minutes after irradiation. Lysates from these cells were immunoprecipitated with GFP beads and the resulting elutions analysed via LC-MS/MS. Three replicates for both GFP control and PLK1-LAP were prepared, and an input sample was also analysed for one replicate of each. Flow cytometry analysis of separate samples prepared in the same way confirmed that the DNA damage checkpoint arrested the damaged cells in G2, albeit somewhat less robustly for the GFP cell line (Figure 4.1B).

Statistical analysis described in Section 2.7.7 identified proteins significantly enriched ($p < 0.05$) in the PLK1-LAP sample over the GFP sample in at least one timepoint. Additionally, to control for naturally abundant proteins, all proteins with a higher average number of PSMs per sample across all input samples compared to across all PLK1-LAP IP samples were discounted.

4.2 Results

Identified PLK1 interaction partners of interest are shown in Figure 4.2, which depicts volcano plots of Signal-to-Noise (STN) ratios and the corresponding p-values of PLK1 binding partners for each timepoint.

4.2.1 PLK1 interaction partners related to the cell cycle

As expected, one of the most abundant proteins detected in PLK1-LAP pull-downs was PLK1's binding partner Bora. Less abundantly, I also detected other known PLK1 interactors: PICH, which localises PLK1 to chromosome arms to promote chromatin condensation [219] [220]; MISP, which PLK1 phosphorylates to promote proper spindle orientation [221]; PRC1, which localises PLK1 to the central spindle during anaphase [222]; and CDC6, which is most widely known as a key factor in replication initiation [223], but which PLK1 has only been found to interact with in anaphase by phosphorylating it to promote chromosome segregation [224]. These proteins interact with PLK1 during mitosis, so this perhaps reflected the small portion of the cells that were mitotic after the 8-hour release.

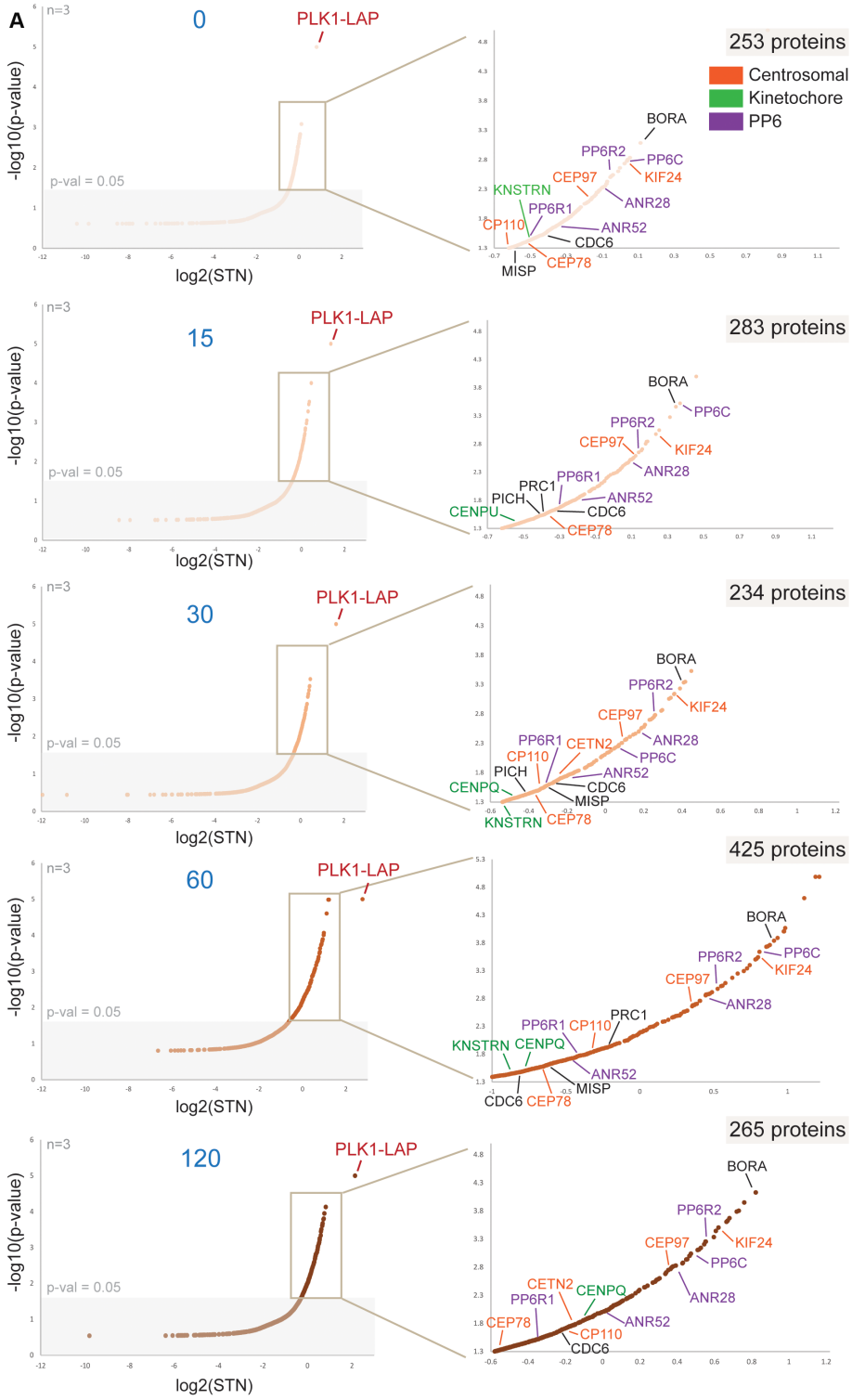
As a reflection of the portion of PLK1 which was localised to kinetochores, I identified centromere proteins CENPU (also known as PBIP), which is known to bind PLK1 and recruit it to pre-kinetochores during G2 [225], and CENPQ, which PLK1 phosphorylates via its binding to CENPU to dissociate it from kinetochores upon mitotic entry [226]. I also found Kinastrin, part of a complex with Astrin which promotes stable microtubule-kinetochore interactions and has been shown to interact with PLK1 [227].

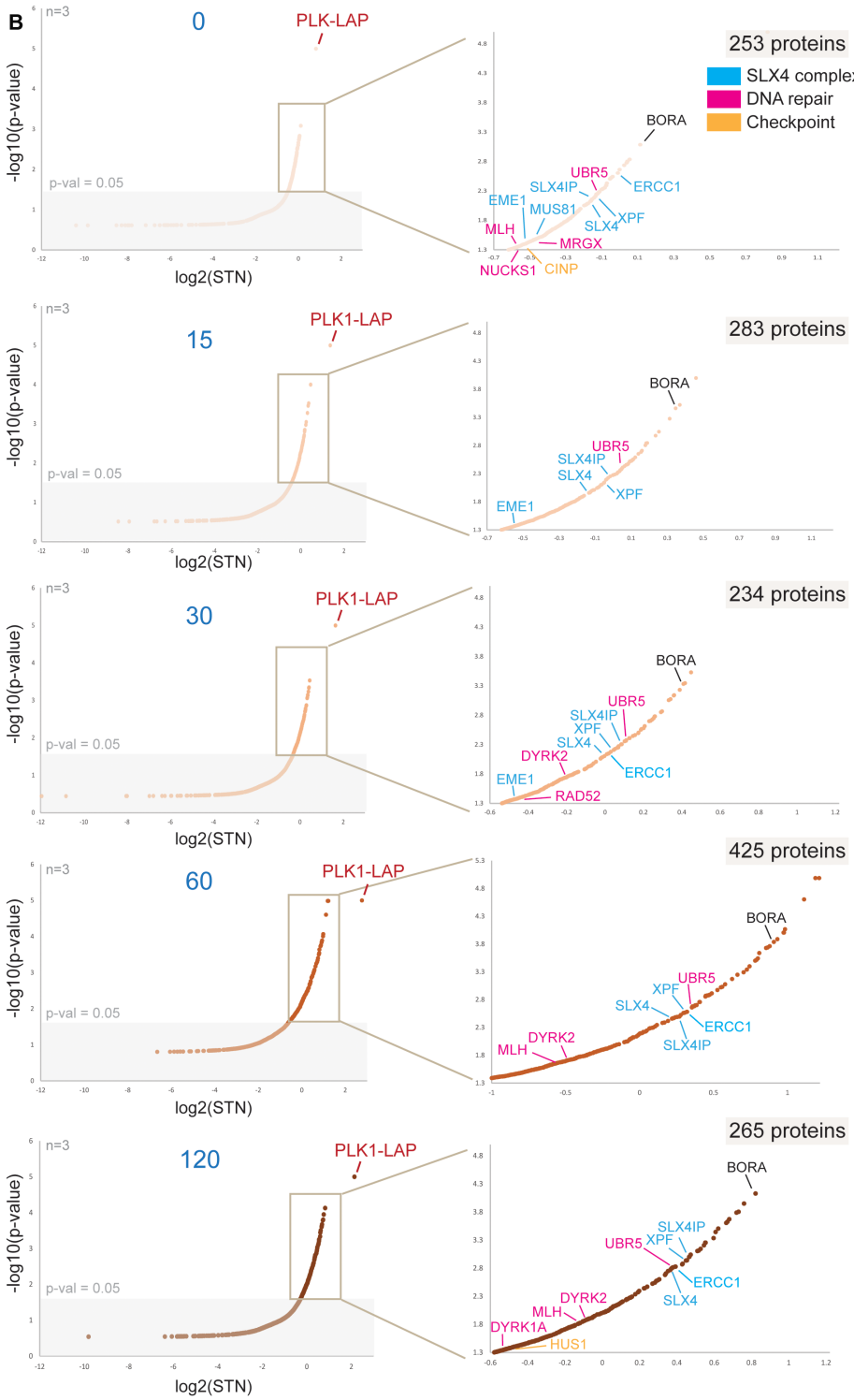
Meanwhile, I identified a number of centrosomal proteins most likely reflecting PLK1's localisation there, although, interestingly, none of these were proteins that have been previously reported to directly interact with PLK1. These proteins were CP110, CEP97, and KIF24, which are involved in cilia disassembly [228] [229], Centrin2 (CETN2), which promotes cilia assembly by removal of CP110 [230], and CEP78, which aids in centriole duplication by recruiting PLK4 [231]. The fact that multiple of these centrosomal proteins identified have similar roles suggests that their detection

here is not random noise but reflects some kind of functional relationship with PLK1. Seeing CP110 and CEP78 here may also be related to the fact that CP110 is ubiquitylated and targeted for degradation by UBR5 in a manner inhibited by CEP78 [232], and UBR5 is another protein identified as a relatively abundant PLK1 binding partner, as will be discussed later. While centriole maturation and cilium biogenesis is not at all the focus of this work, the novel finding that PLK1 associates with these proteins may be of interest to people in the relevant field.

Perhaps one of the most interesting novel associations with PLK1 I identified is that of protein phosphatase 6 (PP6) complex members, all of which were identified with relatively high confidence and abundance. PP6 acts as a heterotrimeric complex [233] (Figure 4.3C) consisting of the catalytic subunit PP6C, a regulatory subunit containing a SAPS domain, of which PP6R1 and PP6R2 were detected here, and a regulatory subunit containing ankyrin repeats, of which ANR28 and ANR52 were detected here. Based on the detected abundances of each subunit – PP6C the highest, PP6R2 and ANR28 the next highest and similar to each other, and then PP6R1 and ANR52 lower and also similar to each other (Figure 4.3D) – the data suggests that PLK1 primarily associates with a PP6C/PP6R2/ANR28 complex and then to a lesser extent with a PP6C/PP6R2/ANR52 complex. The

Figure 4.2: [*following pages*] **Volcano plots of notable significant PLK1 interaction partners.** Signal-to-Noise ratios (STN) were plotted against p-values for all proteins as indicated. Only proteins with positive STN values were included in each graph. Time post-damage in minutes is indicated above each leftmost plot. Right: Zoomed plots showing only proteins with p-values of <0.05. Proteins not enriched in IP over input sample were also included in these plots. **A:** Proteins of interest with functions related to the cell cycle are labelled. **B:** Proteins of interest with functions related to DNA damage are labelled, along with Bora.


A
n=3
0
PLK1-LAP
253 proteins
Centrosomal
Kinetochore
PP6
-log10(p-value)
p-val = 0.05
log2(STN)
BORA
PP6R2
PP6C
KIF24
CEP97
KNSTRN
ANR28
PP6R1
CP110
ANR52
CDC6
CEP78
MISP
n=3
15
PLK1-LAP
283 proteins
-log10(p-value)
p-val = 0.05
log2(STN)
BORA
PP6C
PP6R2
CEP97
KIF24
ANR28
PP6R1
PRC1
PICH
ANR52
CENPU
CDC6
CEP78
n=3
30
PLK1-LAP
234 proteins
-log10(p-value)
p-val = 0.05
log2(STN)
BORA
PP6R2
KIF24
CEP97
PP6R1
CETN2
ANR28
CP110
PP6C
PICH
ANR52
CENPQ
CDC6
MISP
KNSTRN
CEP78
n=3
60
PLK1-LAP
425 proteins
-log10(p-value)
p-val = 0.05
log2(STN)
BORA
PP6C
PP6R2
KIF24
CEP97
ANR28
PP6R1
CP110
PRC1
KNSTRN
CENPQ
ANR52
MISP
CDC6
CEP78
n=3
120
PLK1-LAP
265 proteins
-log10(p-value)
p-val = 0.05
log2(STN)
BORA
PP6R2
CEP97
KIF24
PP6C
CETN2
CENPQ
ANR28
PP6R1
CEP78
ANR52
CP110
CDC6


B
n=3
0
PLK-LAP
253 proteins
SLX4 complex
DNA repair
Checkpoint
-log10(p-value)
p-val = 0.05
log2(STN)
BORA
UBR5
SLX4IP
ERCC1
EME1
MUS81
XPF
SLX4
MLH
MRGX
NUCKS1
CINP
n=3
15
PLK1-LAP
283 proteins
-log10(p-value)
p-val = 0.05
log2(STN)
BORA
UBR5
SLX4IP
SLX4
XPF
EME1
n=3
30
PLK1-LAP
234 proteins
-log10(p-value)
p-val = 0.05
log2(STN)
BORA
UBR5
SLX4IP
XPF
SLX4
DYRK2
ERCC1
EME1
RAD52
n=3
60
PLK1-LAP
425 proteins
-log10(p-value)
p-val = 0.05
log2(STN)
BORA
UBR5
XPF
SLX4
ERCC1
DYRK2
MLH
SLX4IP
n=3
120
PLK1-LAP
265 proteins
-log10(p-value)
p-val = 0.05
log2(STN)
BORA
SLX4IP
UBR5
XPF
ERCC1
DYRK2
SLX4
MLH
DYRK1A
HUS1

association of PLK1 with PP6C, PP6R2 and ANR28 was confirmed by immunoblotting (Figure 4.3A).

Kettenbach *et al* [234] recently published a similar proteomic analysis of PLK1 interaction partners in mitosis. In agreement with my data, they found PLK1 associating with PP6 complex members, with a preference for PP6R2/ANR28 over the other regulatory subunits. They went on to show that PLK1 binding to PP6R2 is PBD-dependent, primed by CDK1, and that PLK1 phosphorylation of PP6R2 prevents PP6C from dephosphorylating Aurora A's T-loop [235], thus creating a positive feedback loop for PLK1's own activation.

4.2.2 PLK1 interaction partners related to the DNA damage response

Several of the PLK1 interaction partners reported in the previous section also have characterised roles in DNA repair. One of these is the PP6 complex: PP6C and PP6R1 are required for DNA-PK activation upon damage [236], although the mechanism for this is unclear. DNA-PK also recruits PP6 to sites of damage where it dephosphorylates γH2AX, which is important for HR [237] [238]. PLK1 has not yet been implicated in anything related to this; it does also interact with DNA-PK and phosphorylate it in mitosis [239], but the purpose of this is currently still unclear and likely involves DNA-PK's additional functions in mitosis that are unrelated to the DNA damage response. As such, it is uncertain whether PLK1's interaction with PP6 has any relevance to DNA repair. I attempted to look into PP6's effect on PLK1 myself, as will be described in Chapter 5, but only briefly.

Another previously-mentioned protein related to DNA damage is CDC6, which is implicated in the S-M phase checkpoint. CDC6 detects replication

stress in S phase and prevents mitotic entry by activating ATR/CHK1 [240] [241]. However, again, since PLK1 already has a characterised interaction with CDC6 that is unrelated to this, it seems unlikely that PLK1 would be playing a role in CDC6's checkpoint function.

A known set of repair-related PLK1 interaction partners that I identified are the members of the SLX4 complex [242] (Figure 4.3E). SLX4 acts as a scaffold for multiple structure-specific endonucleases, including ERCC1 and XPF, which are involved in interstrand cross-link repair, and MUS81 and EME1, which, in conjunction with SLX4, resolve double HJs that form after HR. SLX1 is an additional member of this complex which also plays a role in HJ resolution in conjunction with SLX4, yet SLX1 was the only SLX4 complex member that was not identified as a PLK1 interaction partner here. PLK1 is known to bind to SLX4 in a manner partially dependent on a potential PBD-bound phosphosite at S1453 [243]. As described in Section 1.1.5, PLK1, along with CDK1, temporally regulates the association of SLX4 with MUS81 by phosphorylating SLX4, ensuring that MUS81's HJ resolution function is restricted to late G2 and early mitosis [91].

I also identified several DNA repair-related proteins that had not previously been reported to interact with PLK1. MLH1 is one of several proteins involved in mismatch repair [244], although none of the other proteins involved in this pathway were identified here. HUS1 is part of the RAD9-HUS1-RAD1 9-1-1 clamp complex, which binds to DNA damage and facilitates ATR phosphorylating CHK1 [245]. However, the other two members of the 9-1-1 complex were not identified. Another checkpoint-related protein I identified was CINP, which interacts with ATRIP to aid ATR signalling [246].

Some of the identified proteins have roles in HR. NUCKS1, a paralogue

of RAD51-associated protein 1, has been implicated in promoting efficient HR in a manner which is still not clearly defined [247]. MRGX was recently identified by our lab as a highly abundant binding partner of PALB2 alongside MRG15, though MRGX depletion did not affect PALB2 chromatin association, so its role in regulating PALB2 remains unclear [248]. Perhaps the most interesting HR-related PLK1 binding partner identified is RAD52, which in yeast fills a similar role to that of BRCA2 in humans, being required for RPA-RAD51 exchange on resected ssDNA. Human RAD52 alone is not necessary for efficient HR, but RAD52 mutants are synthetically lethal with mutants in several HR proteins such as BRCA1, BRCA2 and PALB2, suggesting RAD52 plays an important backup role. The exact roles of human RAD52 in HR are still being uncovered, but it can promote ssDNA annealing even in the presence of RPA, aiding the formation of dHJs [249].

One of the most abundant PLK1 interaction partners related to DNA damage I identified was a ubiquitin ligase, UBR5, also known as EDD. Interestingly, although at much lower abundance, I also identified the dual-specificity protein kinase DYRK2, which is required for assembly of the E3 ubiquitin ligase complex containing UBR5 [250], as well as its more well-characterised family member DYRK1A. Finding these proteins was intriguing enough that I decided to follow this up with further investigation, which will be the subject of Chapter 5 of this thesis. As such, a full description of UBR5 and DYRK2's known roles in DNA damage and relation to each other will be saved for then. For now, like for the PP6C complex, association of UBR5 with PLK1 was confirmed by immunoblotting (Figure 4.3A). Unfortunately, due to the lack of a strong enough antibody (as discussed further in Section 5.2.2), the same could not be done for DYRK2.

4.2.3 Change in PLK1 interaction partners upon DNA damage

The main purpose of performing a DNA damage time course with this experiment was to examine proteins for which their extent of interaction with PLK1 changed noticeably after DNA damage induction. However, the majority of proteins simply showed a slight decrease in association with PLK1 across the time course; Figure 4.3B shows the averaged relative association with PLK1 for all proteins which were identified in all five timepoints. This may simply reflect the fact that the amount of PLK1-LAP detected increased slightly throughout the time course, and therefore the calculated PLK1 association of a protein for which the detected abundance remains constant would decrease. Most of the PLK1 interaction partners discussed above, including SLX4 complex members, PP6 complex members, and UBR5, showed a similar gradual decrease across the time course (Figure 4.3D, F, G). Given that this is the same pattern shown by almost every protein detected, even those unrelated to damage, it is difficult to conclude that this reflects any meaningful change in these particular proteins' interaction with PLK1 upon DNA damage.

However, one very notable exception to this is DYRK2. DYRK2 was not detected at all in the 0 minute (undamaged) timepoint, but was present in a very small amount 15 minutes after damage and at higher amounts from 30 minutes onwards (Figure 4.3F). This suggests that DYRK2's interaction with PLK1 is promoted in a damage-dependent manner that occurs during the early timeframe I am interested in, when PLK1 is actively playing a role in DNA repair by phosphorylating RAD51. Meanwhile, the association of the related protein DYRK1A remained relatively constant across the time course (Figure 4.3F), further supporting the idea that DYRK2's PLK1 association is regulated in a specific manner that is not shared by similar

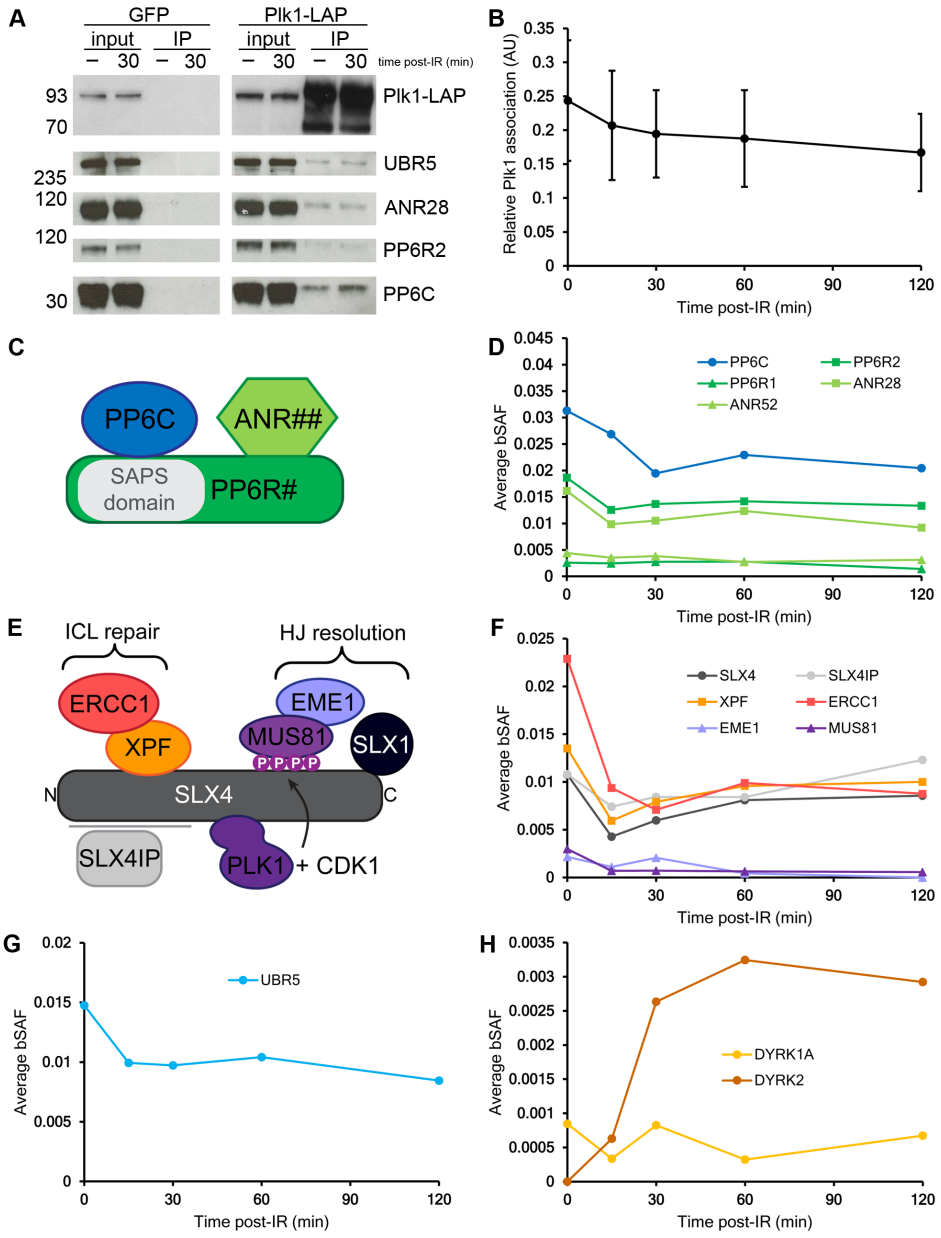

A
GFP
Plk1-LAP
input
IP
input
IP
– 30 – 30 – 30 – 30
time post-IR (min)
93
70
Plk1-LAP
235
120
UBR5
ANR28
120
PP6R2
30
PP6C
B
Relative Plk1 association (AU)
Time post-IR (min)
C
PP6C
ANR##
SAPS domain
PP6R#
D
PP6C
PP6R2
PP6R1
ANR28
ANR52
Average bSAF
Time post-IR (min)
E
ICL repair
HJ resolution
ERCC1
XPF
EME1
MUS81
SLX1
P P P P
N
SLX4
C
SLX4IP
PLK1 + CDK1
F
SLX4
SLX4IP
XPF
ERCC1
EME1
MUS81
Average bSAF
Time post-IR (min)
G
UBR5
Average bSAF
Time post-IR (min)
H
DYRK1A
DYRK2
Average bSAF
Time post-IR (min)

Figure 4.3: **PLK1 interaction partners of interest. A:** GFP and PLK1-LAP cells were synchronised in G2 with an 8-hour release from double thymidine block then either lysed, or irradiated with 4 Gy, allowed to recover for 30 minutes and then lysed. GFP was immunoprecipitated from lysates and input and IP samples were blotted with PLK1, UBR5, ANR28, PP6R2 and PP6C antibodies. **B:** Average bSAF values from the 130 significant protein hits that were identified in all five timepoints were normalised by dividing the average bSAF values at each timepoint by the sum of all five timepoint's average bSAF values for that protein. Using this normalisation, if the level of a protein's association with PLK1 across the time course remained exactly constant, the normalised values should be 0.2 at each timepoint, regardless of the protein's overall abundance. These values were then averaged for all 130 proteins and plotted against time. Error bars = SEM. **C:** Cartoon depiction of the PP6 complex. # denotes multiple possible numbers, due to there being several different SAPS domain-containing and ankyrin repeat subunits. **E:** Cartoon depiction of the SLX4 complex. Of the proteins shown, only SLX1 was not identified here as a PLK1 interaction partner. **D, F-H:** Average bSAF values for the indicated proteins plotted against time. All bSAF values were calculated by normalising the indicated protein's SAF value (a measure of its abundance within the sample [203]) against the bait (PLK1-LAP) SAF value for that sample.

proteins. This is an extremely promising result, which, along with DYRK2's established roles in DNA damage and connection to another novel PLK1 interaction partner UBR5, is another part of the reason I decided to follow up this finding in Chapter 5.

Another protein with an intriguing change in PLK1 interaction across the DNA damage time course was PICH, which was only detected in the 15, 30 and 60 minute timepoints. PICH also plays a role in DNA repair: during anaphase, it binds to ultrafine DNA bridges caused by incomplete chromosome replication and recruits a protein complex that resolves the bridge to allow chromatids to separate without breaking [251]. However, PICH is localised in the cytoplasm during interphase [252] and can only access chromatin after nuclear envelope breakdown. Therefore, the chances of PICH playing a role in DNA repair outside of mitosis seems unlikely.

A number of other proteins were only found associated with PLK1 in certain timepoints across the time course. However, in most cases these were proteins with very low abundance, and none aside from DYRK2 showed a clear trend of increasing association with PLK1 after damage induction. As such, it is difficult to conclude that any of the variation in PLK1 association across the time course seen for these proteins is functionally relevant rather than just a product of the noisiness of the data.

RAD52 is one such protein identified only in the 30 minute timepoint, and given RAD52's role in regulating RAD51, along with PLK1's role in phosphorylating RAD51 at approximately this time post-damage, this could potentially reflect a functional interaction. It is possible that RAD52 could be acting as another scaffold to bridge between PLK1 and RAD51, especially since it contains two potential PBD-binding sites. These sites are at residues 281 and 300, which are close or overlapping with RAD52's RAD51-interaction region at 291-330 [253], making PLK1 or RAD51 binding to a single RAD52 molecule mutually exclusive. However, RAD52 exists as a homoheptameric complex [249], meaning that it could still potentially bridge PLK1 and RAD51 if each of them were bound to different subunits. Investigation into whether this is indeed the case could be a promising avenue to go down in future.

4.3 Discussion

In this chapter, I identified many novel PLK1 interaction partners, several of which have known roles related to DNA repair. In most cases, it is not immediately clear how these proteins could be interacting with and regulating PLK1, if they indeed do so at all, so most of these findings are not being

followed up in this work. Regardless, this dataset still provides a useful source of potential candidates for investigation in the future. I also discovered some novel PLK1 interaction partners unrelated to damage that could be of interest to groups working in different fields.

The original main intent of this proteomics approach was to identify proteins for which their association with PLK1 changes notably across the DNA damage time course, under the belief that such proteins would be regulating PLK1 in a manner relevant to its role in DNA repair. However, the majority of proteins, including many known to have roles in DNA repair, instead merely showed a gradual decrease in association with PLK1 after damage. Given that this trend was seen for almost all proteins, it is quite possible that this is simply some kind of artefact of the experimental setup. Still, this could potentially reflect PLK1 becoming less associated with most of its usual binding partners upon damage as it becomes repurposed for DNA repair. The decrease of PLK1 association with members of the SLX4 complex after damage induction is particularly drastic, more so than for the average interaction partner (Figure 4.3), so this if nothing else is more likely to represent some kind of meaningful removal of PLK1 from this complex in a damage-dependent manner.

Regardless, perhaps the lack of many proteins changing noticeably in their detected interaction with PLK1 upon damage should not be so surprising. As a kinase, many of PLK1's interactions with either its substrates, or other kinases activating its T-loop, would be expected to be transient and dynamic, and therefore a significant change in interaction upon damage may not be possible to detect using this method of analysis. The most stable interactions between PLK1 and other proteins are mediated by its PBD, but this binding is primed largely by CDKs in a cell cycle-dependent manner

and would not necessarily change drastically upon damage. Downregulation of CDK activity by the DNA damage checkpoint may partially explain the general small decrease in PLK1 association for most proteins, however.

Almost the sole example of a protein which did increase notably in association upon DNA damage was DYRK2, and as such this is one of the candidates I chose to follow up with further investigation. In fact, it is remarkable to detect DYRK2 association with PLK1 at all, even at this low of an abundance compared to some of the other PLK1 interaction partners identified (Figure 4.3; compare bSAF values on the Y-axes), considering DYRK2's low copy number in cells. A study to estimate copy numbers of proteins in HeLa cells could not detect DYRK2 at all, while DYRK1A (which was detected associating with PLK1 at abundances similar to DYRK2) and UBR5 have relatively high copy numbers [254]. Thus, it seems even more likely that the association detected here reflects some kind of functional interaction between DYRK2 and PLK1.

Meanwhile, UBR5 was also chosen as a candidate for follow-up investigation for multiple reasons: it was determined to associate with PLK1 at relatively high abundance, and it is a known interaction partner of DYRK2 with roles in the DNA damage response. Like DYRK2, UBR5 will be discussed further in Chapter 5.

PLK1 is already known to interact with several proteins while playing its active role in DNA repair. Of these, the SLX4 complex members were identified in this study, but others, including BRCA2, BRCA1 and TOPBP1, were not. The fact that PLK1 was almost certainly interacting with at least a small amount of these proteins in the cells analysed and yet this interaction was not detected shows the limitations of this analysis: presumably, these proteins were too low in abundance in the PLK1 IPs to be above the sensitivity

threshold of the mass spectrometer used. Since the overall abundance of BRCA1, BRCA2 and TOPBP1 in cells is nonetheless reasonably high and therefore should not be the reason for their lack of detection (BRCA1 and BRCA2's copy numbers are around one-fifth that of UBR5, and TOPBP1's is around one-third) [254], this could be another indication of the transience of PLK1's associations with many of its interaction partners. Alternatively, if PLK1 association with these proteins is stable, it seems likely that only a very small proportion of cellular PLK1 needs to interact with them in order to carry out its functions in repair. The idea that only a subset of PLK1 molecules play an active role in DNA repair would be consistent with my findings in Chapter 3 that only a small portion of nuclear PLK1 becomes recruited to damage sites. Particularly given PLK1's more prominent role in opposing the DNA damage response and overcoming checkpoint arrest, it could be that an overabundance of PLK1 associating with damage sites or interacting with repair-related proteins could have undesired consequences inhibitory to repair.

Thus, while this dataset is an important step forward in finding novel PLK1 interaction partners, it is evidently not comprehensive. This leaves open the possibility that there are also several more currently-unknown PLK1 interaction partners that were not detected with this method and yet could nonetheless be playing important roles in the regulation of PLK1 upon damage.

Chapter 5

PLK1 interaction with DYRK2 and UBR5

5.1 Introduction

The most intriguing novel interaction partner of PLK1 identified in the previous chapter was the protein kinase DYRK2, which increased dramatically in association with PLK1 by 30 minutes after damage, the very timeframe in which PLK1 is likely being regulated in a damage-dependent manner. Additionally, one of the most abundant novel PLK1 interaction partners identified was the ubiquitin ligase UBR5, also known as EDD, which interacts with DYRK2 and has multiple characterised roles in the DNA damage response, and therefore may also be playing a role in PLK1 regulation.

5.1.1 A brief overview of DYRK2

DYRK2 is a dual-specificity serine/threonine and tyrosine kinase; however, it primarily acts through its serine/threonine kinase activity. It has several varied roles, some of which are related to cell cycle progression [255]. In G1

phase, DYRK2 phosphorylates transcription factors c-Jun and c-Myc, targeting them for ubiquitylation by the SCF complex and subsequent degradation, which promotes the G1-S transition [256]. In G2, DYRK2 works together with a different ubiquitin ligase complex known as the EDVP complex, which contains UBR5. Assembly of the EDVP complex is facilitated by DYRK2 in a manner independent of DYRK2's kinase activity and is restricted to G2/M phase [250]. DYRK2 phosphorylation of substrates primes them for ubiquitylation by UBR5, thus targeting them for degradation [257] [258] [232]. One of the proteins targeted this way is Katanin p60; its timely degradation by DYRK2 and UBR5 action is important for mitotic progression [250]. As a side note, the *S. pombe* orthologue of DYRK2, Pom1, also plays a role in G2-M phase transition by detecting cell size and facilitating activation of Cdk when cells are large enough to divide [259].

Some of DYRK2's other functions are related to the DNA damage response. Its localisation is primarily cytoplasmic, but upon damage induction, nuclear DYRK2 is stabilised in an ATM-dependent manner [260] [261], where it interacts with RNF8 to aid in chromatin ubiquitylation [262] and phosphorylates p53 to promote apoptosis [260]. These and DYRK2's cell cycle-related functions give it multiple roles in tumour suppression [255].

My dataset of PLK1 interaction partners included another DYRK2 family member, DYRK1A [263], which has known functions in neurodegeneration but also plays a role in inhibiting apoptosis [264], in contrast to DYRK2 promoting it. However, DYRK1A did not show the same damage-dependent association profile with PLK1, instead remaining relatively constant in its PLK1 association before and after damage. This along with DYRK1A's lack of established damage-related functions outside of apoptosis present it as a less interesting candidate for PLK1 regulation that I did not attempt to

follow up.

Like all members of the DYRK family, DYRK2's target kinase motif has a preference for an R at -2 or -3 and a P at +1 relative to the phosphorylated serine or threonine [265]. The sequence surrounding the threonine residues in PLK1's T-loop is RKK**T**LCG**T**PNY, where the first T is T210 and the second is T214. Both partially fit DYRK2's target motif, so it is possible that DYRK2 could phosphorylate either or both of these threonine residues to activate PLK1. PLK1's S137 has three R residues N-terminal to it and therefore might also be a DYRK2 target, presenting the alternative possibility that DYRK2 could be indirectly activating and mobilising PLK1 by abrogating PBD autoinhibition via S137 [109]. Since many PBD binding sites contain a proline at +1 to the phosphorylated residue, and DYRK2's target motif has a partial preference for a proline in this position, it is also possible that DYRK2 could be priming a PBD binding site on a different protein. This has been shown to occur in the context of *C. elegans* embryogenesis [266], supporting the idea that it could potentially occur in other contexts, too.

As a dual-specificity kinase, DYRK2 has tyrosine kinase as well as a serine/threonine kinase activity. Although initial evidence indicated that its tyrosine kinase activity only occurs co-translationally in order to activate itself [267], later work raises the possibility that it can phosphorylate tyrosines on other proteins, though this is still unclear [268]. Therefore, there is also a small possibility that DYRK2 could phosphorylate the Y217 residue in PLK1's T-loop, the function of which is still unclear but appears to be inhibitory to activity [101].

DYRK2's increased association with PLK1 upon damage, combined with the potential sites that it might phosphorylate given its kinase motif, suggests that DYRK2 could be modulating PLK1's activity upon damage

by phosphorylating the T-loop, relieving PBD autoinhibition by phosphorylating S137, and/or aiding in PLK1's localisation to specific substrates or subcellular locations by priming PBD binding sites.

5.1.2 A brief overview of UBR5

UBR5 has a variety of different roles in the DNA damage response. Similarly to DYRK2, UBR5 also becomes more heavily localised in the nucleus upon DNA damage [269]. It mediates the activation of ATM [270] and CHK2 [269], regulates transcription repression at damaged chromatin [271] and prevents excessive spreading of damage-induced ubiquitylation by reducing levels of RNF8 and RNF168 [198]. Not all of these functions require its ubiquitin ligase activity. These varied damage-related functions of UBR5 are likely the reason its overexpression is associated with certain cancers, while also, paradoxically, mutations disrupting its ubiquitin ligase activity are present in other cancers [272].

One might assume that the PLK1 association with DYRK2 I observed is merely a by-product of PLK1's greater association with UBR5, given that UBR5 and DYRK2 are known to interact as part of the EDVP E3 ubiquitin ligase complex. However, I consider this unlikely due to the different association profiles of UBR5 and DYRK2 with PLK1 across the time course, where UBR5's is constitutive and DYRK2's is damage-dependent. There is no evidence suggesting that DYRK2's interaction with UBR5 is damage-dependent; as such, this difference in association profile instead most likely reflects DYRK2's association with PLK1 being UBR5-independent. I also did not identify any of the other EDVP complex members in my proteomics experiment, suggesting that PLK1's interaction with UBR5 is unrelated to its interaction with DYRK2 and ubiquitin ligase activity within this complex.

UBR5's potential role in regulating PLK1 is less clear, but considering its large size and its relatively high PLK1 association compared to other proteins, it may be acting as a binding scaffold to bring PLK1 closer to other UBR5 binding partners or certain subcellular locations, such as sites of damage. UBR5 has been found to form damage-induced foci upon UV irradiation or etoposide treatment, some of which overlap with γH2AX [271], though its localisation to laser-induced damage sites has yet to be investigated. PLK1 binding to UBR5 could be PBD-mediated, since UBR5 contains three potential PBD-binding sites, two of which are currently known to be phosphorylated [273], and one of these two matches DYRK2's phosphorylation motif.

While I did not have the time to follow these lines of investigation as thoroughly as I had hoped, in this chapter I present the initial data I obtained showing evidence that DYRK2 does indeed play a role in phosphorylating PLK1, including on T210 but also potentially on other residues too. Additionally, I discuss preliminary experiments attempting to investigate PLK1's interaction with UBR5, and UBR5 and DYRK2's effect on PLK1 recruitment to damage, which I was unfortunately not able to reach a satisfying conclusion for but which can hopefully can be completed at some point in the future.

5.2 Results

5.2.1 DYRK2 phosphorylates PLK1 *in vitro*

I first examined whether DYRK2 could phosphorylate PLK1 *in vitro*. I incubated active DYRK2 protein with full-length PLK1, either wild type, or kinase dead (K82R) to remove the possibility of autophosphorylation, and

phosphorylation of PLK1 was detected in both instances (Figure 5.1A). Using a phospho-specific antibody, I also confirmed that T210 was at least one of the PLK1 residues being phosphorylated by DYRK2 in this assay (Figure 5.1A).

The intensity of the pIMAGO band (detecting all phosphorylation) for PLK1 in Figure 5.1A is weaker in the WT lane than in the K82R lane, and yet the intensity of the PLK1 pT210 band is stronger in the WT lane than in the K82R lane. This indicates that a reasonable proportion of the signal in the pIMAGO band for K82R is detecting a phosphorylation other than pT210, meaning that DYRK2 is likely phosphorylating other residues on PLK1 as well.

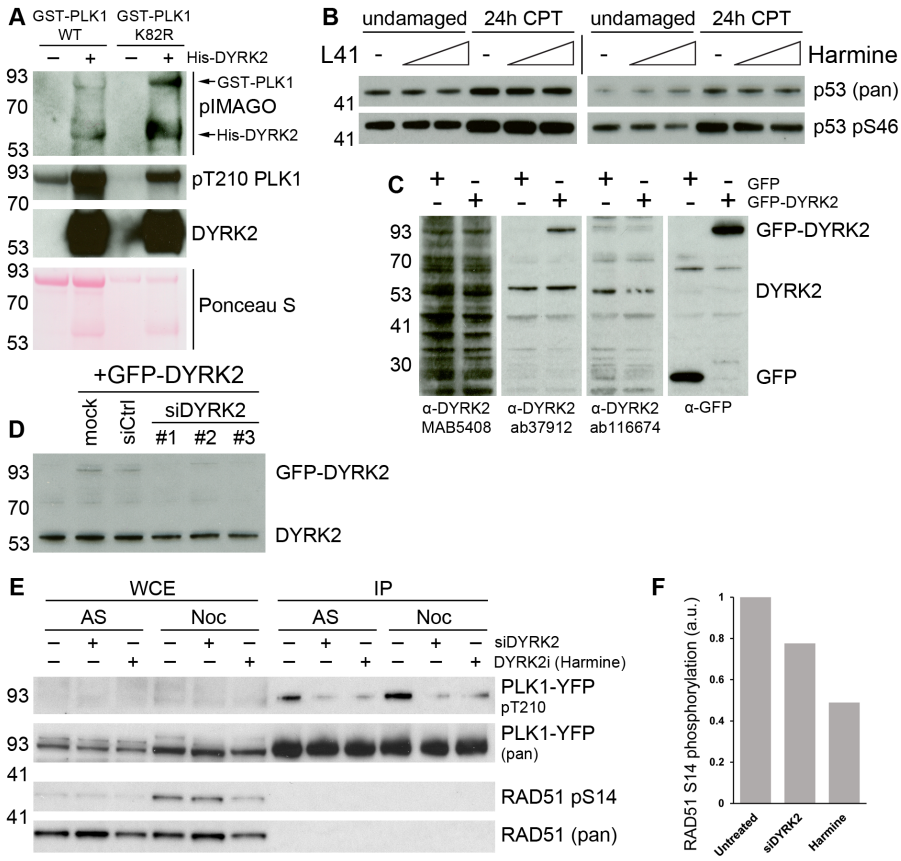
As a follow up to this, I intended to perform further *in vitro* kinase assays using DYRK2 to phosphorylate kinase dead PLK1 and then analyse the phosphorylated PLK1 with LC-MS/MS to identify which sites in particular are phosphorylated. To this end, I generated more GST-tagged K82R PLK1 myself (the stock used for the former experiment was generated previously by Keiko Yata, but had run out) by expressing it in *E. coli* and purifying it. Additionally, rather than continuing to use commercial DYRK2, I generated plasmids containing GFP-tagged DYRK2, either wild-type or different mutants: K251R (kinase dead), F301A or F301G (two different possible analogue-sensitive mutants that can be inhibited with high specificity by a bulky ATP analogue [274]). I expressed these constructs in HEK293T cells and pulled them down using GFP beads, with the intend to use the eluates in an *in vitro* reaction. While there would be a possibility of other kinases also present in the pulldown being able to target PLK1, the kinase-dead DYRK2 would serve as an adequate negative control for this. Unfortunately, I ran out of time to perform the *in vitro* kinase assays myself, but

these resources I generated remain for others in our research group to use in future.

5.2.2 Confirmation of DYRK2 inhibition and knockdown

Next, I planned to investigate the effect DYRK2 had on PLK1 phosphorylation *in vivo*. First, I tested the effectiveness of the following small-molecule inhibitors against DYRK2 kinase activity: Leucettine L41, an inhibitor with approximately equal selectivity for DYRK2 and DYRK1A [275] [276]; and harmine, an inhibitor with greater selectivity for DYRK1A but which still inhibits DYRK2 to a certain extent [277]. As a readout for DYRK2 activity, I used the phosphorylation of p53 at serine 46 [260] upon damage induction with the topoisomerase inhibitor camptothecin. Unfortunately, treatment of cells with L41 did not show a noticeable decrease in p53 phosphorylation. Treatment with harmine, however, did result in a decrease in phospho-S46 p53 (Figure 5.1B), so I settled for using this inhibitor, despite its inhibition of DYRK1A at a greater selectivity than DYRK2.

I had difficulty obtaining an DYRK2 antibody with adequately specific binding. We purchased three different antibodies, but only one of the three, ab37912 from Abcam, showed specificity to DYRK2, based on binding to transiently-transfected GFP-DYRK2 versus a negative control (Figure 5.1C). However, it turned out that this antibody was still not ideal, as evidenced in cells transfected with GFP-DYRK2 and then subjected to siRNA knockdown of DYRK2. As shown in Figure 5.1D, the siRNA treatment fully reduced the GFP-DYRK2 signal displayed by this antibody, but only slightly reduced the endogenous DYRK2 signal. This indicates that this antibody also binds to another protein of the same size as endogenous DYRK2, inconveniently masking most of the genuine DYRK2 signal. Nonetheless, this



experiment confirmed that siRNA knockdown of DYRK2 was successful. If a better antibody cannot be obtained, future experiments that require identification of endogenous DYRK2 via Western blotting would perhaps benefit from the generation of a cell line in which the endogenous DYRK2 protein has been tagged with an epitope using CRISPR/Cas9 gene editing. Such a cell line could also be used to obtain Western blot confirmation of DYRK2 being pulled down with PLK1, as I did for other proteins in Figure 4.3A but was unable to for DYRK2.

Figure 5.1: **DYRK2 phosphorylates PLK1 *in vitro* and *in vivo*. A:** GST-PLK1 wild-type or K82R (kinase dead) was incubated with or without active DYRK2, then blotted with the indicated antibodies (DYRK2 antibody was ab37912) or with pIMAGO-HRP to detect phosphoprotein. Total protein was stained using Ponceau S. **B:** HEK293T cells were treated with either DMSO at 1:1000 or with the indicated DYRK2 inhibitors at either 1 µM or 10 µM, along with 1 µM camptothecin if indicated, for 24 hours. Lysates from these cells were blotted with the indicated antibodies. **C:** HEK293T cells were transfected with plasmids expressing either GFP or GFP-DYRK2 for 24 hours and the lysates blotted with the indicated antibodies. **D:** HEK293T cells were either left untransfected or transfected as indicated with plasmids expressing GFP-DYRK2, grown for 24 hours, transfected again as indicated with either mock transfection, control siRNA at 20 nM or the indicated DYRK2 siRNAs at 100 nM. After another 48 hours, cells were lysed and probed with the ab37912 DYRK2 antibody. **E:** PLK1-YFP cells were left untreated, treated with 20 nM SmartPool DYRK2 siRNA (Dharmacon) 48 hours prior to harvesting or treated with 10 µM harmine 16 hours prior to harvesting as indicated, and also synchronised with nocodazole or not as indicated. GFP was immunoprecipitated from lysates, then whole cell extract (WCE) or IP samples were blotted with phospho-specific or pan PLK1 or RAD51 antibodies. **F:** Quantification of phospho-S14 RAD51 signal from nocodazole-treated samples in **E** relative to pan-RAD51 signal, then normalised so that the value for the untreated sample was equal to 1.

5.2.3 DYRK2 affects PLK1 T210 phosphorylation *in vivo*

In PLK1-YFP cells, I either knocked down DYRK2 using siRNA or inhibited it using harmine, and either grew cells asynchronously or synchronised them in mitosis with a nocodazole block. After pulling down PLK1-YFP, I blotted for pT210. Both siRNA knockdown of DYRK2 and inhibition with harmine resulted in a dramatic decrease in PLK1 phosphorylation at T210, in both asynchronous and mitotic cells (Figure 5.1E). That the decrease is so dramatic is perhaps a reason for caution, since other kinases such as Aurora A should be expected to be able to compensate and still phopshorylate T210 under unperturbed conditions. Nonetheless, the fact that both siRNA knockdown of DYRK2 and inhibition via harmine showed the same effect

does support that this is not an off-target effect and is specific to DYRK2.

As an added readout for PLK1 activity, I also probed for RAD51 S14 phosphorylation and found it to be somewhat decreased in mitotic whole-cell extracts upon DYRK2 knockdown or inhibition compared to untreated cells (Figure 5.1E/F). That this was not such a dramatic decrease as seen for PLK1 T210 phosphorylation suggests either that PLK1 remained active despite not being phosphorylated on T210, perhaps via phosphorylation of a different T-loop residue such as T214, or that a different kinase other than PLK1 is also capable of phosphorylating RAD51 on S14. While I cannot rule out the possibility that the requirement of DYRK2 for PLK1 T-loop phosphorylation *in vivo* is only an indirect effect, this data supports the idea that DYRK2 phosphorylates PLK1 on T210 in unperturbed cells, and that doing so aids PLK1 in its role in phosphorylating RAD51 during mitosis.

5.2.4 PP6 has no effect on PLK1 T210 phosphorylation in mitosis

Since PP6C and several of the regulatory subunits of the PP6 complex were identified as abundant PLK1 binding partners in Chapter 4, I also considered the possibility that PP6's phosphatase activity could have an effect on the phosphorylation status of PLK1 T210. I overexpressed PP6C in HEK293T cells (using this cell line over PLK1-YFP because it is more receptive to being transfected with additional constructs), synchronised cells in mitosis and pulled down PLK1, but found no noticeable difference in PLK1 T210 phosphorylation level compared to a negative control (Figure 5.2A). However, only overexpressing PP6C and not any of its regulatory subunits may have not been sufficient to have an effect on dephosphorylation of its targets. I also tried siRNA knockdown of PP6, this time knocking

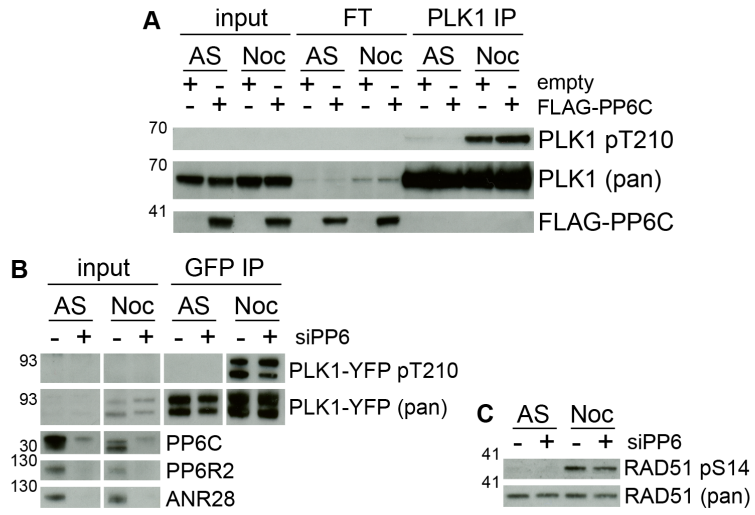


Figure 5.2: **PP6 has no effect on phosphorylation of PLK1 T210 in mitosis. A:** HEK293T cells were transfected with either a FLAG empty vector or plasmids expressing FLAG-PP6C and either grown asynchronously or synchronised in mitosis with nocodazole, then lysed and immunoprecipitated with beads crosslinked to anti-PLK1. Input, flowthrough and elution samples were probed with anti pan-PLK1, anti-pT210 PLK1 and anti-PP6C. **B:** PLK1-YFP cells were treated or not as indicated with SmartPool siRNAs targeting PP6C, PP6R2 and ANR28 (Dharmacon) at 33 nM each, and either grown asynchronously or synchronised in mitosis with nocodazole, then lysed and immunoprecipitated with GFP beads. Input and IP samples were probed with the indicated antibodies. For some reason, PLK1-YFP displayed a doublet of bands here, unlike in similar experiments seen in Figure 5.1. **C:** Lysate samples prepared as in **B** and probed with the indicated antibodies.

down all three of PP6C, PP6R2 and ANR28 simultaneously, in PLK1-YFP cells, and this also showed no effect on PLK1 T210 phosphorylation level in mitosis (Figure 5.2B). Additionally, I again used RAD51 S14 phosphorylation as an added readout for PLK1 activity and found no difference in phosphorylation level upon knockdown of PP6 complex components (Figure 5.2C).

A functional link between the PP6 complex and PLK1 has in fact already been established: PP6 dephosphorylates Aurora A's activatory T-

loop [235], which would in turn reduce or delay activation of PLK1. However, my experiment was not well-designed to show this effect, since the cells were synchronised in mitosis and so PLK1 would have been maximally activated by that time, regardless of whether PP6 overexpression or knockdown caused a decrease or increase in the rate of Aurora A-induced PLK1 activation during G2.

5.2.5 Preliminary experiments on UBR5's interaction with PLK1

UBR5 is a large protein (2799 amino acids) with multiple characterised domains [278]. Aside from its C-terminal HECT domain for ubiquitin ligase activity, these other characterised domains are all likely involved in protein-protein interaction. Additionally, UBR5 also contains three potential binding sites for PLK1's PBD. In order to narrow down which part of UBR5 PLK1 interacts with, I generated five truncations of UBR5, shown in Figure 5.3A.

These truncations were generated via PCR amplification of the relevant regions of UBR5 cDNA using primers which added attB sites to both ends of the fragment to allow for gateway cloning into vectors conferring different tags (Figure 5.3B). Since only fragments UBR5-1 and UBR5-2 contained a known functional NLS [278], I also generated versions of fragments UBR5-3, UBR5-4 and UBR5-5 with an NLS added to their C-termini, in case the versions of these fragments without an NLS did not show nuclear localisation. I then cloned these constructs into plasmids that tagged them with either 3x FLAG or GFP at the N-terminus. Upon testing the nuclear localisation of the FLAG-tagged constructs using immunofluorescence, it turned out that the versions of fragments UBR5-3, UBR5-4 and UBR5-5 without an added NLS showed equal or better nuclear localisation than the fragments

with an NLS (Figure 5.3C). As such, I used only the NLS-free constructs from here on.

I first expressed these five FLAG-tagged UBR5 truncations in PLK1-YFP cells using the same amount of plasmid for each transfection and found that the expression levels of the proteins varied (Figure 5.3D). Based on these expression levels, I normalised the amount of plasmid transfected in an attempt to obtain more even expression for the full experiment in which I pulled down PLK1-YFP. Unfortunately, this attempt at compensation was unsuccessful; in fact, expression levels varied even more to the point that fragments UBR5-1, UBR5-3 and UBR5-5 were barely expressed at all (Figure 5.3E). In an attempt to avoid this apparent issue with expressing the constructs, I switched to using in HEK293T cells which are more receptive to expressing exogenous constructs. Again, I normalised the amount of plasmids used based on the expression levels seen in Figure 5.3D; however, this time this was an overcompensation that resulted in UBR5-2 and UBR5-4 not being expressed at all. Unfortunately, here I ran out of time and was not able to finish optimising this for another attempt at PLK1 IP.

Regardless of these issues with expressing the constructs, I also did not observe any of UBR5-2 or UBR5-4 co-IPing with PLK1-YFP (Figure 5.3E). It is possible that this is only due to the fact that PLK1 does not associate with either of these fragments. However, I also probed for endogenous, full-length UBR5 and did not observe any of it co-IPing with PLK1 either. The reason for this could be that this experiment was carried out in asynchronous cells, whereas the proteomics experiment and the blot in which I confirmed UBR5 association with PLK1 (Figure 4.3A) both used G2-synchronised cells. This suggests that UBR5 association with PLK1 may be restricted to G2 phase and that, aside from better optimising the

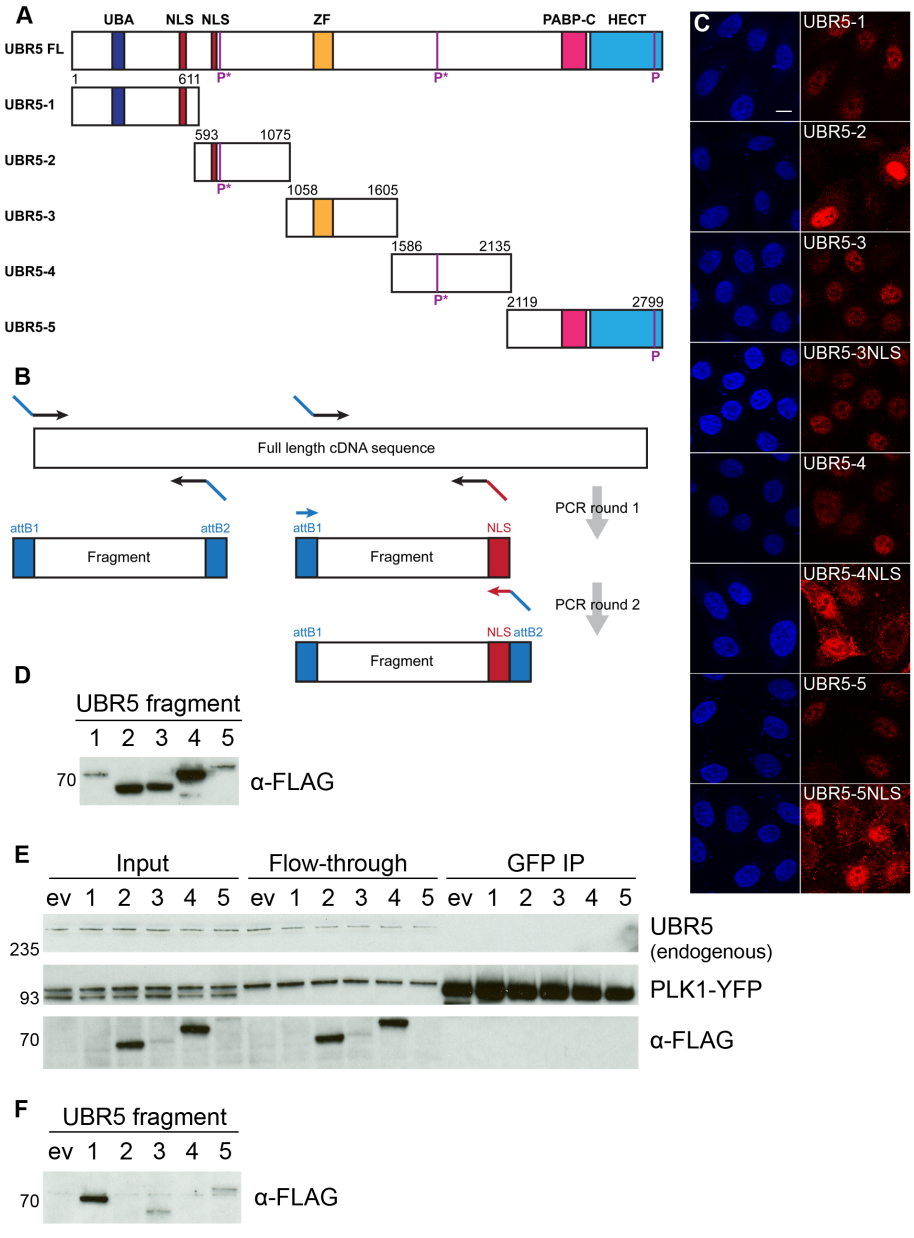

A
UBA
NLS NLS
ZF
PABP-C HECT
UBR5 FL
1
611
P*
P*
P
UBR5-1
593
1075
UBR5-2
P*
1058
1605
UBR5-3
1586
2135
UBR5-4
P*
2119
2799
UBR5-5
P
B
Full length cDNA sequence
attB1
attB2
Fragment
attB1
NLS
Fragment
PCR round 1
PCR round 2
attB1
NLS attB2
Fragment
C
UBR5-1
UBR5-2
UBR5-3
UBR5-3NLS
UBR5-4
UBR5-4NLS
UBR5-5
UBR5-5NLS
D
UBR5 fragment
1 2 3 4 5
70
α-FLAG
E
Input
Flow-through
GFP IP
ev 1 2 3 4 5 ev 1 2 3 4 5 ev 1 2 3 4 5
235
UBR5
(endogenous)
93
PLK1-YFP
70
α-FLAG
F
UBR5 fragment
ev 1 2 3 4 5
70
α-FLAG

Figure 5.3: **Generation and testing of UBR5 truncation constructs. A:** Diagram depicting full-length (FL) UBR5 with its characterised domains [278], and the truncations that I generated. UBA = ubiquitin-associated (found in many ubiquitylation-related proteins; thought to be for protein-protein interaction). NLS = nuclear localisation sequence. ZF = zinc finger (protein-protein interaction). PABP-C = poly-A binding protein carboxyl region (likely also for protein-protein interaction). HECT = homologous to E6-AP carboxylterminus (ubiquitin ligase domain). Lines labelled with a P indicate potential PLK1 PBD binding sites (either SSP or STP). Asterisks represent such sites that are confirmed to be phosphorylated. **B:** PCR setup used to generate truncations from full length UBR5 cDNA. To solely add attB sites, only one PCR round was needed. To add an NLS along with attB sites, two rounds of PCR were needed. Primers are listed in Table 2.1. **C:** PLK1-YFP cells transiently transfected with the indicated FLAG-UBR5 constructs were fixed and stained with DAPI and red immunofluorescence staining targeting FLAG. Images are blue and red channels of representative cells. Scale bar = 10 μm. **D:** PLK1-YFP cells were transfected with the indicated FLAG-UBR5 plasmids at equal concentrations, then lysed and probed with anti-FLAG. **E:** PLK1-YFP cells were transfected with either empty FLAG vector or the indicated FLAG-UBR5 plasmids at concentrations normalised based on the signal in **D** with the intent to give equal expression, then lysed, immunoprecipitated with GFP beads and probed with the indicated antibodies. **F:** HEK293T cells were transfected with either empty FLAG vector or the indicated FLAG-UBR5 plasmids at concentrations normalised as in **E**, then lysed and probed with FLAG antibody.

expression of the truncation constructs, G2 synchronisation would also be needed in future to carry out this experiment successfully.

5.2.6 Laser microirradiation experiments with DYRK2 and UBR5

I was also curious as to whether UBR5 and/or DYRK2 are recruited to damage sites in a similar manner to PLK1. As a pilot experiment for this, I transiently expressed GFP-tagged UBR5 or DYRK2 in HeLa Kyoto mCherry-BP1 cells and performed a laser microirradiation experiment as in Chapter 3. However, I did not observe, nor calculate using my quantification method, any localisation of either GFP-UBR5 or GFP-DYRK2 to laser stripes between 0 and 90 minutes post-bleaching (Figure 5.4A/B). While there is a small chance that the lack of localisation was an effect of the transient protein expression, or the N-terminal GFP tag blocking association, it seemed likely enough that UBR5 and DYRK2 do not localise to laser-induced damage that I did not attempt to follow this up with further experiments in a cell line stably expressing these GFP-tagged proteins.

Given this finding, it seems less likely that UBR5 could be playing a role in recruiting PLK1 to damage sites. This also suggests that, while DYRK2 is likely to be phosphorylating PLK1 according to my other data, this phosphorylation is not specifically taking place at sites of damage, although damage-associated PLK1 could still potentially be phosphorylated by diffusible DYRK2 not stably associated with damage sites.

The other natural question to ask was whether UBR5 and/or DYRK2 had any effect on PLK1 localisation to damage. I first attempted to ask this question with DYRK2 by using harmine to inhibit it prior to a laser microirradiation experiment with PLK1-YFP. Unfortunately, treatment of PLK1-YFP

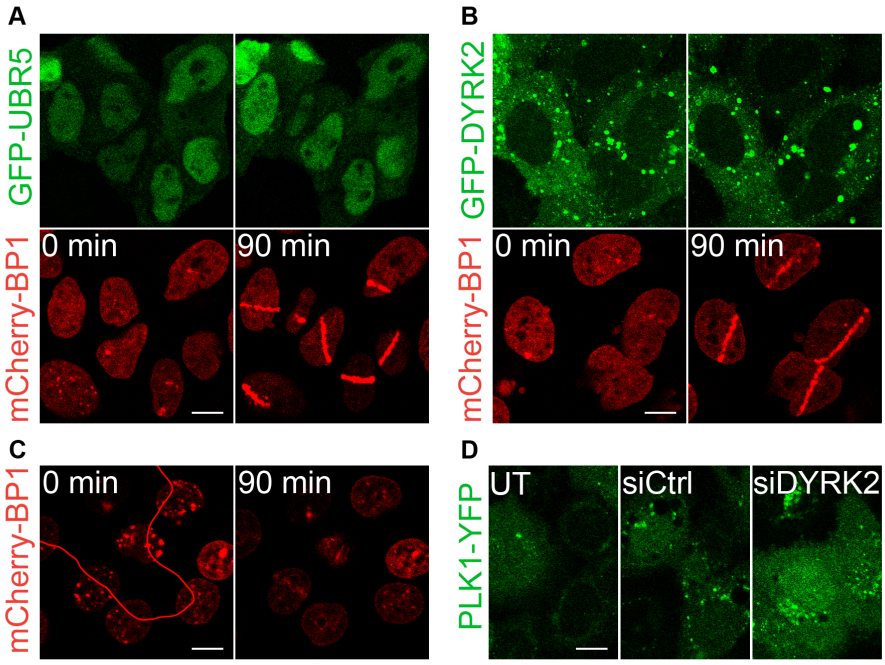


Figure 5.4: **UBR5 and DYRK2 in laser microirradiation experiments. A, B:** HeLa Kyoto mCherry-BP1 cells were transiently transfected with either GFP-UBR5 or GFP-DYRK2, then subjected to laser microirradiation. Images are green and red channels the indicated times after bleaching. **C:** PLK1-YFP mCherry-BP1 cells were treated with 10 µM harmine prior to laser microirradiation. Images are the red channel the indicated times after bleaching. Red line: laser path. **D:** PLK1-YFP cells were either untreated (UT) or treated with 100 nM of either control or DYRK2 siRNA 48 hours prior to imaging. Images are green channel, prior to any bleaching. Note the aggregates of PLK1-YFP in the cytoplasm, as well as large vesicles from which PLK1-YFP is excluded, both of which are specific to siRNA-treated cells.

mCherry-BP1 cells with harmine resulted in the mCherry-BP1 signal being almost nonexistent at sites of damage (Figure 5.4C). This is not too surprising, since DYRK2's role in aiding chromatin ubiquitylation via RNF8 means that upon depletion of DYRK2, 53BP1 foci formation is reduced [262]. However, this makes it impossible to use mCherry-BP1 as a marker for my quantification method in any experiment using harmine. The only way to carry out this experiment while being able to properly quantify the faint PLK1-YFP stripe would be to use a different damage marker that is not affected by loss of ubiquitylation at damaged chromatin. One derived from MDC1 would perhaps be a good candidate for this, since it binds directly to γH2AX.

Instead of using harmine, I then tried knocking down DYRK2 using siRNA in the hope that this would perhaps affect the mCherry-BP1 signal less. The mCherry-BP1 recruitment to damage stripes in siDYRK2 cells was indeed unaffected; on the other hand, the siRNA-treated cells appeared noticeably more unhealthy than usual such that I doubted whether any reduction seen in PLK1-YFP recruitment would necessarily be due to the loss of DYRK2 and not simply the cells being sick due to the siRNA treatment. In support of this idea, cells treated with the same concentration of control siRNA looked similarly unhealthy (Figure 5.4D), and both siCtrl- and siDYRK2-treated cells had a reduced intensity of PLK1-YFP stripe compared to healthy, untreated cells. I also attempted using a different siRNA transfection reagent (Lipofectamine 2000 (Thermo Fisher Scientific) instead of DharmaFECT (Dharmacon)), but this did not improve the health of the transfected cells. As such, siRNA treatment does not seem to be a viable option for this experimental system, so I was unfortunately unable to investigate how UBR5 and DYRK2 affect PLK1 recruitment to damage using this method.

5.2.7 Setup of a CRISPR interference system for live-cell microscopy

As an alternative method for downregulating UBR5 and DYRK2 in laser microirradiation experiments, I attempted to generate cell lines that would use CRISPR interference (CRISPRi) to inducibly silence transcription of the target genes. CRISPRi is adapted from the CRISPR system and utilises a nuclease-dead version of the Cas9 protein (dCas9) along with a single guide RNA (sgRNA) which targets dCas9 to a region near the target gene's transcription start site. While dCas9 cannot cleave the DNA, it causes a steric block that prevents transcription elongation [279]. Specifically, I used a refined version of this system which fuses dCas9 to a KRAB repression domain, thus increasing the efficiency of transcriptional silencing [280] (Figure 5.5A). I aimed to create cell lines stably expressing both dCas9-KRAB under an inducible promoter and *UBR5*- or *DYRK2*-targeted sgRNAs under a constitutive promoter, thus allowing me to induce repression of the target gene upon doxycycline treatment. In theory, this method would have none of the toxic effects on cells that I found siRNA treatment to have and would therefore potentially be a means by which I could investigate UBR5 and DYRK2's effect on PLK1 recruitment to damage. The other benefit of this system over siRNA treatment would be that, as the constructs are stably expressed in all cells and induced by a drug, there should be no cell-to-cell variation in knockdown of the target gene like siRNA treatment would have based on which cells are successfully transfected.

I first transfected PLK1-YFP mCherry-BP1 cells with a plasmid expressing dCas9-KRAB under a doxycycline-inducible promoter, obtained stable clones and confirmed that the clones expressed dCas9-KRAB after doxycycline induction. The next step was to determine which of several sgRNAs

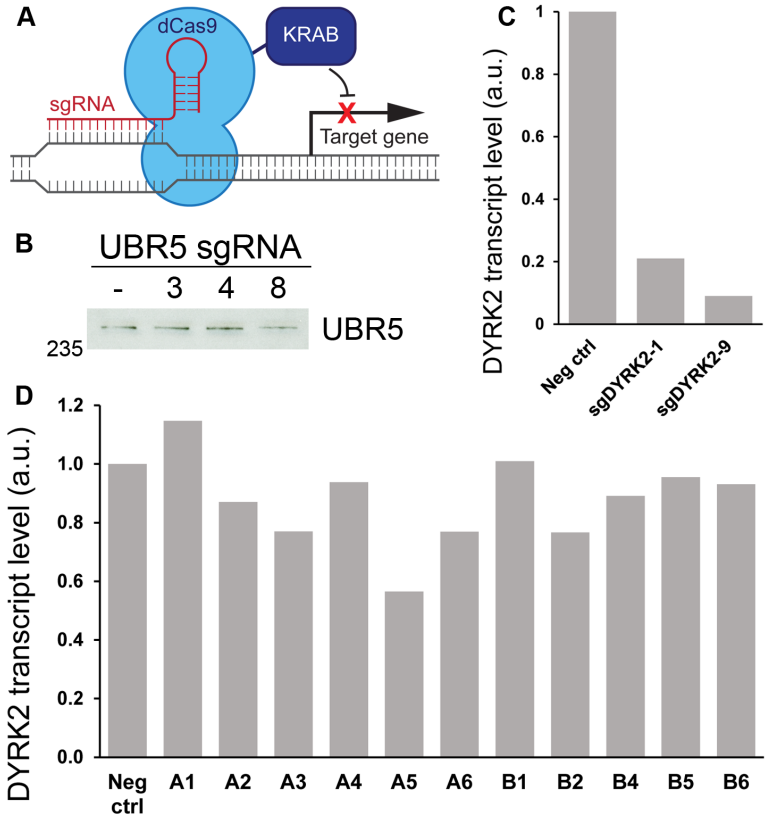


Figure 5.5: **Attempts to set up a CRISPRi system for live-cell experiments. A:** Diagram depicting the mechanism of CRISPRi. A nuclease-dead Cas9 (dCas9) fused to a KRAB repression domain is guided by an sgRNA to bind near the transcription start site of the target gene and repress transcription. **B:** PLK1-YFP mCherry-BP1 dCas9-KRAB cells were untransfected or transiently transfected with constructs expressing the indicated UBR5 sgRNAs, induced with 2 µM doxycycline for 4 days and then lysed and probed for UBR5 expression with antibody A300-573A-T. **C:** PLK1-YFP mCherry-BP1 dCas9-KRAB cells were untransfected or transiently transfected with constructs expressing the indicated DYRK2 sgRNAs and induced with 2 µM doxycycline for 4 days, then cDNA libraries were generated and relative *DYRK2* transcript levels were measured with qPCR by normalisation against transcript levels of the housekeeping gene *HPRT*. Results were further normalised such that the value for the negative control equalled 1. **D:** PLK1-YFP mCherry-BP1 dCas9-KRAB cell lines were stably transfected with constructs expressing DYRK2-9 sgRNA. Several clonal cell lines resulting from this, along with the parental cell line as a negative control, were induced with 2 µM doxycycline for 4 days, then relative *DYRK2* transcript levels were measured with qPCR as in **C**.

for *DYRK2* and *UBR5* caused most efficient repression, to determine which should be stably transfected. To do this, I transiently transfected PLK1-YFP mCherry-BP1 dCas9-KRAB cells with plasmids expressing the appropriate sgRNA while also treating them with doxycycline. Measuring *UBR5* repression was simply a matter of Western blotting for protein level; however, since the DYRK2 antibody could not be used to confirm knockdown (as discussed in Section 5.2.2), I instead used quantitative real-time PCR (qPCR) to asses *DYRK2* transcript level. Transfection with an sgRNA construct and treatment with doxycycline for 2 days did not give notable repression of *UBR5* or *DYRK2* (data not shown). Extending the doxycycline treatment to 4 days gave a much more drastic decrease in *DYRK2* transcript level, 5-fold for sgDYRK2-1 and 10-fold for sgDYRK2-9 (Figure 5.5C), so DYRK2-9 was chosen as the sgRNA to use for *DYRK2*. Unfortunately, even this 4-day treatment did not show a particularly notable effect on *UBR5* repression (Figure 5.5B), but since obtaining a stable cell line takes a long time and I was running low on time remaining in my project, I chose the sgRNA UBR5-8, as it gave a slightly lower UBR5 signal than the others, and hoped to further optimise knockdown conditions once the cell line was obtained.

Once I obtained stable clones of cells expressing either DYRK2-9 or UBR5-8 sgRNAs, the next step was to confirm sgRNA expression by confirming knockdown of the target genes upon doxycycline induction. Since I was waiting for a replacement supply of the main UBR5 antibody I had been using, I initially focused on DYRK2. I took several potential clones that in theory stably expressed DYRK2-9 sgRNA and induced dCas9-KRAB for 4 days with doxycycline, then measured *DYRK2* transcript level using qPCR. The results were not as drastic as the previous time I had done this with transiently-transfected sgRNA constructs: none of the clones showed more

than a 2-fold decrease in *DYRK2* transcript level compared to the parental cell line negative control (Figure 5.5D). The reason for this was perhaps due to the lower expression level of the sgRNA from a stably-integrated plasmid (which would presumably be only a single copy) compared to a transiently-transfected plasmid which would be at a higher copy number.

Unfortunately, here I ran out of time and as such was not able to finish verifying this system and use it in laser microirradiation experiments. The reason for the clones stably expressing DYRK2 sgRNA not showing sufficient knockdown was likely that the doxycycline induction was not long enough. Published work by Mandegar *et al* [199] which set up a similar stable, inducible CRISPRi system in stem cells (and from which I obtained the dCas9-KRAB plasmid construct used here) found that doxycycline induction for 4 days was sufficient for efficient knockdown only for some genes, and others required 7 days before full knockdown was achieved. As such, were I to continue this, I would induce DYRK2 sgRNA-expressing clones with doxycycline for 7 days in the hope that this achieves at least 10-fold knockdown as seen by sgDYRK2-9 in Figure 5.5C. I would also do the same for UBR5 sgRNA-expressing clones and measure UBR5 knockdown by Western blot, hopefully seeing more significant knockdown than was shown in Figure 5.5B. Upon obtaining a suitable clone for each cell line, I would then be able to use them in laser microirradiation experiments to examine PLK1-YFP recruitment to damage sites in the absence of UBR5 or DYRK2.

5.3 Discussion and further work

While much of the work in this chapter is preliminary and some of it did not reach any kind of conclusion, there are still some meaningful findings to take away. Although the *in vitro* kinase assay is only a single experiment, it indicates that DYRK2 can phosphorylate PLK1, including on T210 on its T-loop, and therefore could play a role in activating PLK1. It is likely that T210 is not the only residue on PLK1 phosphorylated by DYRK2; others could be S137, or T214, as these also partially match DYRK2's target motif. Since a phospho-specific antibody for PLK1 T214 does not currently exist, the best method to investigate this would be mass spectrometry analysis of PLK1 phosphorylated *in vitro* by DYRK2, which would also identify any other possible phosphorylation sites.

DYRK2 was also found to be important for PLK1 T210 phosphorylation *in vivo* in unperturbed cells. Observing this effect even outside of damage conditions despite the proteomics experiment only detecting DYRK2 association with PLK1 upon damage suggests that DYRK2 may also interact with PLK1 in unperturbed cells, just at too low of an extent to have been detected by my analysis. Regardless, the increased association of DYRK2 with PLK1 observed after damage implies that DYRK2 might play an even greater role in activating PLK1 upon damage. Experiments both downregulating and overexpressing DYRK2 in damaged cells to see the effect on PLK1 phosphorylation shortly after damage, and the subsequent effect on RAD51 phosphorylation, would be the logical next step to take to determine if this is the case.

Though I very much would have liked to, I was not able to successfully test the effect of DYRK2 or UBR5 on PLK1 localisation to laser-induced

damage, as siRNA treatment proved too toxic for the cells in this system, and small-molecule inhibition of DYRK2 also inhibited the mCherry-BP1 signal I usually used as a marker for quantification. I began setting up cell lines for CRISPR interference, which would in theory have avoided the problem with siRNA transfection, but could not finish verifying them in the time I had; however, continuing with this approach could still be a viable option to try in future. If this also were to prove unsuccessful for one reason or another, other options still exist. Generating PLK1-YFP cell lines with a different fluorescent DNA damage marker, such as one derived from MDC1, should enable use of small molecule inhibitors for DYRK2 in this system. For more specific inhibition of DYRK2, using CRISPR/Cas9 gene editing to generate cell lines with analogue-sensitive DYRK2 that can be specifically inhibited should work, or, more simply, it might also be possible to overexpress kinase-dead DYRK2 to cause a dominant negative effect. Similarly, if necessary, knockout cell lines of UBR5 are an option.

Pilot live-cell microirradiation experiments with GFP-UBR5 and GFP-DYRK2 showed no evidence of either protein being recruited to laser-induced damage sites. This is particularly relevant for UBR5, especially since this runs contrary to published data that UBR5 forms foci upon damage induction by both UV irradiation and DSB-inducing etoposide treatment [271]. The reason for this discrepancy could simply be down to the differing methods of DNA damage induction, or it could be related to the fact that damage-induced UBR5 foci formation in this paper was somewhat unusual in that it was dependent on several members of the polycomb repressive complex 1 but not on any of the main DNA damage response proteins (including ATM), and that only some but not all of the foci overlapped with γH2AX. Regardless, my experiment showing no recruitment of GFP-UBR5 to laser-induced

damage makes the idea that UBR5 plays a role in delivering PLK1 to damage sites seem unlikely, though there is also the possibility that UBR5 shuttles PLK1 to and from damage sites without needing to stably associate with the sites itself. On the other hand, perhaps it may have been optimistic to assume that the PLK1-UBR5 association would necessarily be related to damage, since their level of association does not change notably upon damage and UBR5 also has several damage-independent roles. Whether or not their interaction is damage-related remains unconfirmed, and this question would still be worth looking into further.

Although further experiments are needed to fully confirm this, it seems as though PLK1 association with UBR5 may be G2-specific, which would support the idea that PLK1 may be binding to UBR5 via a PBD site primed by a CDK. Continuing work with UBR5 truncation constructs to narrow down the PLK1 binding region would still be worthwhile. In theory, if the binding region(s) contained a PBD binding site, point mutations could then be introduced at this site to block PBD binding in order to determine if PLK1 binding to UBR5 was PBD-dependent. This could point towards the cell cycle-dependent regulation of the association between PLK1 and UBR5 and potentially a new role of UBR5 in regulating PLK1, or vice versa, in the cell cycle, even if it does prove to be unrelated to the DNA damage response.

Chapter 6

Conclusions and overall discussion

Despite the DNA damage checkpoint downregulating PLK1 by around 3-4 hours after damage induction, there is growing evidence that PLK1 can also play an active role in DNA repair during an earlier timeframe. This work expands upon this idea by investigating the regulation of PLK1 itself during this early timeframe. I identified mechanisms of DNA damage-dependent regulation of PLK1 both in terms of its localisation to DNA damage and its increased interaction with a novel protein partner DYRK2. This final chapter further discusses the most key points of these findings, focusing on the overall picture they present.

6.1 PLK1 localises to sites of DNA damage in S/G2 in a PBD- and CDK2-dependent manner

Laser microirradiation experiments on YFP-tagged PLK1 found that PLK1 localises to DNA damage sites in S/G2 phase. Notably, the appearance

of the PLK1-YFP stripes at damage in S/G2 was punctate, suggesting that PLK1 binds to ssDNA-associated microcompartments where resection has occurred, especially since this pattern matched the one I observed for BRCA2, which is already known to associate with resected DNA [65]. Even though PLK1 is involved in promoting HR, it is still interesting to observe PLK1 potentially localising so directly to resected DNA. PLK1's main known role so far in HR is phosphorylating RAD51 to aid in its recruitment to damage [86], which should not be necessary if both PLK1 and RAD51 are already close to where RAD51 needs to be. This presents the possibility that PLK1 plays other, more direct roles at sites of resection that are currently unknown.

My data shows that PLK1's PBD is required for this localisation in S/G2, as well as the activity of CDK2, presenting a model in which PLK1 binds to a CDK2-phosphorylated substrate at ssDNA-associated microcompartments via its PBD. CDK2 and not CDK1 being the priming kinase for PBD-dependent PLK1 localisation to damage is in keeping with the idea discussed in Section 1.4. While CDK1 is the kinase that is downregulated by the DNA damage checkpoint to halt the cell cycle until damage is repaired, CDK2 remains active upon damage and thus is able to promote S/G2-dependent DNA repair pathways such as resection. Therefore, PLK1 could in theory continue to localise to damage through PBD-dependent binding to CDK2-phosphorylated sites, even when CDK1 activity decreases.

The exact protein or proteins which are phosphorylated by CDK2 and then bound by PLK1's PBD at damage sites remain to be determined. I was hoping for such proteins to be identified by my proteomics analysis in Chapter 4: one might expect PLK1's association with such a protein to increase at around 15-30 minutes post-damage, then remain stable. How-

ever, no proteins with a noticeable and sustained increase in PLK1 association at this timeframe were found except for DYRK2, which is unlikely to be a binding scaffold for PLK1 since it contains no potential PBD binding sites, is a protein kinase with no other characterised domains, and a pilot experiment with GFP-DYRK2 showed no localisation of DYRK2 at damage sites. It is possible, however, that the increase of PLK1 association with its binding scaffold at damage sites was small enough to not be noticeably detected by the LC-MS/MS quantification, especially given that only a fraction of PLK1 associates with damage sites. If this increased-association model is true, then since CDK2 phosphorylation of the scaffold would presumably be present regardless of damage state, another mechanism should exist to increase PLK1 association with the scaffold upon damage. This would most likely be the result of a DNA damage response protein actively promoting their association, or relieving an inhibitory mechanism that blocked their association prior to damage (Figure 6.1A). It is possible that ATM could be the protein providing this regulation, especially given ATM's requirement for PLK1 recruitment to damage sites, which will be discussed further in the next section.

Another perhaps more likely possibility is a stable-association model, in which PLK1 is constitutively bound to the CDK2- and PBD-dependent binding scaffold in S/G2 regardless of damage, and the scaffold is then recruited to damage sites upon their induction, bringing PLK1 along with it (Figure 6.1B). The requirement of ATM could also be on this level, promoting recruitment of the scaffold to damage sites.

I considered the possibility that the scaffold protein in this model could be UBR5, which shows a relatively stable association with PLK1 across the DNA damage time course and contains multiple potential PBD binding

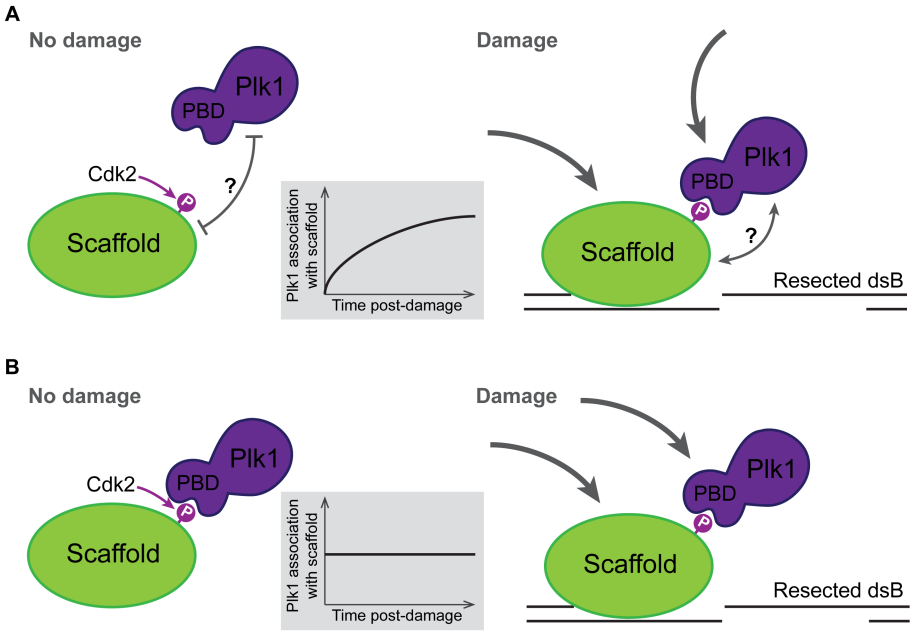


Figure 6.1: **Models for PLK1's interaction with its CDK2- and PBD-dependent binding scaffold upon damage. A:** Increased-association model. Despite constitutive phosphorylation of the scaffold by CDK2 in S/G2 phase, PLK1's interaction with it is only actively promoted by a damage-dependent mechanism, perhaps by the removal of an inhibitory mechanism that was blocking it in unperturbed conditions. This causes PLK1 to only associate with the scaffold after damage induction, at sites of DNA damage. **B:** Stable-association model. PLK1 constitutively interacts with the scaffold in S/G2 phase due to CDK2 phosphorylation, even in unperturbed conditions. Upon damage induction, the scaffold, and therefore PLK1 with it, is recruited to damage sites.

sites (although I was unfortunately unable to confirm in this work whether PLK1 binds to any of these sites). A pilot experiment using transiently-expressed GFP-UBR5 showed no evidence of UBR5 recruitment to laser-induced damage, making it unlikely that UBR5 is the binding scaffold for PLK1 at damage sites. On the other hand, UBR5 foci formation upon damage has been observed [271], so it may still be worth looking into this further to fully confirm or deny UBR5's role here.

Another potential candidate for the scaffold could be RAD52. RAD52

recruitment to damage sites has been documented, with similar kinetics to that of PLK1 [217], and it localises to ssDNA-associated microcompartments [65]. Additionally, RAD52 contains potential PBD binding sites and was identified as a PLK1 binding partner in my proteomics analysis, even if only at a very low abundance in a single timepoint. As such, looking into the effect of RAD52 on the localisation of PLK1 to damage sites could be promising.

While it is possible that the binding scaffold could be RAD52, or perhaps another protein identified by the proteomics analysis that I did not consider because it has no currently-known roles in DNA repair, it also likely that it was simply not identified by this method. Several DNA repair-related proteins already known to interact with PLK1 were not identified either, such as BRCA1, BRCA2 and TOPBP1. This shows that this method is imperfect: evidently, some PLK1 interaction partners were either at low enough abundances to be below the detection threshold of the mass spectrometer used, or interacted weakly or transiently enough with PLK1 that they were not pulled down by this protocol. Given the relatively small fraction of PLK1 that associates with damage, the PBD-dependent binding scaffold for PLK1 at damage sites could be another such protein that was too low in abundance to detect – or low enough to only just barely be detected in a single timepoint, if it is indeed RAD52.

Even though BRCA2 was not detected by mass spectrometry, PLK1 is already known to bind to it in a manner dependent on the PBD and CDK (including CDK2) activity even in undamaged cells [87]. Additionally, BRCA2 interacts with ssDNA, presenting the possibility that it could be the binding scaffold recruiting PLK1 to damage sites. However, this seems unlikely due to the fact that BRCA2 was recruited to damage with faster kinetics

than PLK1. It is reasonable to assume that a portion of BRCA2-associated PLK1 is still recruited to damage sites along with BRCA2, but this must only be a tiny portion of the PLK1 at damage sites, since this faster recruitment of PLK1 is not detectable by my quantification methods compared to the majority of PLK1 that is recruited more slowly. This discrepancy in kinetics could however also be explained by the increased-association model: in such a model, the scaffold's recruitment to damage would potentially be somewhat faster than that of PLK1. While PLK1 association with BRCA2 is already present in undamaged cells, it could potentially be upregulated upon damage as well. Investigating PLK1 localisation to laser-induced damage in the absence of BRCA2 may be worthwhile to properly confirm or deny this possibility.

Regardless, the knowledge that PLK1 appears to be binding to ssDNA-associated microcompartments in S/G2 and requires CDK2 activity and the PBD to do so significantly narrows down the possibilities for what this binding scaffold could be, even though BRCA2 can likely be ruled out as one of them. Performing another bottom-up approach like my proteomics experiment may still fail to identify the protein in question due to similar issues with detection threshold. Instead, a top-down approach testing out proteins containing a PBD binding site which have established ssDNA association and/or similar recruitment kinetics to PLK1 might be more likely to succeed. This should include RAD52, as well as other proteins not positively identified here as PLK1 binding partners. Small interfering RNA-induced knockdown of these candidates in the live-cell microirradiation assay would be one way to test them (along with BRCA2), if it could be optimised to work without the siRNA transfection hindering PLK1-YFP damage association even for the negative control. Otherwise, IP experiments to determine

whether PLK1 binds to candidate proteins in a PBD- and CDK2-dependent manner would be another approach, since Western blotting can be more sensitive at detecting interaction partners than mass spectrometry provided the antibodies are of good quality. After narrowing down the pool of candidates this way, their effect on PLK1 damage recruitment could be tested by generating either knockout cell lines for the candidate proteins containing fluorescently-tagged PLK1 and a DNA damage marker, or by introducing sgRNAs for their genes into my established PLK1-YFP mCherry-BP1 dCas9-KRAB cell line.

6.2 PLK1 localises to damage sites in both G1 and S/G2 in an ATM-dependent manner

Much more surprising than the observation that PLK1 localises to damage sites in S/G2 was the finding that it also does so in G1 cells. PLK1's main characterised roles in DNA repair are related to HR, which does not occur in G1, and additionally PLK1 itself should not be active during G1. Despite this, I observed PLK1 localising to DNA damage sites in G1, suggesting the novel possibility that PLK1 could be playing some kind of currently-unknown role in a DNA repair mechanism other than HR, one which takes place in G1 cells.

PLK1 has in fact recently been implicated in one repair mechanism other than HR, namely microhomology-mediated end joining (MMEJ), a highly error-prone alternative NHEJ pathway separate from the canonical NHEJ pathway mentioned in Section 1.1.1 [281]. While PLK1's role in promoting MMEJ was only examined in G2/M phase [282], it is currently unclear exactly how MMEJ activity is spread across the cell cycle. Most work

seems to suggest it occurs mainly from S phase onwards [283] [284], but one study found it can also be promoted in G1 [285]. Thus, it is possible that PLK1 could play a role in MMEJ in G1 as well, though the evidence is still too sparse to draw a firm conclusion, and it may instead be involved in an entirely different G1 repair mechanism.

The most relevant clue from my data towards what PLK1's damage-related role in G1 may be is that its localisation to damage in G1 is dependent on ATM activity. While ATM's function in promoting DNA resection is G2 specific, most of its other roles are carried out regardless of cell cycle phase. Testing the effect of various factors downstream of ATM on PLK1 recruitment in G1 would be a good place to start looking into this further.

Another consideration in narrowing down what to look into could be the fact that ATM activity is also required for PLK1 localisation in S/G2. One possibility for ATM's requirement in S/G2 is that it is directly regulating either PLK1's binding to its PBD- and CDK2-dependent scaffold upon damage, or the recruitment of said scaffold to damage sites, and in this case, this would be separate from the fact that ATM is also important in G1, when the PBD and CDK2 are not relevant. On the other hand, the requirement of ATM in S/G2 could be due to a much more general upstream mechanism that also applies in the same way in G1 cells. This general mechanism could potentially be ATM's involvement in the generation of damage-induced chromatin containing γH2AX, which could be helping to concentrate PLK1 or its binding scaffold near damage in S/G2 to facilitate its more direct binding to sites of resection, but which PLK1 could also be associating with through a different mechanism in G1.

Even so, it is important to remember that while the portion of PLK1 that associates with damage sites in G1 is a similar proportion of nuclear

PLK1 to the proportion that associates in S/G2, it is nonetheless a much lower absolute amount of PLK1, since PLK1 is so much less abundant in G1, particularly in the nucleus. Additionally, if the mechanism behind ATM's requirement is the same in both phases of the cell cycle, then PLK1 recruitment in G1 may simply be a passive side-effect of the fact that ATM is also important in S/G2 when PLK1 has a functional role in repair, and not necessarily a reflection of the fact that PLK1 has any repair function in G1.

One way of being more certain about whether PLK1 really is playing a role in DNA repair at damage sites in G1 is to consider its activation level. PLK1 is usually largely inactive during G1; if it were to be carrying out a specific function upon damage, it would likely need to have its activity actively upregulated first. In line with the model discussed in Section 1.4 and Figure 1.7 and potentially backed up by the FRET data from Dr. Lindqvist, it is possible that PLK1 activity is upregulated upon damage when it is initially too low to carry out its repair functions such as RAD51 phosphorylation. If this is the case, it might also apply in G1 as well as in S/early G2, if PLK1 does indeed play a role in G1 repair. This possibility will be discussed further in the next section while considering the regulation of PLK1 by DYRK2.

If the activation state of PLK1 is indeed rising significantly upon damage in G1 cells, this could be playing a role in its localisation to damage. In fact, this would make more sense than the idea that PLK1 activity could be related to its localisation to damage in S/G2 cells, since in G2 cells, PLK1 is already highly activated regardless of damage state. Currently, in terms of the relation of PLK1 activity level to its localisation to damage, the picture presented by my data is very unclear. In part, this is due to the fact that I could not determine the cell cycle phase for cells expressing PLK1 activity mutants. For example, the constitutively-active T210D mutant showed

slightly increased recruitment to damage sites; however, this could be an effect which is only relevant in S/G2 due to the T210D mutation freeing up the PBD to bind more to CDK2-phosphorylated sites, since the PBD and the T-loop are mutually autoinhibitory [109] (Figure 1.5).

Since the question of whether PLK1 activation affects its recruitment to damage is perhaps most relevant to G1 cells, it would be useful to introduce a fluorescent marker of cell cycle phase into these cell lines for future work. Assuming that PLK1 does become significantly more activated upon damage in G1, the following questions present themselves: is PLK1's activation connected to its localisation to damage sites? If so, which is upstream of the other: is PLK1 activation a prerequisite for its recruitment, or is only the fraction of PLK1 that is associated with damage sites able to be locally activated by another damage-associated factor? Along with using PLK1 activity mutants together with a cell cycle marker to answer this question, another useful approach could be to combine the FRET sensor for PLK1 activity with laser microirradiation to observe the spatial regulation of PLK1 activation relative to the location of damage sites.

6.3 A novel PLK1 interaction partner, DYRK2, increases association with PLK1 upon damage and likely aids in its activation

While my proteomics analysis identified many novel DNA damage-related and unrelated interaction partners of PLK1, some of which are discussed in more detail in Chapter 4, the most intriguing new partner is the protein kinase DYRK2. DYRK2 interaction with PLK1 was not detected prior to damage, however, upon damage, its association with PLK1 increased dra-

matically within 30 minutes and remained relatively constant until at least 2 hours after damage. Despite this, given my evidence that DYRK2 affects PLK1 phosphorylation in unperturbed cells, it is likely that DYRK2 does still interact with PLK1 to some extent prior to damage and this interaction was simply too transient or low in abundance to be detected by the LC-MS/MS system until it increased upon damage.

The majority of nuclear DYRK2 is usually degraded via ubiquitination by MDM2 in unperturbed cells. Upon damage, phosphorylation of DYRK2 by ATM prevents MDM2 from ubiquitinating it, stabilising it in the nucleus [261]. It is possible that the increased association of DYRK2 with PLK1 upon damage is purely due to this mechanism: perhaps DYRK2 has a constitutive low-level association with PLK1, which then increases as the abundance of nuclear DYRK2 increases upon damage. The paper that discovered this nuclear stabilisation of DYRK2 only measured it at 24 hours post-damage and no earlier, however, so it remains to be seen whether DYRK2 already becomes more abundant in the nucleus as early as 30 minutes post-damage. If it turns out that it does not, then a different mechanism must be behind the association of PLK1 and DYRK2 upon damage, perhaps involving some kind of scaffold protein bridging the two. It could also simply be a result of both PLK1 and DYRK2 being recruited to damage sites, although my pilot experiment looking at GFP-DYRK2's response to microirradiation did not detect it localising at damage.

My preliminary evidence indicates a strong possibility that DYRK2 can activate PLK1. The *in vitro* kinase assay showed DYRK2 phosphorylating PLK1, including at T210 in its T-loop, while the *in vivo* experiment showed a requirement of DYRK2 for PLK1 T210 phosphorylation in unperturbed cells, both asynchronous and in mitosis. Although I did not have a chance

to determine this, it is likely that DYRK2 can phosphorylate more than just the T210 residue of PLK1. The S137 residue on PLK1 is a potential target of DYRK2, through which DYRK2 would be able to indirectly aid PLK1's activation by relieving the PBD autoinhibition [109]. A phosphospecific antibody for this residue exists and would be worth testing in the context of DYRK2. Another possible target residue for DYRK2 is T214 on the T-loop. PLK1's T214 residue has not been well-studied, but recent evidence suggests that T214 phosphorylation is also important in promoting PLK1 activity [99]. Aurora A, the kinase initially responsible for phosphorylating PLK1 T210 in cell cycle progression, would be incapable of phosphorylating T214 due to the proline residue immediately following it [96]. However, given its preference for a proline at the +1 position, DYRK2 is more likely to be able to do so. While this is currently only speculation, it is possible that regulation of PLK1 activity through T214 could be primarily occurring through the action of DYRK2. Further investigation of this, including generation of a phosphospecific antibody for PLK1 T214 to make doing so easier, might be worthwhile potentially even outside the context of DNA repair. Future mass spectrometry analysis of PLK1 phosphorylated *in vitro* by DYRK2 would help to confirm which other residues DYRK2 is capable of phosphorylating, thus confirming whether these possibilities are worth investigating.

Given the evidence suggesting DYRK2 can activate PLK1 and the increased association of DYRK2 with PLK1 upon damage, it is also very likely that DYRK2 can increase the activation level of PLK1 upon damage. DYRK2 and PLK1's increase in association occurs between 15-30 minutes post-damage, which matches the timeframe of the increase in RAD51 phosphorylation upon damage [86] and the potential increase in PLK1 activation from basal levels seen by the FRET data from Dr. Lindqvist. PLK1

activation upon damage in specifically G1 and S cells and the possible contribution of DYRK2 to this might be worth investigating further. In particular, this could link to my finding that PLK1 localises to damage in G1 and provide more support for the idea that this indicates a novel function of PLK1 in DNA repair outside of HR. While my proteomics experiment only confirmed the association of DYRK2 with PLK1 in G2 cells, DYRK2 does also have functions in G1, promoting the G1-S transition [256], so it is still possible that it could be playing a role related to PLK1 in G1/S cells as well.

I was not able to confirm or deny whether DYRK2 is also involved in the recruitment of PLK1 to damage sites. DYRK2's ability to phosphorylate sites adjacent to prolines makes it possible that it could be priming PBD binding sites. The PBD-dependent localisation of PLK1 to damage sites in S/G2 appears to be almost entirely regulated by CDK2, based on the fact that CDK2 inhibition almost completely abrogates localisation (Figure 3.3C). However, NU-6102, the CDK2 inhibitor I used, also inhibits DYRK1A at a 30-fold lower selectivity than CDK2 [211], so it is possible that it could be inhibiting DYRK2 as well to some extent. Therefore, the data showing reduced PLK1 recruitment upon NU-6102 treatment could at least partially be reflecting the effect of a loss in DYRK2 activity. Further work to confirm whether or not NU-6102 does in fact inhibit DYRK2, and if so, repeating the CDK2 inhibition experiment with a different inhibitor that does not affect DYRK2, would be worth looking into. Meanwhile, in G1 cells, if a damage-induced increase in activity does prove to be relevant to PLK1 association to damage, DYRK2 could easily be important for this, given its effect on PLK1 activation. Successfully optimising a way to downregulate DYRK2 during laser microirradiation while still being able to quantify PLK1-YFP localisation and having a functional negative control will be necessary to be

able to determine this in future. The CRISPRi cell lines for inducibly silencing DYRK2 transcription that I almost finished generating should prove useful for this if they can be verified.

6.4 Concluding remarks

The evidence presented in this work sheds light on the DNA damage-dependent regulation of PLK1 during early timeframes prior to its downregulation by the checkpoint, thus expanding on the recently-developed idea that during these timeframes PLK1 can play an active role in DNA repair. In particular, I show that PLK1 begins to localise directly to sites of DNA damage in both S/G2 and G1 cells within 15 minutes of damage induction in an ATM-dependent manner. PLK1 recruitment in S/G2 is also dependent on its PBD binding to a CDK2-primed phosphorylation on a currently-unknown scaffold that can hopefully be identified in future. Meanwhile, I discovered novel DNA repair-related interaction partners of PLK1, including UBR5 and DYRK2. I was not able to shed much light onto UBR5's role in regulating PLK1, but this is still potentially worth looking into further. More promisingly, I found that DYRK2 increases in association with PLK1 upon damage and is able to phosphorylate PLK1's T-loop, making it likely to be involved in activating PLK1 under damage conditions. Although further work is required to confirm that this is indeed the case and examine the full extent of DYRK2's role in activating PLK1, this promises to provide new insight into the regulation of PLK1 activity, particularly during the timeframes in which it is actively involved in DNA repair.

Perhaps most interestingly, some of my evidence presents the possibility that PLK1 could be playing novel roles in DNA repair outside of simply

phosphorylating RAD51. PLK1's localisation pattern at damage stripes indicates direct association with resected DNA, which should not be necessary merely for its function of RAD51 phosphorylation, while PLK1 association with damage sites in G1 implies a role entirely outside of HR. Thus, even aside from my specific findings about the damage-dependent regulation of PLK1 through its localisation to damage sites and its interaction with DYRK2, this work suggests the potential for entirely new avenues of research into the roles PLK1 plays in DNA repair.

References

1. Jackson, S. P. & Bartek, J. The DNA-damage response in human biology and disease. *Nature.* ISSN: 00280836. doi:10.1038/nature08467 (2009).
2. Lieber, M. R. The mechanism of double-strand DNA break repair by the nonhomologous DNA end-joining pathway. *Annual Review of Biochemistry.* ISSN: 0066-4154. doi:10.1146/annurev.biochem.052308.093131 (2010).
3. Morrical, S. W. DNA-pairing and annealing processes in homologous recombination and homology-directed repair. *Cold Spring Harbor Perspectives in Biology* **7.** ISSN: 19430264. doi:10.1101/cshperspect.a016444 (2015).
4. Mari, P.-O. *et al.* Dynamic assembly of end-joining complexes requires interaction between Ku70/80 and XRCC4. *Proceedings of the National Academy of Sciences.* ISSN: 0027-8424. doi:10.1073/pnas.0609061103 (2006).
5. Rupnik, A., Lowndes, N. F. & Grenon, M. MRN and the race to the break. *Chromosoma.* ISSN: 00095915. doi:10.1007/s00412-009-0242-4 (2010).
6. De Jager, M. *et al.* Human Rad50/Mre11 is a flexible complex that can tether DNA ends. *Molecular Cell.* ISSN: 10972765. doi:10.1016/S1097-2765(01)00381-1 (2001).
7. Carson, C. T. *et al.* The Mre11 complex is required for ATM activation and the G2/M checkpoint. *EMBO Journal.* ISSN: 02614189. doi:10.1093/emboj/cdg630 (2003).
8. Uziel, T. *et al.* Requirement of the MRN complex for ATM activation by DNA damage. *EMBO Journal.* ISSN: 02614189. doi:10.1093/emboj/cdg541 (2003).
9. Burma, S, Chen, B. P., Murphy, M, Kurimasa, A & Chen, D. J. ATM phosphorylates histone H2AX in response to DNA double-strand breaks. *Journal of Biological Chemistry.* ISSN: 0021-9258. doi:10.1074/jbc.C100466200 (2001).

10. Stucki, M. *et al.* MDC1 directly binds phosphorylated histone H2AX to regulate cellular responses to DNA double-strand breaks. *Cell.* ISSN: 00928674. doi:10.1016/j.cell.2005.09.038 (2005).

11. Goldberg, M. *et al.* MDC1 is required for the intra-S-phase DNA damage checkpoint. *Nature.* ISSN: 00280836. doi:10.1038/nature01445 (2003).

12. Stewart, G. S., Wang, B., Bignell, C. R., Taylor, A. M. R. & Elledge, S. J. MDC1 is a mediator of the mammalian DNA damage checkpoint. *Nature.* ISSN: 0028-0836. doi:10.1038/nature01446 (2003).

13. Lou, Z. *et al.* MDC1 maintains genomic stability by participating in the amplification of ATM-dependent DNA damage signals. *Molecular Cell.* ISSN: 10972765. doi:10.1016/j.molcel.2005.11.025 (2006).

14. Celeste, A. *et al.* Genomic instability in mice lacking histone H2AX. *Science.* ISSN: 00368075. doi:10.1126/science.1069398 (2002).

15. Huen, M. S. Y. *et al.* RNF8 transduces the DNA-damage signal via histone ubiquitylation and checkpoint protein assembly. *Cell.* ISSN: 00928674. doi:10.1016/j.cell.2007.09.041 (2007).

16. Kolas, N. K. *et al.* Orchestration of the DNA-damage response by the RNF8 ubiquitin ligase. *Science.* ISSN: 00368075. doi:10.1126/science.1150034 (2007).

17. Mailand, N. *et al.* RNF8 ubiquitylates histones at DNA double-strand breaks and promotes assembly of repair proteins. *Cell.* ISSN: 00928674. doi:10.1016/j.cell.2007.09.040 (2007).

18. Doil, C. *et al.* RNF168 binds and amplifies ubiquitin conjugates on damaged chromosomes to allow accumulation of repair proteins. *Cell.* ISSN: 00928674. doi:10.1016/j.cell.2008.12.041 (2009).

19. Stewart, G. S. *et al.* The RIDDLE syndrome protein mediates a ubiquitin-dependent signaling cascade at sites of DNA damage. *Cell.* ISSN: 00928674. doi:10.1016/j.cell.2008.12.042 (2009).

20. Fradet-Turcotte, A. *et al.* 53BP1 is a reader of the DNA-damage-induced H2A Lys 15 ubiquitin mark. *Nature.* ISSN: 00280836. doi:10.1038/nature12318 (2013).

21. Sobhian, B. *et al.* RAP80 targets BRCA1 to specific ubiquitin structures at DNA damage sites. *Science.* ISSN: 00368075. doi:10.1126/science.1139516 (2007).

22. Wang, B. *et al.* Abraxas and RAP80 form a BRCA1 protein complex required for the DNA damage response. *Science (New York, N.Y.)* ISSN: 1095-9203. doi:10.1126/science.1139476 (2007).

23. Wang, B. & Elledge, S. J. Ubc13/Rnf8 ubiquitin ligases control foci formation of the Rap80/Abraxas/Brca1/Brcc36 complex in response to DNA damage. *Proceedings of the National Academy of Sciences.* ISSN: 0027-8424. doi:10.1073/pnas.0710061104 (2007).

24. Yan, J. *et al.* The ubiquitin-interacting motif-containing protein RAP80 interacts with BRCA1 and functions in DNA damage repair response. *Cancer Research.* ISSN: 00085472. doi:10.1158/0008-5472.CAN-07-0924 (2007).

25. Wang, M. *et al.* PARP-1 and Ku compete for repair of DNA double strand breaks by distinct NHEJ pathways. *Nucleic Acids Research.* ISSN: 03051048. doi:10.1093/nar/gkl840 (2006).

26. Schreiber, V., Dantzer, F., Amé, J. C. & De Murcia, G. Poly(ADP-ribose): Novel functions for an old molecule. *Nature Reviews Molecular Cell Biology.* ISSN: 14710072. doi:10.1038/nrm1963 (2006).

27. Haince, J. F. *et al.* Ataxia telangiectasia mutated (ATM) signaling network is modulated by a novel poly(ADP-ribose)-dependent pathway in the early response to DNA-damaging agents. *Journal of Biological Chemistry.* ISSN: 00219258. doi:10.1074/jbc.M608406200 (2007).

28. Haince, J. F. *et al.* PARP1-dependent kinetics of recruitment of MRE11 and NBS1 proteins to multiple DNA damage sites. *Journal of Biological Chemistry.* ISSN: 00219258. doi:10.1074/jbc.M706734200 (2008).

29. Li, M. & Yu, X. Function of BRCA1 in the DNA Damage Response Is Mediated by ADP-Ribosylation. *Cancer Cell.* ISSN: 15356108. doi:10.1016/j.ccr.2013.03.025 (2013).

30. Orthwein, A. *et al.* Mitosis inhibits DNA double-strand break repair to guard against telomere fusions. *Science.* ISSN: 10959203. doi:10.1126/science.1248024 (2014).

31. Giunta, S., Belotserkovskaya, R. & Jackson, S. P. DNA damage signaling in response to double-strand breaks during mitosis. *Journal of Cell Biology.* ISSN: 00219525. doi:10.1083/jcb.200911156 (2010).

32. Zhang, W., Peng, G., Lin, S.-Y. & Zhang, P. DNA damage response is suppressed by the high cyclin-dependent kinase 1 activity in mitotic mammalian cells. *Journal of Biological Chemistry.* ISSN: 1083-351X. doi:10.1074/jbc.M111.267690 (2011).

33. Terasawa, M., Shinohara, A. & Shinohara, M. Canonical non-homologous end joining in mitosis induces genome instability and is suppressed by M-phase-specific phosphorylation of XRCC4. *PLoS Genetics.* ISSN: 15537404. doi:10.1371/journal.pgen.1004563 (2014).

34. Garcia, V., Phelps, S. E. L., Gray, S. & Neale, M. J. Bidirectional resection of DNA double-strand breaks by Mre11 and Exo1. *Nature.* ISSN: 00280836. doi:10.1038/nature10515 (2011).

35. Wold, M. S. Replication protein A: a heterotrimeric, single-stranded DNA-binding protein required for eukaryotic DNA metabolism. *Annual Review of Biochemistry.* ISSN: 0066-4154. doi:10.1146/annurev.biochem.66.1.61 (1997).

36. Sartori, A. A. *et al.* Human CtIP promotes DNA end resection. *Nature.* ISSN: 14764687. doi:10.1038/nature06337 (2007).

37. Huertas, P., Cortés-Ledesma, F., Sartori, A. A., Aguilera, A. & Jackson, S. P. CDK targets Sae2 to control DNA-end resection and homologous recombination. *Nature.* ISSN: 00280836. doi:10.1038/nature07215 (2008).

38. Huertas, P. & Jackson, S. P. Human CtIP mediates cell cycle control of DNA end resection and double strand break repair. *Journal of Biological Chemistry.* ISSN: 0021-9258. doi:10.1074/jbc.M808906200 (2009).

39. Buis, J., Stoneham, T., Spehalski, E. & Ferguson, D. O. Mre11 regulates CtIP-dependent double-strand break repair by interaction with CDK2. *Nature Structural and Molecular Biology.* ISSN: 15459993. doi:10.1038/nsmb.2212 (2012).

40. You, Z. *et al.* CtIP links DNA double-strand break sensing to resection. *Molecular Cell.* ISSN: 10972765. doi:10.1016/j.molcel.2009.12.002 (2009).

41. Wang, H. *et al.* The interaction of CtIP and Nbs1 connects CDK and ATM to regulate HR-mediated double-strand break repair. *PLoS Genetics.* ISSN: 15537390. doi:10.1371/journal.pgen.1003277 (2013).

42. Lafranchi, L. *et al.* APC/C(Cdh1) controls CtIP stability during the cell cycle and in response to DNA damage. *EMBO Journal.* ISSN: 1460-2075. doi:10.15252/embj.201489017 (2014).

43. Tomimatsu, N. *et al.* Phosphorylation of EXO1 by CDKs 1 and 2 regulates DNA end resection and repair pathway choice. *Nature Communications.* ISSN: 20411723. doi:10.1038/ncomms4561 (2014).

44. Bolderson, E. *et al.* Phosphorylation of Exo1 modulates homologous recombination repair of DNA double-strand breaks. *Nucleic Acids Research.* ISSN: 03051048. doi:10.1093/nar/gkp1164 (2010).

45. Shibata, A. *et al.* Factors determining DNA double-strand break repair pathway choice in G2 phase. *The EMBO Journal.* ISSN: 02614189. doi:10.1038/emboj.2011.27 (2011).

46. Chanut, P., Britton, S., Coates, J., Jackson, S. P. & Calsou, P. Coordinated nuclease activities counteract Ku at single-ended DNA double-strand breaks. *Nature Communications.* ISSN: 20411723. doi:10.1038/ncomms12889 (2016).

47. Langerak, P., Mejia-Ramirez, E., Limbo, O. & Russell, P. Release of Ku and MRN from DNA ends by Mre11 nuclease activity and Ctp1 is required for homologous recombination repair of double-strand breaks. *PLoS Genetics.* ISSN: 15537390. doi:10.1371/journal.pgen.1002271 (2011).

48. Sun, J., Lee, K. J., Davis, A. J. & Chen, D. J. Human Ku70/80 protein blocks exonuclease 1-mediated DNA resection in the presence of human Mre11 or Mre11/Rad50 protein complex. *Journal of Biological Chemistry.* ISSN: 00219258. doi:10.1074/jbc.M111.306167 (2012).

49. Chen, L., Nievera, C. J., Lee, A. Y.-L. & Wu, X. Cell cycle-dependent complex formation of BRCA1.CtIP.MRN is important for DNA double-strand break repair. *Journal of Biological Chemistry.* ISSN: 0021-9258. doi:10.1074/jbc.M710245200 (2008).

50. Yun, M. H. & Hiom, K. CtIP-BRCA1 modulates the choice of DNA double-strand-break repair pathway throughout the cell cycle. *Nature.* ISSN: 00280836. doi:10.1038/nature07955 (2009).

51. Reczek, C. R., Szabolcs, M., Stark, J. M., Ludwig, T. & Baer, R. The interaction between CtIP and BRCA1 is not essential for resection-mediated DNA repair or tumor suppression. *Journal of Cell Biology.* ISSN: 00219525. doi:10.1083/jcb.201302145 (2013).

52. Polato, F. *et al.* CtIP-mediated resection is essential for viability and can operate independently of BRCA1. *Journal of Experimental Medicine.* ISSN: 0022-1007. doi:10.1084/jem.20131939 (2014).

53. Cruz-García, A., López-Saavedra, A. & Huertas, P. BRCA1 accelerates CtIP-ediated DNA-end resection. *Cell Reports.* ISSN: 22111247. doi:10.1016/j.celrep.2014.08.076 (2014).

54. Bouwman, P. *et al.* 53BP1 loss rescues BRCA1 deficiency and is associated with triple-negative and BRCA-mutated breast cancers. *Nature Structural and Molecular Biology.* ISSN: 15459985. doi:10.1038/nsmb.1831 (2010).

55. Bunting, S. F. *et al.* 53BP1 inhibits homologous recombination in brca1-deficient cells by blocking resection of DNA breaks. *Cell.* ISSN: 00928674. doi:10.1016/j.cell.2010.03.012 (2010).

56. Chapman, J. R. *et al.* RIF1 Is essential for 53BP1-dependent nonhomologous end joining and suppression of DNA double-strand break resection. *Molecular Cell.* ISSN: 10972765. doi:10.1016/j.molcel.2013.01.002 (2013).

57. Di Virgilio, M. *et al.* Rif1 prevents resection of DNA breaks and promotes immunoglobulin class switching. *Science.* ISSN: 10959203. doi:10.1126/science.1230624 (2013).

58. Escribano-Díaz, C. *et al.* A cell cycle-dependent regulatory circuit composed of 53BP1-RIF1 and BRCA1-CtIP controls DNA repair pathway choice. *Molecular Cell.* ISSN: 10972765. doi:10.1016/j.molcel.2013.01.001 (2013).

59. Feng, L., Fong, K. W., Wang, J., Wang, W. & Chen, J. RIF1 counteracts BRCA1-mediated end resection during DNA repair. *Journal of Biological Chemistry.* ISSN: 00219258. doi:10.1074/jbc.M113.457440 (2013).

60. Zimmermann, M., Lottersberger, F., Buonomo, S. B., Sfeir, A. & De Lange, T. 53BP1 regulates DSB repair using Rif1 to control 5' end resection. *Science.* ISSN: 10959203. doi:10.1126/science.1231573 (2013).

61. Mirman, Z. *et al.* 53BP1–RIF1–shieldin counteracts DSB resection through CST- and Polα-dependent fill-in. *Nature.* ISSN: 14764687. doi:10.1038/s41586-018-0324-7 (2018).

62. Isono, M. *et al.* BRCA1 directs the repair pathway to homologous recombination by promoting 53BP1 dephosphorylation. *Cell Reports.* ISSN: 22111247. doi:10.1016/j.celrep.2016.12.042 (2017).

63. Hu, Y. *et al.* RAP80-directed tuning of BRCA1 homologous recombination function at ionizing radiation-induced nuclear foci. *Genes and Development.* ISSN: 08909369. doi:10.1101/gad.2011011 (2011).

64. Huen, M. S., Sy, S. M. & Chen, J. BRCA1 and its toolbox for the maintenance of genome integrity. *Nature Reviews Molecular Cell Biology.* ISSN: 14710072. doi:10.1038/nrm2831 (2010).

65. Bekker-Jensen, S. *et al.* Spatial organization of the mammalian genome surveillance machinery in response to DNA strand breaks. *Journal of Cell Biology.* ISSN: 0021-9525. doi:10.1083/jcb.200510130 (2006).

66. Chapman, J. R., Sossick, A. J., Boulton, S. J. & Jackson, S. P. BRCA1-associated exclusion of 53BP1 from DNA damage sites underlies temporal control of DNA repair. *Journal of Cell Science.* ISSN: 0021-9533. doi:10.1242/jcs.105353 (2012).

67. Kakarougkas, A. *et al.* Co-operation of BRCA1 and POH1 relieves the barriers posed by 53BP1 and RAP80 to resection. *Nucleic Acids Research.* ISSN: 03051048. doi:10.1093/nar/gkt802 (2013).

68. Baumann, P. & West, S. C. Role of the human RAD51 protein in homologous recombination and double-stranded-break repair. *Trends in Biochemical Sciences.* ISSN: 09680004. doi:10.1016/S0968-0004(98)01232-8 (1998).

69. Carreira, A. *et al.* The BRC repeats of BRCA2 modulate the DNA-binding selectivity of RAD51. *Cell.* ISSN: 00928674. doi:10.1016/j.cell.2009.02.019 (2009).

70. Jensen, R. B., Carreira, A. & Kowalczykowski, S. C. Purified human BRCA2 stimulates RAD51-mediated recombination. *Nature.* ISSN: 00280836. doi:10.1038/nature09399 (2010).

71. Thorslund, T. *et al.* The breast cancer tumor suppressor BRCA2 promotes the specific targeting of RAD51 to single-stranded DNA. *Nature Structural and Molecular Biology.* ISSN: 15459993. doi:10.1038/nsmb.1905 (2010).

72. Liu, J., Doty, T., Gibson, B. & Heyer, W. D. Human BRCA2 protein promotes RAD51 filament formation on RPA-covered single-stranded DNA. *Nature Structural and Molecular Biology.* ISSN: 15459993. doi:10.1038/nsmb.1904 (2010).

73. Xia, B. *et al.* Control of BRCA2 cellular and clinical functions by a nuclear partner, PALB2. *Molecular Cell.* ISSN: 10972765. doi:10.1016/j.molcel.2006.05.022 (2006).

74. Sy, S. M. H., Huen, M. S. Y. & Chen, J. PALB2 is an integral component of the BRCA complex required for homologous recombination repair. *Proceedings of the National Academy of Sciences.* ISSN: 0027-8424. doi:10.1073/pnas.0811159106 (2009).

75. Zhang, F. *et al.* PALB2 Links BRCA1 and BRCA2 in the DNA-Damage Response. *Current Biology.* ISSN: 09609822. doi:10.1016/j.cub.2009.02.018 (2009).

76. Bleuyard, J. Y., Buisson, R., Masson, J. Y. & Esashi, F. ChAM, a novel motif that mediates PALB2 intrinsic chromatin binding and facilitates DNA repair. *EMBO Reports.* ISSN: 1469221X. doi:10.1038/embor.2011.243 (2012).

77. Sy, S. M. H., Huen, M. S. Y. & Chen, J. MRG15 is a novel PALB2-interacting factor involved in homologous recombination. *Journal of Biological Chemistry.* ISSN: 00219258. doi:10.1074/jbc.C109.023937 (2009).

78. Hayakawa, T. *et al.* MRG15 binds directly to PALB2 and stimulates homology-directed repair of chromosomal breaks. *Journal of Cell Science.* ISSN: 0021-9533. doi:10.1242/jcs.060178 (2010).

79. Li, L. & Wang, Y. Cross-talk between the H3K36me3 and H4K16ac histone epigenetic marks in DNA double-strand break repair. *Journal of Biological Chemistry.* ISSN: 1083351X. doi:10.1074/jbc.M117.788224 (2017).

80. Buisson, R. *et al.* Cooperation of breast cancer proteins PALB2 and piccolo BRCA2 in stimulating homologous recombination. *Nature Structural and Molecular Biology.* ISSN: 15459993. doi:10.1038/nsmb.1915 (2010).

81. Dray, E. *et al.* Enhancement of RAD51 recombinase activity by the tumor suppressor PALB2. *Nature Structural and Molecular Biology*. ISSN: 15459993. doi:10.1038/nsmb.1916 (2010).

82. Yang, H. *et al.* BRCA2 function in DNA binding and recombination from a BRCA2-DSS1-ssDNA structure. *Science.* ISSN: 00368075. doi:10.1126/science.297.5588.1837 (2002).

83. Zhang, F., Shi, J., Bian, C. & Yu, X. Poly(ADP-Ribose) mediates the BRCA2-dependent early DNA damage response. *Cell Reports.* ISSN: 22111247. doi:10.1016/j.celrep.2015.09.040 (2015).

84. Siaud, N. *et al.* Plasticity of BRCA2 function in homologous recombination: Genetic interactions of the PALB2 and DNA binding domains. *PLoS Genetics.* ISSN: 15537390. doi:10.1371/journal.pgen.1002409 (2011).

85. Tarsounas, M., Davies, D. & West, S. C. BRCA2-dependent and independent formation of RAD51 nuclear foci. *Oncogene.* ISSN: 09509232. doi:10.1038/sj.onc.1206263 (2003).

86. Yata, K. *et al.* Plk1 and CK2 act in concert to regulate Rad51 during DNA double strand break repair. *Molecular Cell.* ISSN: 10972765. doi:10.1016/j.molcel.2011.12.028 (2012).

87. Yata, K. *et al.* BRCA2 coordinates the activities of cell-cycle kinases to promote genome stability. *Cell Reports.* ISSN: 22111247. doi:10.1016/j.celrep.2014.04.023 (2014).

88. Moudry, P. *et al.* TOP BP1 regulates RAD51 phosphorylation and chromatin loading and determines PARP inhibitor sensitivity. *Journal of Cell Biology.* ISSN: 15408140. doi:10.1083/jcb.201507042 (2016).

89. West, S. C. *et al.* Resolution of recombination intermediates: Mechanisms and regulation. *Cold Spring Harbor Symposia on Quantitative Biology.* ISSN: 19434456. doi:10.1101/sqb.2015.80.027649 (2016).

90. Wyatt, H. D. M., Sarbajna, S., Matos, J. & West, S. C. Coordinated actions of SLX1-SLX4 and MUS81-EME1 for holliday junction resolution in human cells. *Molecular Cell.* ISSN: 10972765. doi:10.1016/j.molcel.2013.08.035 (2013).

91. Duda, H. *et al.* A mechanism for controlled breakage of underreplicated chromosomes during mitosis. *Developmental Cell.* ISSN: 1534-5807. doi:10.1016/j.devcel.2016.11.017 (2016).

92. Uchiumi, T, Longo, D. L. & Ferris, D. K. Cell cycle regulation of the human polo-like kinase (PLK) promoter. *Journal of Biological Chemistry.* ISSN: 0021-9258 (1997).

93. Akopyan, K. *et al.* Assessing kinetics from fixed cells reveals activation of the mitotic entry network at the S/G2 transition. *Molecular Cell.* ISSN: 10972765. doi:10.1016/j.molcel.2014.01.031 (2014).

94. Petronczki, M., Lénárt, P. & Peters, J. M. Polo on the rise: From mitotic entry to cytokinesis with Plk1. *Developmental Cell.* ISSN: 15345807. doi:10.1016/j.devcel.2008.04.014 (2008).

95. Nakojima, H., Toyoshima-Morimoto, F., Taniguchi, E. & Nishida, E. Identification of a consensus motif for PlK (Polo-like kinase) phosphorylation reveals Myt1 as a Plk1 substrate. *Journal of Biological Chemistry.* ISSN: 00219258. doi:10.1074/jbc.C300126200 (2003).

96. Alexander, J. *et al.* Spatial exclusivity combined with positive and negative selection of phosphorylation motifs is the basis for context-dependent mitotic signaling. *Science Signaling.* ISSN: 19450877. doi:10.1126/scisignal.2001796 (2011).

97. Qian, Y.-W., Erikson, E. & Maller, J. L. Mitotic effects of a constitutively active mutant of the Xenopus Polo-like kinase Plx1. *Molecular and Cellular Biology.* ISSN: 0270-7306. doi:10.1128/MCB.19.12.8625 (1999).

98. Jang, Y. J., Ma, S., Terada, Y. & Erikson, R. L. Phosphorylation of threonine 210 and the role of serine 137 in the regulation of mammalian polo-like kinase. *Journal of Biological Chemistry.* ISSN: 00219258. doi:10.1074/jbc.M202172200 (2002).

99. Lasek, A. L., McPherson, B. M., Trueman, N. G. & Burkard, M. E. The functional significance of posttranslational modifications on polo-like kinase 1 revealed by chemical genetic complementation. *PLoS ONE.* ISSN: 19326203. doi:10.1371/journal.pone.0150225 (2016).

100. Macůrek, L. *et al.* Polo-like kinase-1 is activated by aurora A to promote checkpoint recovery. *Nature.* ISSN: 00280836. doi:10.1038/nature07185 (2008).

101. Caron, D. *et al.* Mitotic phosphotyrosine network analysis reveals that tyrosine phosphorylation regulates Polo-like kinase 1 (PLK1). *Science Signaling.* ISSN: 19379145. doi:10.1126/scisignal.aah3525 (2016).

102. Elia, A. E. H., Cantley, L. C. & Yaffe, M. B. Proteomic screen finds pSer/pThr-binding domain localizing Plk1 to mitotic substrates. *Science.* ISSN: 00368075. doi:10.1126/science.1079079 (2003).

103. Elia, A. E. *et al.* The molecular basis for phosphodependent substrate targeting and regulation of Plks by the Polo-box domain. *Cell.* ISSN: 00928674. doi:10.1016/S0092-8674(03)00725-6 (2003).

104. Lowery, D. M., Mohammed, D. H., Elia, A. E. & Yaffe, M. B. The Polo-box domain: A molecular integrator of mitotic kinase cascades and Polo-like kinase function. *Cell Cycle.* ISSN: 15514005. doi:10.4161/cc.3.2.660 (2004).

105. Neef, R. *et al.* Choice of Plk1 docking partners during mitosis and cytokinesis is controlled by the activation state of Cdk1. *Nature Cell Biology.* ISSN: 14657392. doi:10.1038/ncb1557 (2007).

106. Lee, K. S. *et al.* Mechanisms of mammalian polo-like kinase 1 (Plk1) localization: Self- versus non-self-priming. *Cell Cycle.* ISSN: 15514005. doi:10.4161/cc.7.2.5272 (2008).

107. Jang, Y.-J., Lin, C.-Y., Ma, S. & Erikson, R. L. Functional studies on the role of the C-terminal domain of mammalian polo-like kinase. *Proceedings of the National Academy of Sciences.* ISSN: 0027-8424. doi:10.1073/pnas.042689299 (2002).

108. Johnson, T. M., Antrobus, R. & Johnson, L. N. Plk1 activation by Ste20-like kinase (Slk) phosphorylation and polo-box phosphopeptide binding assayed with the substrate translationally controlled tumor protein (TCTP). *Biochemistry.* ISSN: 00062960. doi:10.1021/bi702134c (2008).

109. Xu, J., Shen, C., Wang, T. & Quan, J. Structural basis for the inhibition of Polo-like kinase 1. *Nature Structural and Molecular Biology.* ISSN: 1545-9985. doi:10.1038/nsmb.2623 (2013).

110. Kachaner, D. *et al.* Coupling of Polo kinase activation to nuclear localization by a bifunctional NLS is required during mitotic entry. *Nature Communications.* ISSN: 20411723. doi:10.1038/s41467-017-01876-8 (2017).

111. Taniguchi, E., Toyoshima-Morimoto, F. & Nishida, E. Nuclear translocation of Plk1 mediated by its bipartite nuclear localization signal. *Journal of Biological Chemistry.* ISSN: 00219258. doi:10.1074/jbc.M206307200 (2002).

112. Bruinsma, W. *et al.* Spatial separation of Plk1 phosphorylation and activity. *Frontiers in Oncology.* ISSN: 2234-943X. doi:10.3389/fonc.2015.00132 (2015).

113. Seki, A., Coppinger, J. A., Jang, C. Y., Yates, J. R. & Fang, G. Bora and the kinase Aurora A cooperatively activate the kinase Plk1 and control mitotic entry. *Science.* ISSN: 00368075. doi:10.1126/science.1157425 (2008).

114. Tavernier, N. *et al.* Cdk1 phosphorylates SPAT-1/Bora to trigger PLK-1 activation and drive mitotic entry in C. elegans embryos. *Journal of Cell Biology.* ISSN: 15408140. doi:10.1083/jcb.201408064 (2015).

115. Thomas, Y. *et al.* Cdk1 phosphorylates SPAT-1/Bora to promote Plk1 activation in C. elegans and human cells. *Cell Reports.* ISSN: 22111247. doi:10.1016/j.celrep.2016.03.049 (2016).

116. Gheghiani, L., Loew, D., Lombard, B., Mansfeld, J. & Gavet, O. PLK1 activation in late G2 sets up commitment to mitosis. *Cell Reports.* ISSN: 22111247. doi:10.1016/j.celrep.2017.05.031 (2017).

117. Cascales, H. S. *et al.* Cyclin A2 localises in the cytoplasm at the S/G2 transition to activate Plk1. *bioRxiv.* doi:10.1101/191437 (2017).

118. Vigneron, S. *et al.* Cyclin A-cdk1-dependent phosphorylation of Bora is the triggering factor promoting mitotic entry. *Developmental Cell.* ISSN: 18781551. doi:10.1016/j.devcel.2018.05.005 (2018).

119. O'Farrell, P. H. Triggering the all-or-nothing switch into mitosis. *Trends in Cell Biology.* ISSN: 09628924. doi:10.1016/S0962-8924(01)02142-0 (2001).

120. Watanabe, N. *et al.* M-phase kinases induce phospho-dependent ubiquitination of somatic Wee1 by SCF -TrCP. *Proceedings of the National Academy of Sciences.* ISSN: 0027-8424. doi:10.1073/pnas.0307700101 (2004).

121. Kumagai, A. & Dunphy, W. G. Purification and molecular cloning of Plx1, a Cdc25-regulatory kinase from Xenopus egg extracts. *Science.* ISSN: 00368075. doi:10.1126/science.273.5280.1377 (1996).

122. Qian, Y. W., Erikson, E, Taieb, F. E. & Maller, J. L. The polo-like kinase Plx1 is required for activation of the phosphatase Cdc25C and cyclin B-Cdc2 in Xenopus oocytes. *Molecular Biology of the Cell.* ISSN: 1059-1524. doi:10.1091/mbc.12.6.1791 (2001).

123. Toyoshima-Morimoto, F., Taniguchi, E. & Nishida, E. Plk1 promotes nuclear translocation of human Cdc25C during prophase. *EMBO Reports.* ISSN: 1469221X. doi:10.1093/embo-reports/kvf069 (2002).

124. Lobjois, V., Jullien, D., Bouché, J. P. & Ducommun, B. The polo-like kinase 1 regulates CDC25B-dependent mitosis entry. *Biochimica et Biophysica Acta - Molecular Cell Research.* ISSN: 01674889. doi:10.1016/j.bbamcr.2008.12.015 (2009).

125. Van Vugt, M. A., Brás, A. & Medema, R. H. Polo-like kinase-1 controls recovery from a G2 DNA damage-induced arrest in mammalian cells. *Molecular Cell.* ISSN: 10972765. doi:10.1016/j.molcel.2004.07.015 (2004).

126. Lénárt, P. *et al.* The small-molecule inhibitor BI 2536 reveals novel insights into mitotic roles of Polo-like Kinase 1. *Current Biology.* ISSN: 09609822. doi:10.1016/j.cub.2006.12.046 (2007).

127. Aspinall, C. F., Zheleva, D., Tighe, A. & Taylor, S. S. Mitotic entry: Non-genetic heterogeneity exposes the requirement for Plk1. *Oncotarget.* ISSN: 1949-2553. doi:10.18632/oncotarget.5507 (2015).

128. Golsteyn, R. M., Mundt, K. E., Fry, A. M. & Nigg, E. A. Cell cycle regulation of the activity and subcellular localization of PLK1, a human protein kinase implicated in mitotic spindle function. *Journal of Cell Biology.* ISSN: 00219525. doi:10.1083/jcb.129.6.1617 (1995).

129. Arnaud, L., Pines, J. & Nigg, E. A. GFP tagging reveals human Polo-like kinase 1 at the kinetochore/centromere region of mitotic chromosomes. *Chromosoma.* ISSN: 00095915. doi:10.1007/s004120050326 (1998).

130. Kishi, K., van Vugt, M. a.T. M., Okamoto, K.-i., Hayashi, Y. & Yaffe, M. B. Functional dynamics of Polo-like kinase 1 at the centrosome. *Molecular and Cellular Biology.* ISSN: 0270-7306. doi:10.1128/MCB.01663-08 (2009).

131. Sunkel, C. E. & Glover, D. M. polo, a mitotic mutant of Drosophila displaying abnormal spindle poles. *Journal of Cell Science.* ISSN: 0021-9533. doi:10.1016/j (1988).

132. Lane, H. A. & Nigg, E. A. Antibody microinjection reveals an essential role for human polo-like kinase 1 (Plk1) in the functional maturation of mitotic centrosomes. *Journal of Cell Biology.* ISSN: 00219525. doi:10.1083/jcb.135.6.1701 (1996).

133. Sumara, I. *et al.* Roles of polo-like kinase 1 in the assembly of functional mitotic spindles. *Current Biology.* ISSN: 09609822. doi:10.1016/j.cub.2004.09.049 (2004).

134. Mardin, B. R., Agircan, F. G., Lange, C. & Schiebel, E. Plk1 controls the Nek2A-PP1γ antagonism in centrosome disjunction. *Current Biology.* ISSN: 09609822. doi:10.1016/j.cub.2011.05.047 (2011).

135. Arquint, C. & Nigg, E. A. The PLK4–STIL–SAS-6 module at the core of centriole duplication. *Biochemical Society Transactions.* ISSN: 0300-5127. doi:10.1042/bst20160116 (2016).

136. Cizmecioglu, O. *et al.* Plk2 regulates centriole duplication through phosphorylation-mediated degradation of Fbxw7 (human Cdc4). *Journal of Cell Science.* doi:10.1242/jcs.095075 (2012).

137. Carmena, M. *et al.* The chromosomal passenger complex activates Polo kinase at centromeres. *PLoS Biology.* ISSN: 15449173. doi:10.1371/journal.pbio.1001250 (2012).

138. Van Vugt, M. A.T. M. *et al.* Polo-like kinase-1 is required for bipolar spindle formation but is dispensable for anaphase promoting complex/Cdc20 activation and initiation of cytokinesis. *Journal of Biological Chemistry.* ISSN: 00219258. doi:10.1074/jbc.M313681200 (2004).

139. Hanisch, A., Wehner, A., Nigg, E. A. & Silljé, H. H. W. Different Plk1 functions show distinct dependencies on Polo-Box domain-mediated targeting. *Mol Biol Cell.* ISSN: 1059-1524. doi:10.1091/mbc.E05-08-0801 (2006).

140. Elowe, S., Hümmer, S., Uldschmid, A., Li, X. & Nigg, E. A. Tension-sensitive Plk1 phosphorylation on BubR1 regulates the stability of kinetochore-microtubule interactions. *Genes and Development.* ISSN: 08909369. doi:10.1101/gad.436007 (2007).

141. Brennan, I. M., Peters, U., Kapoor, T. M. & Straight, A. F. Polo-like kinase controls vertebrate spindle elongation and cytokinesis. *PLoS ONE.* ISSN: 19326203. doi:10.1371/journal.pone.0000409 (2007).

142. Burkard, M. E. *et al.* Chemical genetics reveals the requirement for Polo-like kinase 1 activity in positioning RhoA and triggering cytokinesis in human cells. *Proceedings of the National Academy of Sciences.* ISSN: 0027-8424. doi:10.1073/pnas.0701140104 (2007).

143. Petronczki, M., Glotzer, M., Kraut, N. & Peters, J. M. Polo-like kinase 1 triggers the initiation of cytokinesis in human cells by promoting recruitment of the RhoGEF Ect2 to the central spindle. *Developmental Cell.* ISSN: 15345807. doi:10.1016/j.devcel.2007.03.013 (2007).

144. Santamaria, A. *et al.* Use of the novel Plk1 inhibitor ZK-thiazolidinone to elucidate functions of Plk1 in early and late stages of mitosis. *Molecular Biology of the Cell.* ISSN: 1059-1524. doi:10.1091/mbc.E07-05-0517 (2007).

145. Shaltiel, I. A., Krenning, L., Bruinsma, W. & Medema, R. H. The same, only different - DNA damage checkpoints and their reversal throughout the cell cycle. *Journal of Cell Science.* ISSN: 0021-9533. doi:10.1242/jcs.163766 (2015).

146. Matsuoka, S., Huang, M. & Elledge, S. J. Linkage of ATM to cell cycle regulation by the Chk2 protein kinase. *Science.* ISSN: 00368075. doi:10.1126/science.282.5395.1893 (1998).

147. Lukas, C., Falck, J., Bartkova, J., Bartek, J. & Lukas, J. Distinct spatiotemporal dynamics of mammalian checkpoint regulators induced by DNA damage. *Nature Cell Biology.* ISSN: 14657392. doi:10.1038/ncb945 (2003).

148. Jazayeri, A. *et al.* ATM- and cell cycle-dependent regulation of ATR in response to DNA double-strand breaks. *Nature Cell Biology.* ISSN: 14657392. doi:10.1038/ncb1337 (2006).

149. Zou, L. & Elledge, S. J. Sensing DNA damage through ATRIP recognition of RPA-ssDNA complexes. *Science.* ISSN: 00368075. doi:10.1126/science.1083430 (2003).

150. Mordes, D. A., Glick, G. G., Zhao, R. & Cortez, D. TopBP1 activates ATR through ATRIP and a PIKK regulatory domain. *Genes and Development.* ISSN: 08909369. doi:10.1101/gad.1666208 (2008).

151. Liu, Q. *et al.* Chk1 is an essential kinase that is regulated by Atr and required for the G2/M DNA damage checkpoint. *Genes and Development.* ISSN: 08909369. doi:10.1101/gad.14.12.1448 (2000).

152. Kumagai, A., Kim, S. M. & Dunphy, W. G. Claspin and the activated form of ATR-ATRIP collaborate in the activation of Chk1. *Journal of Biological Chemistry.* ISSN: 00219258. doi:10.1074/jbc.M408353200 (2004).

153. Christiano, C., Chini, S. & Chen, J. Human claspin is required for replication checkpoint control. *Journal of Biological Chemistry.* ISSN: 00219258. doi:10.1074/jbc.M301136200 (2003).

154. Smits, V. A., Reaper, P. M. & Jackson, S. P. Rapid PIKK-dependent release of Chk1 from chromatin promotes the DNA-damage checkpoint response. *Current Biology.* ISSN: 09609822. doi:10.1016/j.cub.2005.11.066 (2006).

155. Donzelli, M. & Draetta, G. F. Regulating mammalian checkpoints through Cdc25 inactivation. *EMBO Reports.* ISSN: 1469221X. doi:10.1038/sj.embor.embor887 (2003).

156. Peng, C. Y. *et al.* Mitotic and G2 checkpoint control: Regulation of 14-3-3 protein binding by phosphorylation of Cdc25c on serine-216. *Science.* ISSN: 00368075. doi:10.1126/science.277.5331.1501 (1997).

157. Sanchez, Y. *et al.* Conservation of the Chk1 checkpoint pathway in mammals: Linkage of DNA damage to Cdk regulation through Cdc25. *Science.* ISSN: 00368075. doi:10.1126/science.277.5331.1497 (1997).

158. Falck, J., Mailand, N., Syljuåsen, R. G., Bartek, J. & Lukas, J. The ATM-Chk2-Cdc25A checkpoint pathway guards against radioresistant DNA synthesis. *Nature.* ISSN: 00280836. doi:10.1038/35071124 (2001).

159. Jin, J., Ang, X. L., Ye, X., Livingstone, M. & Harper, J. W. Differential roles for checkpoint kinases in DNA damage-dependent degradation of the Cdc25A protein phosphatase. *Journal of Biological Chemistry.* ISSN: 00219258. doi:10.1074/jbc.M802474200 (2008).

160. Xie, S. *et al.* Plk3 functionally links DNA damage to cell cycle arrest and apoptosis at least in part via the p53 pathway. *Journal of Biological Chemistry.* ISSN: 00219258. doi:10.1074/jbc.M106050200 (2001).

161. Xie, S. *et al.* Genotoxic stress-induced activation of Plk3 is partly mediated by Chk2. *Cell cycle (Georgetown, Tex.)* ISSN: 15384101. doi:10.4161/cc.1.6.271 (2002).

162. Bahassi, E. M., Myer, D. L., McKenney, R. J., Hennigan, R. F. & Stambrook, P. J. Priming phosphorylation of Chk2 by polo-like kinase 3 (Plk3) mediates its full activation by ATM and a downstream checkpoint in response to DNA damage. *Mutation Research - Fundamental and Molecular Mechanisms of Mutagenesis.* ISSN: 00275107. doi:10.1016/j.mrfmmm.2005.12.002 (2006).

163. Ouyang, B. *et al.* The physical association and phosphorylation of Cdc25C protein phosphatase by Prk. *Oncogene.* ISSN: 09509232. doi:10.1038/sj.onc.1202983 (1999).

164. Myer, D. L. *et al.* Absence of polo-like kinase 3 in mice stabilizes Cdc25A after DNA damage but is not sufficient to produce tumors. *Mutation Research - Fundamental and Molecular Mechanisms of Mutagenesis.* ISSN: 00275107. doi:10.1016/j.mrfmmm.2011.02.006 (2011).

165. Smits, V. A. *et al.* Polo-like kinase-1 is a target of the DNA damage checkpoint. *Nature Cell Biology.* ISSN: 1465-7392. doi:10.1038/35023629 (2000).

166. Van Vugt, M. A.T. M., Smits, V. A. J., Klompmaker, R. & Medema, R. H. Inhibition of Polo-like Kinase-1 by DNA damage occurs in an ATM- or ATR-dependent fashion. *Journal of Biological Chemistry.* ISSN: 00219258. doi:10.1074/jbc.M101831200 (2001).

167. Tsvetkov, L. & Stern, D. F. Phosphorylation of Plk1 at S137 and T210 is inhibited in response to DNA damage. *Cell Cycle.* ISSN: 15514005. doi:10.4161/cc.4.1.1348 (2005).

168. Krystyniak, A., Garcia-Echeverria, C., Prigent, C. & Ferrari, S. Inhibition of Aurora A in response to DNA damage. *Oncogene.* ISSN: 09509232. doi:10.1038/sj.onc.1209056 (2006).

169. Qin, B., Gao, B., Yu, J., Yuan, J. & Lou, Z. Ataxia telangiectasia-mutated- and Rad3-related protein regulates the DNA damage-induced G2/M checkpoint through the Aurora A cofactor Bora protein. *Journal of Biological Chemistry.* ISSN: 00219258. doi:10.1074/jbc.M113.456780 (2013).

170. Bruinsma, W *et al.* Inhibition of Polo-like kinase 1 during the DNA damage response is mediated through loss of Aurora A recruitment by Bora. *Oncogene.* ISSN: 1476-5594. doi:10.1038/onc.2016.347 (2016).

171. Yuan, J.-H. *et al.* Polo-like kinase 1 inactivation following mitotic DNA damaging treatments is independent of ataxia telangiectasia mutated kinase. *Molecular Cancer Research.* ISSN: 1541-7786. doi:2/7/417[pii] (2004).

172. Jang, Y. J., Ji, J. H., Choi, Y. C., Chun, J. R. & Ko, S. Y. Regulation of polo-like kinase 1 by DNA damage in mitosis: Inhibition of mitotic PLK-1 by protein phosphatase 2A. *Journal of Biological Chemistry.* ISSN: 00219258. doi:10.1074/jbc.M605480200 (2007).

173. Lee, H. J., Hwang, H. I. & Jang, Y. J. Mitotic DNA damage response: Polo-like kinase-1 is dephosphorylated through ATM-Chk1 pathway. *Cell Cycle.* ISSN: 15514005. doi:10.4161/cc.9.12.11904 (2010).

174. Skoufias, D. A., Lacroix, F. B., Andreassen, P. R., Wilson, L. & Margolis, R. L. Inhibition of DNA decatenation, but not DNA damage, arrests cells at metaphase. *Molecular Cell.* ISSN: 10972765. doi:10.1016/j.molcel.2004.08.018 (2004).

175. Wang, L., Guo, Q., Fisher, L. A., Liu, D. & Peng, A. Regulation of polo-like kinase 1 by DNA damage and PP2A/B55α. *Cell Cycle.* ISSN: 15514005. doi:10.4161/15384101.2014.986392 (2015).

176. Bassermann, F. *et al.* The Cdc14B-Cdh1-Plk1 axis controls the G2 DNA-damage-response checkpoint. *Cell.* ISSN: 00928674. doi:10.1016/j.cell.2008.05.043 (2008).

177. Zhou, Z. *et al.* P53 Suppresses E2F1-dependent PLK1 expression upon DNA damage by forming p53-E2F1-DNA complex. *Experimental Cell Research.* ISSN: 10902422. doi:10.1016/j.yexcr.2013.09.012 (2013).

178. Mailand, N., Bekker-Jensen, S., Bartek, J. & Lukas, J. Destruction of Claspin by SCFβTrCP restrains Chk1 activation and facilitates recovery from genotoxic stress. *Molecular Cell.* ISSN: 10972765. doi:10.1016/j.molcel.2006.06.016 (2006).

179. Mamely, I. *et al.* Polo-like kinase-1 controls proteasome-dependent degradation of Claspin during checkpoint recovery. *Current Biology.* ISSN: 09609822. doi:10.1016/j.cub.2006.08.026 (2006).

180. Peschiaroli, A. *et al.* SCFβTrCP-mediated degradation of claspin regulates recovery from the DNA replication checkpoint response. *Molecular Cell.* ISSN: 10972765. doi:10.1016/j.molcel.2006.06.013 (2006).

181. Van Vugt, M. A. *et al.* A mitotic phosphorylation feedback network connects Cdk1, Plk1, 53BP1, and Chk2 to inactivate the G2/M DNA damage checkpoint. *PLoS Biology.* ISSN: 15449173. doi:10.1371/journal.pbio.1000287 (2010).

182. Liang, H. *et al.* Homeostatic control of polo-like kinase-1 engenders non-genetic heterogeneity in G2 checkpoint fidelity and timing. *Nature Communications.* ISSN: 20411723. doi:10.1038/ncomms5048 (2014).

183. Wohlbold, L. & Fisher, R. P. Behind the wheel and under the hood: Functions of cyclin-dependent kinases in response to DNA damage. *DNA Repair.* ISSN: 15687864. doi:10.1016/j.dnarep.2009.04.009 (2009).

184. Wohlbold, L. *et al.* Chemical genetics reveals a specific requirement for Cdk2 activity in the DNA damage response and identifies Nbs1 as a Cdk2 substrate in human cells. *PLoS Genetics.* ISSN: 15537390. doi:10.1371/journal.pgen.1002935 (2012).

185. Myers, J. S., Zhao, R., Xu, X., Ham, A. J. L. & Cortez, D. Cyclin-dependent kinase 2-dependent phosphorylation of ATRIP regulates the G2-M checkpoint response to DNA damage. *Cancer Research.* ISSN: 00085472. doi:10.1158/0008-5472.CAN-07-0495 (2007).

186. Müller-Tidow, C. *et al.* The cyclin A1-CDK2 complex regulates DNA double-strand break repair. *Molecular and Cellular Biology.* ISSN: 0270-7306. doi:10.1128/MCB.24.20.8917-8928.2004 (2004).

187. Chow, J. P. *et al.* Differential contribution of inhibitory phosphorylation of CDC2 and CDK2 for unperturbed cell cycle control and DNA integrity checkpoints. *Journal of Biological Chemistry.* ISSN: 00219258. doi:10.1074/jbc.M306683200 (2003).

188. Sanchez, Y. *et al.* Control of the DNA damage checkpoint by Chk1 and Rad53 protein kinases through distinct mechanisms. *Science.* ISSN: 00368075. doi:10.1126/science.286.5442.1166 (1999).

189. Gerber, H. B., Pikman, Y. & Fisher, R. P. The CDK-activating kinase (CAK) Csk1 is required for normal levels of homologous recombination and resistance to DNA damage in fission yeast. *PLoS ONE.* ISSN: 19326203. doi:10.1371/journal.pone.0001492 (2008).

190. Weimer, A. K. *et al.* The plant-specific CDKB 1 -CYCB 1 complex mediates homologous recombination repair in Arabidopsis. *The EMBO Journal.* ISSN: 0261-4189. doi:10.15252/embj.201593083 (2016).

191. Chabalier-Taste, C. *et al.* Polo-like kinase 1 mediates BRCA1 phosphorylation and recruitment at DNA double-strand breaks. *Oncotarget.* ISSN: 1949-2553. doi:10.18632/oncotarget.6825 (2016).

192. Hukasova, E., Silva Cascales, H., Kumar, S. R. & Lindqvist, A. Monitoring kinase and phosphatase activities through the cell cycle by ratiometric FRET. *Journal of Visualized Experiments.* doi:10.3791/3410 (2012).

193. Poser, I. *et al.* BAC TransgeneOmics: A high-throughput method for exploration of protein function in mammals. *Nature Methods.* ISSN: 15487091. doi:10.1038/nmeth.1199 (2008).

194. McKinley, K. L. & Cheeseman, I. M. Polo-like kinase 1 licenses CENP-a deposition at centromeres. *Cell.* ISSN: 10974172. doi:10.1016/j.cell.2014.06.016 (2014).

195. Lekomtsev, S., Gerlich, D. W., Pozniakovsky, A., Petronczki, M. & Guizetti, J. Evidence that the tumor-suppressor protein BRCA2 does not regulate cytokinesis in human cells. *Journal of Cell Science.* ISSN: 0021-9533. doi:10.1242/jcs.068015 (2010).

196. Dimitrova, N., Chen, Y. C. M., Spector, D. L. & De Lange, T. 53BP1 promotes non-homologous end joining of telomeres by increasing chromatin mobility. *Nature.* ISSN: 00280836. doi:10.1038/nature07433 (2008).

197. Johannessen, C. M. *et al.* COT drives resistance to RAF inhibition through MAP kinase pathway reactivation. *Nature.* ISSN: 00280836. doi:10.1038/nature09627 (2010).

198. Gudjonsson, T. *et al.* TRIP12 and UBR5 suppress spreading of chromatin ubiquitylation at damaged chromosomes. *Cell.* ISSN: 00928674. doi:10.1016/j.cell.2012.06.039 (2012).

199. Mandegar, M. A. *et al.* CRISPR interference efficiently induces specific and reversible gene silencing in human iPSCs. *Cell Stem Cell.* ISSN: 18759777. doi:10.1016/j.stem.2016.01.022 (2016).

200. Ran, F. *et al.* Genome engineering using the CRIPR-Cas9 system. *Nature.* ISSN: 1750-2799. doi:10.1038/nprot.2013.143 (2013).

201. Cong, L. *et al.* Multiplex genome engineering using CRISPR/Cas systems. *Science.* ISSN: 10959203. doi:10.1126/science.1231143 (2013).

202. Chen, B. *et al.* Dynamic imaging of genomic loci in living human cells by an optimized CRISPR/Cas system. *Cell.* ISSN: 10974172. doi:10.1016/j.cell.2013.12.001 (2013).

203. Florens, L. *et al.* Analyzing chromatin remodeling complexes using shotgun proteomics and normalized spectral abundance factors. *Methods.* ISSN: 10462023. doi:10.1016/j.ymeth.2006.07.028 (2006).

204. Pavelka, N. *et al.* Statistical similarities between transcriptomics and quantitative shotgun proteomics data. *Molecular & Cellular Proteomics* **7,** 631–644. ISSN: 1535-9476 (2008).

205. Pavelka, N. *et al.* A power law global error model for the identification of differentially expressed genes in microarray data. *BMC Bioinformatics.* ISSN: 14712105. doi:10.1186/1471-2105-5-203 (2004).

206. Zgheib, O., Pataky, K., Brugger, J. & Halazonetis, T. D. An oligomerized 53BP1 tudor domain suffices for recognition of DNA double-strand breaks. *Molecular and Cellular Biology.* ISSN: 0270-7306. doi:10.1128/MCB.01011-08 (2009).

207. Huyen, Y. *et al.* Methylated lysine 79 of histone H3 targets 53BP1 to DNA double-strand breaks. *Nature.* ISSN: 00280836. doi:10.1038/nature03114 (2004).

208. Lindon, C. & Pines, J. Ordered proteolysis in anaphase inactivates Plk1 to contribute to proper mitotic exit in human cells. *Journal of Cell Biology.* ISSN: 00219525. doi:10.1083/jcb.200309035 (2004).

209. Lukas, C. *et al.* 53BP1 nuclear bodies form around DNA lesions generated by mitotic transmission of chromosomes under replication stress. *Nature Cell Biology.* ISSN: 14657392. doi:10.1038/ncb2201 (2011).

210. Vassilev, L. T. *et al.* Selective small-molecule inhibitor reveals critical mitotic functions of human CDK1. *Proceedings of the National Academy of Sciences.* ISSN: 0027-8424. doi:10.1073/pnas.0600447103 (2006).

211. Davies, T. G. *et al.* Structure-based design of a potent purine-based cyclin-dependent kinase inhibitor. *Nature Structural Biology.* ISSN: 10728368. doi:10.1038/nsb842 (2002).

212. Hardcastle, I. R. *et al.* N2-substituted O6-cyclohexylmethylguanine derivatives: Potent inhibitors of cyclin-dependent kinases 1 and 2. *Journal of Medicinal Chemistry.* ISSN: 00222623. doi:10.1021/jm0311442 (2004).

213. Hickson, I. *et al.* Identification and characterization of a novel and specific inhibitor of the ataxia-telangiectasia mutated kinase ATM. *Cancer Research.* ISSN: 00085472. doi:10.1158/0008-5472.CAN-04-2727 (2004).

214. Bakkenist, C. J. & Kastan, M. B. DNA damage activates ATM through intermolecular autophosphorylation and dimer dissociation. *Nature.* ISSN: 00280836. doi:10.1038/nature01368 (2003).

215. Golding, S. E. *et al.* Improved ATM kinase inhibitor KU-60019 radiosensitizes glioma cells, compromises insulin, AKT and ERK prosurvival signaling, and inhibits migration and invasion. *Molecular Cancer Therapeutics.* ISSN: 1535-7163. doi:10.1158/1535-7163.MCT-09-0519 (2009).

216. Sakaue-Sawano, A. *et al.* Visualizing Spatiotemporal Dynamics of Multicellular Cell-Cycle Progression. *Cell.* ISSN: 00928674. doi:10.1016/j.cell.2007.12.033 (2008).

217. Aleksandrov, R. *et al.* Protein dynamics in complex DNA lesions. *Molecular Cell.* ISSN: 10974164. doi:10.1016/j.molcel.2018.02.016 (2018).

218. Li, W. *et al.* A methylation-phosphorylation switch determines Plk1 kinase activity and function in DNA damage repair. *Science Advances,* 1–15 (2019).

219. Leng, M., Bessuso, D., Jung, S. Y., Wang, Y. & Qin, J. Targeting Plk1 to chromosome arms and regulating chromosome compaction by the PICH ATPase. *Cell Cycle.* ISSN: 15514005. doi:10.4161/cc.7.10.5951 (2008).

220. Kurasawa, Y. & Yu-Lee, L. y. PICH and cotargeted Plk1 coordinately maintain prometaphase chromosome arm architecture. *Molecular Biology of the Cell.* ISSN: 1059-1524. doi:10.1091/mbc.E09-11-0950 (2010).

221. Zhu, M. *et al.* MISP is a novel Plk1 substrate required for proper spindle orientation and mitotic progression. *Journal of Cell Biology.* ISSN: 00219525. doi:10.1083/jcb.201207050 (2013).

222. Rape, M. Cell Cycle: On-Time Delivery of Plk1 during Cytokinesis. *Current Biology.* ISSN: 09609822. doi:10.1016/j.cub.2007.04.032 (2007).

223. Borlado, L. R. & Méndez, J. CDC6: From DNA replication to cell cycle checkpoints and oncogenesis. *Carcinogenesis.* ISSN: 01433334. doi:10.1093/carcin/bgm268 (2008).

224. Yim, H., Erikson, R. L. & Plk, C. Cell division cycle 6 , a mitotic substrate of polo-like kinase 1 , regulates chromosomal segregation mediated by cyclin-dependent kinase 1 and separase. *Proceedings of the National Academy of Sciences.* ISSN: 0027-8424. doi:10.1073/pnas.1013557107 (2010).

225. Kang, Y. H. *et al.* Self-regulated Plk1 recruitment to kinetochores by the Plk1-PBIP1 interaction is critical for proper chromosome segregation. *Molecular Cell.* ISSN: 10972765. doi:10.1016/j.molcel.2006.10.016 (2006).

226. Kang, Y. H. *et al.* Mammalian polo-like kinase 1-dependent regulation of the PBIP1-CENP-Q complex at kinetochores. *Journal of Biological Chemistry.* ISSN: 00219258. doi:10.1074/jbc.M111.224105 (2011).

227. Chung, H. J., Park, J. E., Lee, N. S., Kim, H. & Jang, C. Y. Phosphorylation of astrin regulates its kinetochore function. *Journal of Biological Chemistry.* ISSN: 1083351X. doi:10.1074/jbc.M115.712745 (2016).

228. Spektor, A., Tsang, W. Y., Khoo, D. & Dynlacht, B. D. Cep97 and CP110 Suppress a Cilia Assembly Program. *Cell.* ISSN: 00928674. doi:10.1016/j.cell.2007.06.027 (2007).

229. Kobayashi, T., Tsang, W. Y., Li, J., Lane, W. & Dynlacht, B. D. Centriolar kinesin Kif24 interacts with CP110 to remodel microtubules and regulate ciliogenesis. *Cell.* ISSN: 00928674. doi:10.1016/j.cell.2011.04.028 (2011).

230. Prosser, S. L. & Morrison, C. G. Centrin2 regulates CP110 removal in primary cilium formation. *Journal of Cell Biology.* ISSN: 15408140. doi:10.1083/jcb.201411070 (2015).

231. Brunk, K. *et al.* Cep78 is a new centriolar protein involved in Plk4-induced centriole overduplication. *Journal of Cell Science.* ISSN: 0021-9533. doi:10.1242/jcs.184093 (2016).

232. Hossain, D., Javadi Esfehani, Y., Das, A. & Tsang, W. Y. Cep78 controls centrosome homeostasis by inhibiting EDD-DYRK2-DDB1 Vpr BP. *EMBO Reports.* ISSN: 1469-221X. doi:10.15252/embr.201642377 (2017).

233. Ohama, T. The multiple functions of protein phosphatase 6. *Biochimica et Biophysica Acta - Molecular Cell Research.* ISSN: 18792596. doi:10.1016/j.bbamcr.2018.07.015 (2018).

234. Kettenbach, A. N. *et al.* Global assessment of its network dynamics reveals that the kinase Plk1 inhibits the phosphatase PP6 to promote Aurora A activity. *Science Signaling.* ISSN: 19379145. doi:10.1126/scisignal.aaq1441 (2018).

235. Zeng, K., Bastos, R. N., Barr, F. A. & Gruneberg, U. Protein phosphatase 6 regulates mitotic spindle formation by controlling the T-loop phosphorylation state of Aurora A bound to its activator TPX2. *Journal of Cell Biology.* ISSN: 00219525. doi:10.1083/jcb.201008106 (2010).

236. Mi, J., Dziegielewski, J., Bolesta, E., Brautigan, D. L. & Larner, J. M. Activation of DNA-PK by ionizing radiation is mediated by protein phosphatase 6. *PLoS ONE.* ISSN: 19326203. doi:10.1371/journal.pone.0004395 (2009).

237. Douglas, P. *et al.* Protein Phosphatase 6 interacts with the DNA-dependent protein kinase catalytic subunit and dephosphorylates gamma H2AX. *Molecular and Cellular Biology.* ISSN: 0270-7306. doi:10.1128/MCB.00741-09 (2010).

238. Zhong, J. *et al.* Protein phosphatase PP6 is required for homology-directed repair of DNA double-strand breaks. *Cell Cycle.* ISSN: 15514005. doi:10.4161/cc.10.9.15479 (2011).

239. Douglas, P. *et al.* Polo-like kinase 1 (PLK1) and protein phosphatase 6 (PP6) regulate DNA-dependent protein kinase catalytic subunit (DNA-PKcs) phosphorylation in mitosis. *Bioscience Reports.* ISSN: 0144-8463. doi:10.1042/BSR20140051 (2014).

240. Clay-Farrace, L., Pelizon, C., Santamaria, D., Pines, J. & Laskey, R. A. Human replication protein Cdc6 prevents mitosis through a checkpoint mechanism that implicates Chk1. *EMBO Journal.* ISSN: 02614189. doi:10.1093/emboj/cdg046 (2003).

241. Yoshida, K. *et al.* CDC6 interaction with ATR regulates activation of a replication checkpoint in higher eukaryotic cells. *Journal of Cell Science.* ISSN: 0021-9533. doi:10.1242/jcs.058693 (2010).

242. Guervilly, J.-H. & Gaillard, P.-H. L. SLX4: multitasking to maintain genome stability. *Critical Reviews in Biochemistry and Molecular Biology* **53,** 1–40. ISSN: 1040-9238 (2018).

243. Svendsen, J. M. *et al.* Mammalian BTBD12/SLX4 assembles a holliday junction resolvase and is required for DNA repair. *Cell.* ISSN: 00928674. doi:10.1016/j.cell.2009.06.030 (2009).

244. Marti, T. M., Kunz, C. & Fleck, O. DNA mismatch repair and mutation avoidance pathways. *Journal of Cellular Physiology.* ISSN: 00219541. doi:10.1002/jcp.10077 (2002).

245. Parrilla-Castellar, E. R., Arlander, S. J. H. & Karnitz, L. Dial 9-1-1 for DNA damage: The Rad9-Hus1-Rad1 (9-1-1) clamp complex. *DNA Repair.* ISSN: 15687864. doi:10.1016/j.dnarep.2004.03.032 (2004).

246. Lovejoy, C. A. *et al.* Functional genomic screens identify CINP as a genome maintenance protein. *Proceedings of the National Academy of Sciences.* ISSN: 1091-6490. doi:10.1073/pnas.0909345106 (2009).

247. Parplys, A. C. *et al.* NUCKS1 is a novel RAD51AP1 paralog important for homologous recombination and genome stability. *Nucleic Acids Research.* ISSN: 13624962. doi:10.1093/nar/gkv859 (2015).

248. Bleuyard, J.-Y. *et al.* MRG15-mediated tethering of PALB2 to unperturbed chromatin protects active genes from genotoxic stress. *Proceedings of the National Academy of Sciences.* ISSN: 0027-8424. doi:10.1073/pnas.1620208114 (2017).

249. Hanamshet, K., Mazina, O. M. & Mazin, A. V. Reappearance from obscurity: Mammalian Rad52 in homologous recombination. *Genes.* ISSN: 20734425. doi:10.3390/genes7090063 (2016).

250. Maddika, S. & Chen, J. Protein kinase DYRK2 is a scaffold that facilitates assembly of an E3 ligase. *Nature Cell Biology.* ISSN: 14657392. doi:10.1038/ncb1848 (2009).

251. Liu, Y., Nielsen, C. F., Yao, Q. & Hickson, I. D. The origins and processing of ultra fine anaphase DNA bridges. *Current Opinion in Genetics and Development.* ISSN: 18790380. doi:10.1016/j.gde.2014.03.003 (2014).

252. Kaulich, M., Cubizolles, F. & Nigg, E. A. On the regulation, function, and localization of the DNA-dependent ATPase PICH. *Chromosoma.* ISSN: 00095915. doi:10.1007/s00412-012-0370-0 (2012).

253. Shen, Z., Cloud, K. G., Chen, D. J. & Park, M. S. Specific interactions between the human RAD51 and RAD52 proteins. *Journal of Biological Chemistry.* ISSN: 00219258. doi:10.1074/jbc.271.1.148 (1996).

254. Kulak, N. A., Pichler, G., Paron, I., Nagaraj, N. & Mann, M. Minimal, encapsulated proteomic-sample processing applied to copy-number estimation in eukaryotic cells. *Nature Methods.* ISSN: 15487105. doi:10.1038/nmeth.2834 (2014).

255. Taira Nihira, N. & Yoshida, K. Engagement of dyrk2 in proper control for cell division. *Cell Cycle.* ISSN: 15514005. doi:10.1080/15384101.2015.1007751 (2015).

256. Taira, N. *et al.* DYRK2 priming phosphorylation of c-Jun and c-Myc modulates cell cycle progression in human cancer cells. *Journal of Clinical Investigation.* ISSN: 1558-8238. doi:10.1172/JCI60818 (2012).

257. Jung, H. Y., Wang, X., Jun, S. & Park, J. I. Dyrk2-associated EDD-DDB1-VprBP E3 ligase inhibits telomerase by TERT degradation. *Journal of Biological Chemistry.* ISSN: 00219258. doi:10.1074/jbc.M112.416792 (2013).

258. Ong, S. S. *et al.* Stability of the human pregnane X receptor is regulated by E3 ligase UBR5 and serine/threonine kinase DYRK2. *Biochemical Journal.* ISSN: 0264-6021. doi:10.1042/BJ20130558 (2014).

259. Wood, E. & Nurse, P. Sizing up to divide: Mitotic cell-size control in fission yeast. *Annual Review of Cell and Developmental Biology.* ISSN: 1081-0706. doi:10.1146/annurev-cellbio-100814-125601 (2015).

260. Taira, N., Nihira, K., Yamaguchi, T., Miki, Y. & Yoshida, K. DYRK2 is targeted to the nucleus and controls p53 via Ser46 phosphorylation in the apoptotic response to DNA damage. *Molecular Cell.* ISSN: 10972765. doi:10.1016/j.molcel.2007.02.007 (2007).

261. Taira, N., Yamamoto, H., Yamaguchi, T., Miki, Y. & Yoshida, K. ATM augments nuclear stabilization of DYRK2 by inhibiting MDM2 in the apoptotic response to DNA damage. *Journal of Biological Chemistry.* ISSN: 00219258. doi:10.1074/jbc.M109.042341 (2010).

262. Yamamoto, T. *et al.* Interaction between RNF8 and DYRK2 is required for the recruitment of DNA repair molecules to DNA double-strand breaks. *FEBS Letters* **591,** 842–853. ISSN: 18733468 (2017).

263. Becker, W. *et al.* Sequence characteristics, subcellular localization, and substrate specificity of DYRK-related kinases, a novel family of dual specificity protein kinases. *Journal of Biological Chemistry.* ISSN: 00219258. doi:10.1074/jbc.273.40.25893 (1998).

264. Guo, X., Williams, J. G., Schug, T. T. & Li, X. DYRK1A and DYRK3 promote cell survival through phosphorylation and activation of SIRT1. *Journal of Biological Chemistry.* ISSN: 00219258. doi:10.1074/jbc.M110.102574 (2010).

265. Campbell, L. E. & Proud, C. G. Differing substrate specificities of members of the DYRK family of arginine-directed protein kinases. *FEBS Letters.* ISSN: 00145793. doi:10.1016/S0014-5793(01)03221-5 (2002).

266. Nishi, Y., Rogers, E., Robertson, S. M. & Lin, R. Polo kinases regulate C. elegans embryonic polarity via binding to DYRK2-primed MEX-5 and MEX-6. *Development.* ISSN: 0950-1991. doi:10.1242/dev.013425 (2008).

267. Lochhead, P. A., Sibbet, G., Morrice, N. & Cleghon, V. Activation-loop autophosphorylation is mediated by a novel transitional intermediate form of DYRKs. *Cell.* ISSN: 00928674. doi:10.1016/j.cell.2005.03.034 (2005).

268. Walte, A. *et al.* Mechanism of dual specificity kinase activity of DYRK1A. *FEBS Journal.* ISSN: 1742464X. doi:10.1111/febs.12411 (2013).

269. Henderson, M. J. *et al.* EDD mediates DNA damage-induced activation of CHK2. *Journal of Biological Chemistry.* ISSN: 00219258. doi:10.1074/jbc.M602818200 (2006).

270. Zhang, T., Cronshaw, J., Kanu, N., Snijders, A. P. & Behrens, A. UBR5-mediated ubiquitination of ATMIN is required for ionizing radiation-induced ATM signaling and function. *Proceedings of the National Academy of Sciences.* ISSN: 0027-8424. doi:10.1073/pnas.1400230111 (2014).

271. Sanchez, A. *et al.* BMI1–UBR5 axis regulates transcriptional repression at damaged chromatin. *Proceedings of the National Academy of Sciences.* ISSN: 0027-8424. doi:10.1073/pnas.1610735113 (2016).

272. Shearer, R. F., Iconomou, M., Watts, C. K. W. & Saunders, D. N. Functional roles of the E3 ubiquitin ligase UBR5 in cancer. *Molecular Cancer Research.* ISSN: 1541-7786. doi:10.1158/1541-7786.mcr-15-0383 (2015).

273. Bethard, J. R., Zheng, H., Roberts, L. & Eblen, S. T. Identification of phosphorylation sites on the E3 ubiquitin ligase UBR5/EDD. *Journal of Proteomics.* ISSN: 18743919. doi:10.1016/j.jprot.2011.08.023 (2011).

274. Lopez, M. S., Kliegman, J. I. & Shokat, K. M. The logic and design of analog-sensitive kinases and their small molecule inhibitors. *Methods in Enzymology.* ISSN: 15577988. doi:10.1016/B978-0-12-397918-6.00008-2 (2014).

275. Debdab, M. *et al.* Leucettines, a class of potent inhibitors of cdc2-like kinases and dual specificity, tyrosine phosphorylation regulated kinases derived from the marine sponge leucettamine B: Modulation of alternative pre-RNA splicing. *Journal of Medicinal Chemistry.* ISSN: 00222623. doi:10.1021/jm200274d (2011).

276. Tahtouh, T. *et al.* Selectivity, cocrystal structures, and neuroprotective properties of leucettines, a family of protein kinase inhibitors derived from the marine sponge alkaloid leucettamine B. *Journal of Medicinal Chemistry.* ISSN: 00222623. doi:10.1021/jm301034u (2012).

277. Göckler, N. *et al.* Harmine specifically inhibits protein kinase DYRK1A and interferes with neurite formation. *FEBS Journal.* ISSN: 1742464X. doi:10.1111/j.1742-4658.2009.07346.x (2009).

278. Henderson, M. J. *et al.* EDD, the human hyperplastic discs protein, has a role in progesterone receptor coactivation and potential involvement in DNA damage response. *Journal of Biological Chemistry.* ISSN: 00219258. doi:10.1074/jbc.M203527200 (2002).

279. Larson, M. H. *et al.* CRISPR interference (CRISPRi) for sequence-specific control of gene expression. *Nature Protocols.* ISSN: 17542189. doi:10.1038/nprot.2013.132 (2013).

280. Gilbert, L. A. *et al.* CRISPR-mediated modular RNA-guided regulation of transcription in eukaryotes. *Cell.* ISSN: 10974172. doi:10.1016/j.cell.2013.06.044 (2013).

281. Seol, J. H., Shim, E. Y. & Lee, S. E. Microhomology-mediated end joining: Good, bad and ugly. *Mutation Research - Fundamental and Molecular Mechanisms of Mutagenesis.* ISSN: 18792871. doi:10.1016/j.mrfmmm.2017.07.002 (2018).

282. Wang, H. *et al.* PLK1 targets CtIP to promote microhomology-mediated end joining. *Nucleic Acids Research.* ISSN: 13624962. doi:10.1093/nar/gky810 (2018).

283. Wu, W. *et al.* Repair of radiation induced DNA double strand breaks by backup NHEJ is enhanced in G2. *DNA Repair.* ISSN: 15687864. doi:10.1016/j.dnarep.2007.11.008 (2008).

284. Shi, L. Z. *et al.* Microhomology-mediated End Joining and Homologous Recombination share the initial end resection step to repair DNA double-strand breaks in mammalian cells. *Proceedings of the National Academy of Sciences.* ISSN: 0027-8424. doi:10.1073/pnas.1213431110 (2013).

285. Xiong, X. *et al.* 53BP1 promotes microhomology-mediated end-joining in G1-phase cells. *Nucleic Acids Research.* ISSN: 13624962. doi:10.1093/nar/gku1406 (2015).